UNIVERSITY OF LATVIA
FACULTY OF PHYSICS AND MATHEMATIC
Natalja Zorina

ANALYSIS OF SPECTRAL LINE SHAPES IN LOW – TEMPERATURE PLASMA BY MEANS OF INVERSE ILL POSED PROBLEM SOLUTION

Doctor thesis

Riga, 2017

The doctoral thesis was carried out: at the Institute of Atomic Physics and Spectroscopy (IAPS), University of Latvia, from 2004 to 2016

The thesis contains the introduction, 7 chapters, reference list, 6 appendices.
Form of the thesis: dissertation in Physics, Theoretical Physics
Supervisors : Dr.phys. Atis Skudra, leader researcher LU IAPS;
Dr.phys., Gita Revalde, Assoc.Prof. RTU
Reviewers:

1) *Dr. phys.* ***Rita Veilande****, leader researcher LU IAPS;*
2) *Dr. habil. phys.* ***Andris Ozols****, Prof. RTU;*
3) *Dr. phys.* ***Natalja Denisova****, leader researcher Institute of Theoretical and Applied Mechanics, Novosibirsk, Russia.*

The thesis will be defended at the public session of the Doctoral Committee of Physics and Astronomy, University of Latvia, at 15.00 on March 29, 2017 LU IAPS Šķūņu 4, 4. floor auditoria.

The thesis is available at the Library of the University of Latvia, Kalpaka blvd. 4.

This thesis is accepted for the commencement of the degree of Doctor of Physics on December 16, 2016 by the Doctoral Committee of Physics, University of Latvia.

Chairman of the Doctoral Committe_____/Prof., *Dr habil. phys Jānis Spigulis./*

(paraksts)

Secretary of the Doctoral Committe _____/ *Laureta Buševica/*

(paraksts)

Anotācija

Promocijas darbs izstrādāts Latvijas Universitātes Atomfizikas un Spektroskopijas institūtā(ASI), laika posmā no 2004. līdz 2016. gadam.

Darbs sastāv no ievada, 7 nodaļām, literatūras saraksta, 6 pielikumiem.

Darba forma: disertācija Fizikas nozarē, Teorētiskās fizikas apakšnozarē

Darba zinātniskais vadītāji : Dr.fiz. Atis Skudra, vadošais pētnieks LU ASI; Dr.fiz. , Assoc.Prof. Gita Revalde, RTU

Promocijas darbs ir veltīts zemtemperatūras plazmas diagnostikas metodes attīstīšanai, augstfrekvences bezelektrodu lampām (ABL).

Šajā darbā tika izstrādāta jauna metode spektroskopisko attēlu apstrādei un reālo (patieso) spektrāllīniju kontūru noteikšanai, risinot nekorekto apgriezto uzdevumu, kas balstās uz Tihonova regularizācijas algoritmu.

Šī darba ietvaros izstrādātā metode tika pielietota, lai pētītu eksperimentālās dzīvsudraba spektrāllīnijas, kas emitētas no specialas formas mikro ABL, kas izgatavotas LU ASI. Izmantotās metodes ticamība tika pārbaudīta, risinot modeļu piemērus un salīdzinot ar rezultātiem, kas iegūti ar matemātiskās modelēšanas palīdzību. Šajā darbā regularizācijas parametrs tika aprēķināts ar divām neatkarīgām metodēm.

Pirmo reizi šajā darbā jaunā diagnostikas metode tika testēta, aprēķinot patiesās profilu formas, izmantojot eksperimentāli iegūtās Hg rezonanses 184.9nm (6^1P_1-6^1S_0 pāreja), 253.7 nm (6^3P_1-6^1S_0 pāreja) līnijas, Hg redzamā tripleta līnijām (7^3S_1-$6^3P_{0,1,2}$ pārejas ar viļņa garumiem 404,7 nm, 435.8 nm, 546.1 nm) magnētiskajā laukā un bez magnētiskā lauka.

Nekorekta apgriezta uzdevuma risināšanas praktiskai realizācijai tika izveidota programmatūra gadījumiem, kad spektrālas līnijas tika mērītas ar Zēmana spektrometru, Fabrī-Pero interferometru, Furjē spektrometru. Skaitļošanas programmā nodrošināta iespēja izmantot dažādas aparatūras funkcijas dažādiem spektrometriem, gan analītiskas izteiksmes veidā, ka arī eksperimentālā datu masīvā veidā.

Šī darba ietvaros tika analizēta aparatūras funkcijas ietekme uz spektrālās līnijas formu un pusplatumu. Tika pierādīts, ka aparatūras funkcijas neņemšana vērā zemtemperatūras plazmas gadījumā var ieviest lielu neprecizitāti, nosakot profilu formu un platumu un, sekojoši, ABL temperatūru. Tika analizēta arī atkarība no bufergāzes veida.

Šī darba rezultāti tika nopublicēti **3** zinātniskas žurnālos (SCOPUS), **8** konferenču rakstu krājumos (5- SCOPUS) un **8** tēzes.

Abstract

This thesis is dedicated to the development of the diagnostic methods of the low temperature plasma in case of high-frequency electrodeless discharge lamps (HFEDLs) by means of the restoration of the real spectral line profiles from measured ones by means of ill posed inverse task solution.

Within the framework of PhD thesis, the new method of the restoring the real profile of the measured spectral lines based on Tikhonov regularizing algorithm was developed. the elaborated method was applied for case of real Hg spectral line profiles, emitted from special design microsize light sources, manufactured at LU IAPS. The reliability of the solution method was verified by means of solution of the model tasks and comparison with results obtained by means of a non-linear multi-parameter chi-square fit. The regularization parameter was obtained by means of two independed methods in this thesis.

The new diagnostic method was tested using experimental spectral line shapes without and with presence of magnetic field.The solutions for the profiles of the Hg resonance 184.9nm(6^1P_1 -6^1S_0 transitions), 253.7 nm(6^3P_1 -6^1S_0 transitions) line profiles, Hg visible triplet 7^3S_1-$6^3P_{0,1,2}$ transitions (with the wave lengths Hg 404,7 nm, 435.8 nm, 546.1 nm respectively) in magnetic field and without magnetic field were performed for the first time.

Within the framework of this thesis the software was developed for practical realization of the solution of ill posed inverse task in cases when real Hg spectral line profiles were measured by mean of Zeeman spectrometer, Fabry-Perrot interferometer, Fourier transform spectrometer. The program provides an opportunity to use different instrumental function of different spectrometers and use instrumental functions as analytical expressions as well as the experimental data array.

Within the framework of this work the influence of the instrumental function on the form and FWHM of the lines profiles were analyzed. It was proved that the neglecting the instrument function, in the case of low –pressure or cold plasma when instrument function is on the same order that experimental profile, gives huge error for the FWHM estimation and consequently for discharge temperature estimation. The dependence of the FWHM of the type of buffer gas can be observed also.

The results of this work are presented in **3** scientific journals (all in Scopus), **8** Proceedings of International Conferences (5- Scopus) and **8** books of the abstracts. (The names of the publications can be seen in sections IV-VI: *"List of publication"*, but the full texts of publications and proceedings (Scopus) in *"Appendix"*.)

Contents

Main legends

Text abbreviations

AAS- atomic absorption spectrometers

HFEDL - high-frequency electrodeless discharge lamps

FWHM - the full width at half maximum

SLE- system of the linear equation

Main legends (separation by section)

Literature review
Types of the spectral line profiles

$\Delta\nu$ - line width

$\Delta\lambda$ - line width in wavelength scale

ν - frequency

ν_0 – frequency at maximum

k(ν)- function of the brightness

k_0-value of the distribution function of brightness at maximum

μ- atomic mass

R- gas constant

T- absolute temperature of the emitting gas

$\kappa_0 l$ – optical density

l- optical path

$S(\kappa_0 l)$ – Ladenburg –Levi function

κ_0- the absorption coefficient in the centre of the line of the Doppler profile

e - charge of an electron

m_0 - mass of an electron

f_{ik} – strength of oscillator

n_i – density

γ – excitation coefficient

τ_k and τ_i – life times of the energy levels N_k and N_i between which the transition occurs and radiation is emitted with frequency ν_{ki}

A_{ki} -transition probability

g_i un g_k - statistical weights

N_0- number of the particles in the volume unit

Spectral apparatus for registration of spectral line profiles

σ^2 –effective cross section

μ- molecular weight

p- pressure

$N_A = 6{,}022\ 141\ 79(30)\times 10^{23}\ \mathrm{mol}^{-1}$(Avogadro's number)

σ- free spectral range

t- distance between the mirrors of the interferometer ;

n- coefficient of the refraction of the environment

φ- angle of falling rays

k- order of the interference;

λ- wavelength of falling light

A(ν)- Airy function

Δ – difference of the optical ways

r- effective refraction coefficient of the mirrors

$\vec{H}$ - intensity of magnetic field

L- difference between two optical path lengths (optical path difference)

Ill-posed tasks

$f(\nu)$ -measured (experimental) spectral line

$y\left(\nu^{'}\right)$- real line profile

$A\left(\nu,\nu^{'}\right)$- instrumental function

n - integer characterizing the homogeneity of the radiation source

$P(\nu-\nu_0)$ - the line profile of radiation in a unity volume

$M_{\alpha}\left[y,\tilde{f}\right]$- smoothing functional (Tikhonov's functional)

δ - error of experimental $f(x)$ profile

ξ - error of kernel of instrumental function

$\left\|\tilde{A}y - \tilde{f}\right\|_F^2$ - discrepancy

Ω- stabilizing functional

α- regularization parameter

$\Delta\nu_D$- FWHM of Doppler function

$\Delta\nu_L$- FWHM of Lorentz function

$\Delta\nu_{Instr-}$ FWHM of instrumental function

Aim of this work

The aim of this thesis is:

a) to develop the method of restoring the real form of the measured spectral lines, by means of ill-posed inverse task solution, which allows making with high accuracy the procedure of the instrumental function separating from the data obtained in the experiment;

b) to develop the software for practical realization of this method;

c) to test the method on spectral line shapes emitted from low-temperature high-frequency electrodeless lamps

It gives possibility to restore the real profiles of the spectral lines measured by means of Zeeman spectrometer, Fabry-Perot interferometer, Fourier transform spectrometer, using expressions of its instrumental function, as well as, in case when instrumental function is given as data array.

Tasks of this work

The tasks of this thesis are:

1. to develop the method of the restoring the real profile of the measured spectral lines based on Tikhonov regularizing algorithm;
2. to estimate the limits of credibility of the proposed model by means of model tasks solution;

3. to define the best approximation of the instrumental function of the Fourier transform spectrometer;

4. to develop the software for practical realization of this method for cases:

a) the spectral lines measured by means of Zeeman spectrometer (instrumental function is approximated by Gauss or Lorentz or Voigt function);

b) the spectral lines measured by means of Fabry-Perot interferometer (instrumental function is expressed by the Airy function);

c) the spectral lines measured by means of Fourier transform spectrometer (as instrumental function use defined in the task Nr.3 approximation);
d) the instrumental function is given as experimental data array

5. to validate the proposed method for the restoring the real line profiles from measured profiles, emitted from low temperature plasma sources and measured by different spectrometers:
a) Hg resonance 184.9nm line profile, 6^1P_1 -6^1S_0 transitions
b) Hg resonance 253.7 nm line profile, 6^3P_1 -6^1S_0 transitions
c) Hg visible triplet 7^3S_1-$6^3P_{0,1,2}$ transitions (with the wave lengths Hg 404,7 nm, 435.8 nm, 546.1 nm respectively) in magnetic field
d) Hg visible triple 7^3S_1-$6^3P_{0,1,2}$ transitions (with the wave lengths Hg 404,7 nm, 435.8 nm, 546.1 nm respectively) without magnetic field.

Preface

Assumed that low-temperature plasma is ionized gas with the mean energy(temperature) less then hydrogen ionization potential (13,53eV).The low-temperature plasma is viewed in case of high-frequency electrodeless lamp in this work.

Electrodeless discharge lamps are known as bright radiators of narrow and intensive spectral lines, covering the spectrum from vacuum-ultraviolet to infrared. The high-frequency electrodeless discharge lamps (HFEDLs) are widely used in different scientific devices such as radiation and absorption spectrometers, spectrometers for angle and glass refractive index measurements, and frequency standards, magnetometers **[1,2]** Novel type AA analysers are developed for detection of heavy metals, benzene, toluene and other pollutants in air, water and food in real time[**3**]. High selectivity and very low limits of detection depend on the quality of the emitted spectral line shapes.

For optimization and development of the HFEDLs it is necessary to make diagnostic. The diagnostic technique allows determinate the best source filling and operation regimes for each concrete application.

1. Actuality of this work

Line shape diagnostics is crucial in the cases when light sources with well-defined shapes of the emission lines are necessary.

Spectral line shapes are known as important tools for emission plasma diagnostics in different type of plasma since the form of the line is determined by the all plasma processes. However many processes act on the same time and it is not easy to resolve partial effects on the total line shape. In addition, the influence of the processes often correlates with each other. Also we have to take into account that spectral line shapes need to be registered by spectral apparatus which also has influence on the resulting line shape. Reconstructing the real line shape from the measured one is so called inverse ill-posed task since small uncertainties in the measurement give large deviations in solution. Since it is complicated task, sometimes the instrumental function is neglected. It can be done if the width of the instrumental function is much smaller than the real spectral line shape what in general is true in high temperatures and dense plasmas. However in the case of low –pressure or cold

plasma the instrumental function is on the same order that experimental profile and it has to be taken into account. As well known [**4]** the measured profile is the convolution of the real spectral line and instrumental function. The instrumental function can destroy the real spectral line shape significantly, for example, it changes the width of the spectral line that leads to the uncertainties in the determination of such important plasma parameters like temperature. The instrumental function can cover detailed structure of the spectral line, like the dip in the line centre caused by the self-absorption (self-reversal) and characterizing the radiation trapping. The Tikhonov's regularization algorithm is one of the most useful tools for solving the ill-posed inverse task. By minimizing the Tikhonov functional, we obtain correct inverse task instead of the incorrect, for the further solution by means of the classical methods.

Therefore, the Doctoral thesis is dedicated to develop the diagnostic technique of the low-temperature plasma that was tested and used for optimisation needs for special type of low pressure lamps HFEDLS for their application in atomic absorption spectrometers (AAS).

Diagnostic technique includes:

1. spectral line intensity measurements by means of :
   - Fabry-Perot interferometer,
   - Zeeman spectrometer,
   - Fourier transform spectrometer ;
2. subsequent model tasks ;
3. spectral line profile studies by means of solution of the ill-posed inverse tasks for real spectral lines shapes obtaining, using Tikhonov regularization.

2. Scientific novelty of this work

First time, in this thesis:

- The method is created for the solving of ill posed task for the spectral line shape deconvolution based on the Tikhonov algorithm, that was tested

and applied for case of real Hg spectral line profiles, emitted from special design microsize low-temperature plasma sources* :

- ✓ Hg resonance 184.9nm line profile, 6^1P_1 -6^1S_0 transitions
- ✓ Hg resonance 253.7 nm line profile, 6^3P_1 -6^1S_0 transitions
- ✓ Hg visible triple 7^3S_1-$6^3P_{0,1,2}$ transitions (with the wave lengths Hg 404,7 nm, 435.8 nm, 546.1 nm respectively) in magnetic field
- ✓ Hg visible triple 7^3S_1-$6^3P_{0,1,2}$ transitions (with the wave lengths Hg 404,7 nm, 435.8 nm, 546.1 nm respectively) without magnetic field.

• The software was developed for practical realization of the new method based on the Tikhonov algorithm in cases when Hg spectral line profiles were measured by means of:

- ✓ Zeeman spectrometer (instrumental function is approximated Gauss or Lorentz or Voigt function)
- ✓ Fabry-Perot interferometer (instrumental function is expressed by the Airy function)
- ✓ Fourier transform spectrometer (defined approximation of the instrumental function(see task Nr.2))
- ✓ the instrumental function is given as data array

**Microsize light sources manufactured at LU IAPS (Institute of Atomic Physics and Spectroscopy at University of Latvia)*

I. Literature review

1.Broadening and types of the spectral line profiles.

The line profile is the distribution of the spectral intensity within the spectral line. The maximum value of the line profile function is the peak intensity, and the broadening of the line profile is usually **[5]** represented by the width measured at half of the maximum of intensity. This line width, Δν, is also called - the full width at half maximum (FWHM). Sometimes in the literature also half of the width at the half of maximum (HWHM) is used.

In low-temperature plasma the major causes of the line broadening effects are the Doppler effect due to the heat motion of plasma particles, the natural and the collisional broadening and self-absorption.

1.1. Doppler profile

The broadening which originates from the heat motion of emitting atoms is called by Doppler broadening and can be described by means of the Doppler profile.

Distribution function of the brightness k(ν) of it is described by the following equation, called Gauss function:

$$k(\nu) = k_0 e^{-\beta c^2 (\nu - \nu_0/\nu_0)^2}, \tag{I.1}$$

where k_0-value of the distribution function of brightness at maximum, ν_0 – frequency at maximum and

$$\beta = \frac{\mu}{2RT}, \tag{I.2}$$

where μ- atomic mass; R- gas constant, T- absolute temperature of the emitting gas

The motion of atoms in accordance to the Maxwell law is isotropic in the space and thus the FWHM ($\Delta\nu_D$) corresponding to the Doppler effect is **[6]:**

$$\Delta\nu_D = \frac{2\nu_0}{c}\sqrt{\frac{\ln 2}{\beta}} = \frac{2\nu_0}{c}\sqrt{\frac{2\ln 2RT}{\mu}} \quad or \quad \Delta\nu_D = 7.16\times10^{-7}\nu_0\sqrt{\frac{T}{\mu}}\ . \tag{I.3}$$

where μ- atomic mass; R- gas constant, T- absolute temperature of the emitting atoms, c – speed of light.

Or in wavelength scale:

$$\Delta\lambda_D = \frac{2\lambda_0}{c}\sqrt{\frac{2\ln 2RT}{\mu}} \quad or \quad \Delta\lambda_D = 7.16\times10^{-7}\lambda_0\sqrt{\frac{T}{\mu}}\ . \tag{I.4}$$

Taking into account equation (1.3) the absolute temperature of the emitting gas atoms can be expressed in the following form**[6,7]**

$$T = \frac{\mu}{\left(7.16\times10^{-7}\nu_0\right)^2}\Delta\nu_D^2\ , \tag{I.5}$$

Taking into account (I.3) instead of expression (I.1) the distribution function of the brightness of Doppler profile (Fig.I.1) can be described by following equation:

$$k(\nu) = k_0 e^{-4\ln 2(\nu-\nu_0/\Delta\nu_D)^2}\ . \tag{I.6}$$

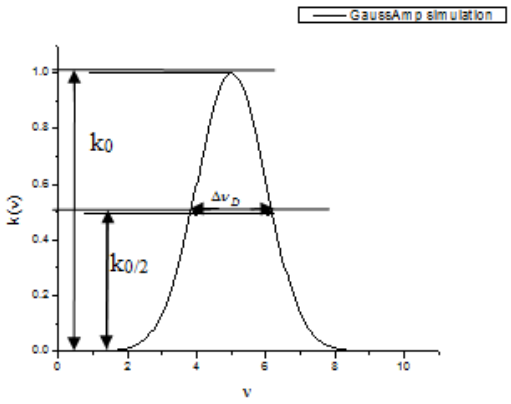

Fig. I.1. Doppler profile (expression I.6)

In the case of Doppler profile the self-absorption can be taken into account by the following expression, containing the Ladenburg-Levi function [**6**]:

$$A_G = \frac{1}{2}\sqrt{\frac{\pi}{\ln 2}} \cdot \Delta\nu_D \cdot \kappa_0 l \cdot S(\kappa_0 l) \qquad \text{(I.7)}$$

where

$\kappa_0 l$ – optical density;

l- optical way;

$S(\kappa_0 l)$ – Ladenburg –Levi function :

$$S(\kappa_0 l) = \frac{1}{\sqrt{\pi}\kappa_0 l}\int_{-\infty}^{\infty}\left(1 - e^{-\kappa_0 l \cdot e^{-\omega^2}}\right)d\omega = 1 - \frac{\kappa_0 l}{2!\sqrt{2}} + \frac{(\kappa_0 l)^2}{3!\sqrt{3}} + \cdots \qquad \text{(I.8)}$$

κ_0- the absorption coefficient in the centre of the line of the Doppler profile:

$$\kappa_0 = 2\sqrt{\frac{\ln 2}{\pi}} \cdot \frac{\pi e^2}{m_0 c} \cdot \frac{f_{ik}}{\Delta\nu_D} \cdot n_i \quad , \qquad \text{(I.9)}$$

where e and m_0 are charge and mass of an electron respectively, f_{ik}- oscillator strength, n_i- particle density, c – speed of light.

.

1.2 Lorentz profile.

Two main effects of the spectral line broadening can be described by means of Lorentz profile. These are: natural broadening and collisional broadening**[6]**.

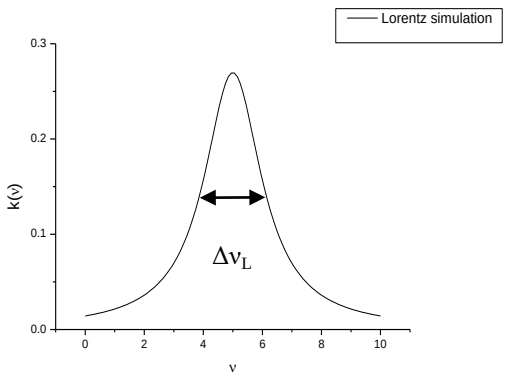

Fig.I.2 Lorentz profile

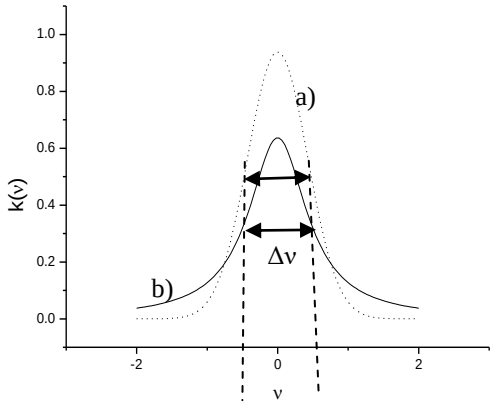

Fig.I.3 a)Doppler profile b)Lorentz profile; $\Delta\nu_D = \Delta\nu_L = \Delta\nu$

Distribution function of the brightness k(ν) of it is described by the following equation:

$$k(\nu) = k_0 \frac{(\gamma/2)^2}{4\pi^2(\nu-\nu_0)^2 + (\gamma/2)^2}, \qquad \text{(I.10)}$$

where γ –extinction coefficient.

Corresponding to the natural broadening, the extinction coefficient is:

$$\gamma = \gamma_k + \gamma_i = \frac{1}{\tau_k} + \frac{1}{\tau_i}, \qquad \text{(I.11)}$$

where: τ_k and τ_i – life times of the energy levels N_k and N_i (Fig.I.4) between which the transition occurs and radiation is emitted with frequency ν_{ki}.

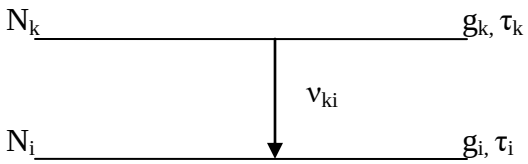

Fig. I.4 Energy levels scheme.

For given spectral line τ_k and τ_i are constants. Their connection with the transition probability A_{ki} is given by following expression:

$$\frac{1}{\tau_k} = \gamma_k = \sum_i A_{ki}, \tag{I.12}$$

and with strength of oscillator f_{ik} by:

$$\frac{1}{\tau_k} = \sum_i \frac{g_i}{g_k} \frac{8\pi^2 e^2 \nu_{ik}^2}{m_0 c^3} f_{ik}, \tag{I.13}$$

where g_i un g_k are the statistical weights; e and m_0 –electron charge and mass accordingly.

The FWHM corresponding to the natural broadening is:

$$\Delta\nu_L = \frac{\gamma_k + \gamma_i}{2\pi}. \tag{I.14}$$

Or in wavelength scale:

$$\Delta\lambda_L = \frac{\gamma\lambda_0^2}{2\pi c}. \tag{I.15}$$

In case of collisional broadening according to the kinetic theory of gases, the average time between two collisions is:

$$\frac{1}{\overline{\tau}_{collissional.}} = 4\sigma^2 N_0 \sqrt{\frac{\pi RT}{\mu}}\ , \qquad \text{(I.16)}$$

where N_0- number of the particles in the volume unit; σ^2 –effective cross section; μ- molecular weight.

Therefore the FWHM corresponding to the collisional broadening can be expressed by following equation:

$$\Delta\nu_L = 4\sigma^2 N_0 \sqrt{\frac{RT}{\pi\mu}} \qquad \text{(I.17)}$$

This broadening is also called pressure broadening, because its magnitude depends on the number of collisions, and therefore, on the pressure.

$$\Delta\nu_L = \frac{4\sigma^2 N_A p}{\sqrt{\pi\mu RT}} \qquad \text{(I.18)}$$

where p- pressure, N_A = 6,022 141 79(30)×10^{23} mol^{-1}(Avogadro's number).

Or in wavelength scale:

$$\Delta\lambda_L = \frac{4\sigma^2 N_A p\lambda_0^2}{c\sqrt{\pi\mu RT}} \approx 6.6*10^5 \frac{\sigma^2 p}{\sqrt{\mu T}}\lambda_0^2 \qquad \text{(I.19)}$$

The self absorption in case of Lorentz profile can be taken into account using following equation, containing the Ladenburg-Reihe function [**6**]:

$$A_G = \frac{\pi}{2}\cdot\Delta\nu_L\cdot\kappa_0 l\cdot S^{'}\left(\kappa_0 l\right) \qquad \text{(I.20)}$$

where

$\kappa_0 l$ – optical density;

l- optical way;

$S'(\kappa_0 l)$ – Ladenburg –Reihe function :

$$S(\kappa_0 l) = \left.\begin{array}{l} e^{-x}\left[I_0(ix) - iI_1(ix)\right], \\ x = \dfrac{\kappa_0 l}{2}. \end{array}\right\} \quad , \tag{I.21}$$

where $I_0(ix)$and $I_1(ix)$-Bessel functions of zero and first order:

$$\left.\begin{array}{l} I_0(ix) = \dfrac{1}{2\pi} \cdot \int\limits_{-\pi}^{\pi} e^{-x\cos y} dy; \\ I_1(ix) = \dfrac{1}{2\pi i} \cdot \int\limits_{-\pi}^{\pi} \cos y e^{-x\cos y} dy. \end{array}\right\} \quad , \tag{I.22}$$

κ_0- the absorption coefficient in the centre of the line of the Lorentz profile:

$$\kappa_0 = \frac{2e^2}{m_0 c} \cdot \frac{f_{ik}}{\Delta\nu_L} \cdot n_i \quad , \tag{I.23}$$

where e and m_0 are charge and mass of an electron respectively, f_{ik}- oscillator strength, n_i- particle density, c – speed of light.

1.3. Voigt profile.

In case when the spectral line profile broadening originates due to the Doppler effect and collisional broadening together, the shape of the spectral line can be described by the Voigt profile**[8,9,10].**

This profile is the convolution of the Doppler and Lorentz profiles.

Distribution function of the brightness k(ν) of it is described by the following equation:

$$k(\nu) = k_0 \frac{a}{\pi} \int\limits_{-\infty}^{+\infty} \frac{e^{-y^2} dy}{a^2 + (\omega - y)^2}, \tag{I.24}$$

where

$$\omega = \frac{2\sqrt{\ln 2}\left(\nu - \nu_0\right)}{\Delta\nu_D}; \tag{I.25}$$

$$a = \frac{\Delta\nu_L}{\Delta\nu_D}\sqrt{\ln 2}; \tag{I.26}$$

y- constant of integration

The shape of Voigt profile depends on *a*, on ratio of the widths of the Lorentz and Doppler profiles.

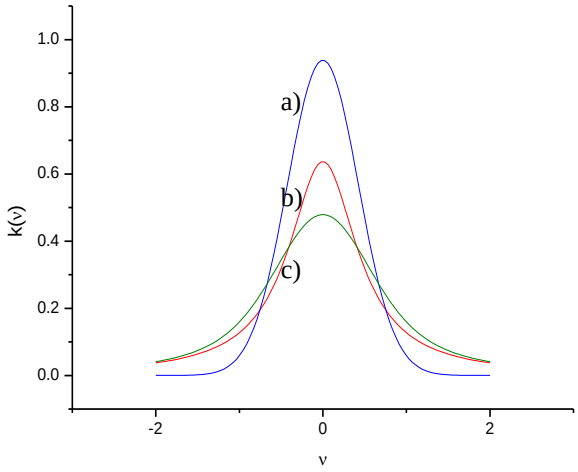

Fig.I.5 a)Doppler profile (blue line); b)Lorentz profile(red line);c) Voigt profile (green line); $\Delta\nu_D$=$\Delta\nu_L$=1 ($\Delta\nu_D$= 0,85; $\Delta\nu_L$=1 - simulation in Origin)

The self absorption in case of Voigt profile can be taken into account using following equation

$$A_G = \frac{e}{\sqrt{m_0 c}} \cdot \sqrt{f_{ik}\gamma_{ik}\ell\, n_i} \quad , \tag{I.27}$$

where: e and m_0 are charge and mass of an electron respectively, f_{ik}- oscillator strength, l- optical way, n_i-particle density, γ_{ik} extinction coefficient.

2. Spectral apparatus for registration of spectral line profiles.

2.1.High-resolution scanning Fabry-Perot interferometer

The standard way to measure line profiles is by means of a high-resolution scanning Fabry–Perot interferometer [**11].**

The experimental set-up is shown in Fig.I.6.

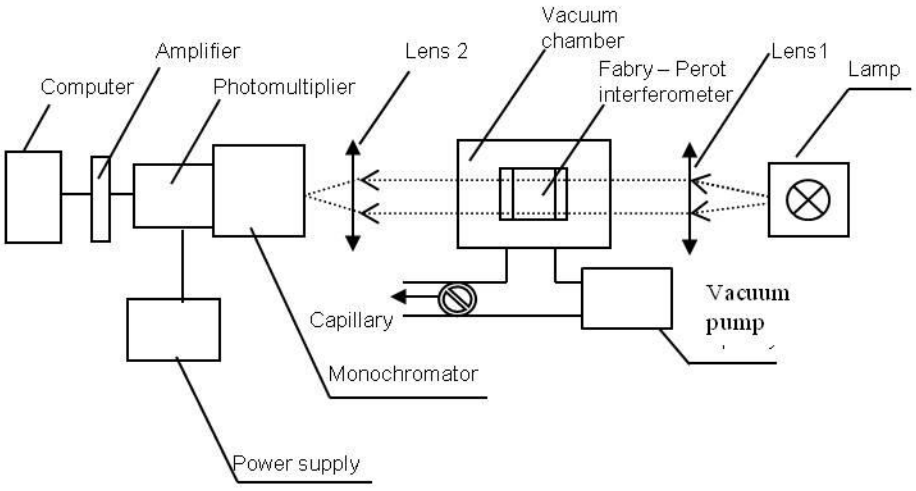

Fig.I.6. High-resolution scanning Fabry-Perot interferometer

The working principles of the interferometer are following: the radiation from the Hg light source, which is placed in focus of lens 1 (Fig.I.6), as parallel sheaf falls on Fabry - Perot interferometer. Interferometer is placed in a vacuum chamber. The air to the chamber is given gradually through the capillaries. Lens 2 focuses the picture of the interference on the circular diaphragm, which is placed in the place of the entrances gap of the monochromator. Light stream changes are registered with the photomultiplier and the results are saved in the computer.

The Fabry – Perot interferometer is characterized with a free spectral range. It is an interval of the frequencies, which corresponds to the distance between two next peaks:

$$\sigma = \frac{1}{2t}\left(cm^{-1}\right) \tag{I.28}$$

The condition of an appearance of the maximums of the interference is following:

$$2tn\cos\varphi = k\lambda \tag{I.29}$$

where:

t- distance between the mirrors of the interferometer ;

n- coefficient of the refraction of the environment

φ- angle of falling rays

k- order of the interference;

λ- wavelength of falling light.

2.1.1 Instrumental function for the Fabry - Perot interferometer

The instrumental function of the Fabry - Perot interferometer is described by the Airy function **[12]**:

$$A(\nu) = A_{\max}\frac{1}{1+\frac{4r}{(1-r)^2}\sin^2\frac{\delta}{2}} \quad , \tag{I.30}$$

where:

$$\delta = \frac{2\pi\Delta}{\lambda}$$

Δ – difference of the optical ways

r- an effective refraction coefficient of the mirrors.

2.2. Zeeman spectrometer

The type of spectrometer based on application of the Zeeman effect, so-called Zeeman spectrometer, offers and advantages of a simple experimental set-up [**13,14**]

The experimental set-up of the Zeeman spectrometer is shown in Fig.I.7.

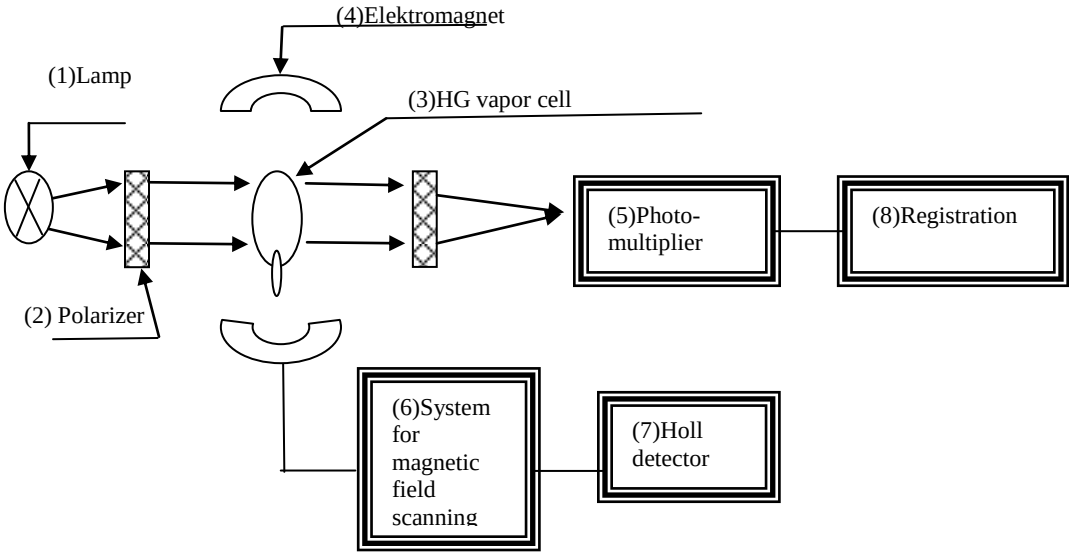

Fig.I.7. Experimental set-up of Zeeman spectrometer

The working principles of spectrometer are following: radiation from the Hg light source (1) passes through a polarizer (2), where it has been separated into σ+ and σ- components. After that, in order to use the Zeeman scanning for the analysis of emission lines, one component has to traverse the same metal vapour cell(3). The mercury absorption line is separated due longitudinal Zeeman effect in the magnetic field of the electromagnet(4). The separation is proportional to intensity of magnetic field:

$$\Delta\nu = \frac{1}{4\pi c}\frac{e}{m}\vec{H}. \qquad \text{(I.31)}$$

Or, in wavelength scale:

$$\Delta\lambda = \frac{1}{4\pi c^2}\left(\frac{e}{m}\right)\lambda^2\vec{H}. \qquad \text{(I.32)}$$

By scanning of the magnetic field intensity using block (6), the distance between the separated lines is changing as shown in formula (I.32). When absorption line of Hg cell coincidences with the radiation line, emitted from the lamp, the level of lighting of photodetector (5) gets low. It allows registering the spectra of investigated lamp. The Holl detector (7) is applied for the scale obtaining.

The advantage of Zeeman spectrometer in comparison with commonly used Fabry-Perot interferometer is quite narrow instrumental function. Due to it, this type of spectrometers has been used to study absorption line profiles.

2.2.1 Instrumental function for the Zeeman spectrometer

For the Zeeman spectrometer, the instrumental function is the absorption spectral line profile, determined by the Doppler broadening for vapour temperature in the absorption cell and collisional broadening described by a Lorentz function. Therefore the approximation by Gauss, Lorentz and Voigt functions were used in this work(see in chapter I).

2.3 Fourier transform spectrometer

A Fourier transform spectrometer is basically a Michelson interferometer **[15, 16]**
The beamsplitter(1) divides an incoming light beam(2) in two parts. The first part is reflected on a fixed mirror(3) whereas the second part is reflected on a mobile mirror(4). The two beams are recombined at the beamsplitter and shone on a detector(5). The principal scheme is shown below (Fig.I.8). The detector registers the interferogram- the intensity of exiting light beam dependence on optical path difference. The interferogram contains complete information of the spectral composition of the incoming light beam. Signal of the sum of cosine waves is expressed by following equation:

$$I(x) = \int_{-\infty}^{\infty} B(\nu)\cos(2\pi x\nu)d\nu, \quad , \tag{I.33}$$

where: *I(x)*- intensity of light, *x*- shift of mobile mirror(4) in cm, $B(\nu)$ - intensity of source as function of wave number ν in cm^{-1}.

Then Fourier-transform converts the interferogram (1.33) into the spectrum:

$$B(\nu) = \int_{-\infty}^{\infty} I(x)\cos(2\pi x\nu)dx, \quad , \tag{I.34}$$

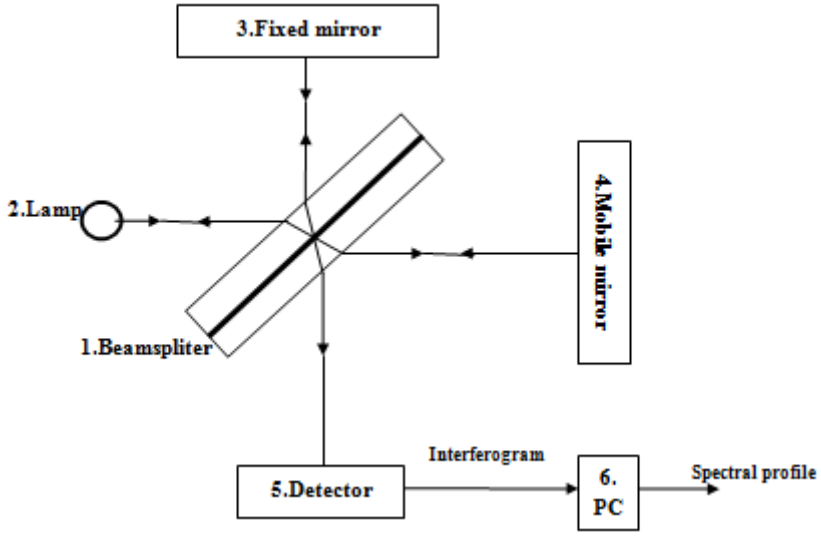

Fig.I.8: Scheme of Fourier transform spectrometer as a Michelson interferometer.

Fourier transforms are inverse integral conversions: the spectrum- is the Fourier image of the interferogram on cosines, and the interferogram - is the Fourier image of spectrum on cosines.

2.3.1. Instrumental function for Fourier transform spectrometer

Usually, as instrumental function for Fourier transform spectrometer use experimentally measured He spectral line of 632.8 nm wavelength emitted from the single mode He/Ne laser.

The function, which is known as sinc(x) function can be used too. **[12]**:

$$I(x) = 2L \bmod \left\{\operatorname{sinc}\left[2\pi(x_0 - x)L\right]\right\} \quad , \tag{I.35}$$

where L- difference between two optical path lengths (optical path difference).

3. High-frequency electrodeless discharge lamps (HF EDLs)

Because of high intensity, the HFEDLs are exploited as intensive emission spectra sources in scientific experiments, such as double-resonance experiments, sensitized fluorescence experiments, shifts and broadening of spectral lines. A discharge in the lamp is excited by means of electrodes, which are located outside the lamp. The electrodeless lamps, in principle, can be excited by four discharge mechanisms i.e. inductive or H-discharges [**17**], capacitive or E-discharges **[18,2**], microwave discharges and travelling wave discharges (e.g. SWDs)[**19].**

In this thesis will be observed HFEDLs excited by two of them: H and E-discharges. HF electrodeless discharge excitation by means of H and E-discharges was realized in the 1930. The excitation mechanisms of both discharge types are different. The E-discharge is excited by the scalar electric field (the force lines of the electrical field are not closed) and the H-discharge by the induced electric field associated
with the HF magnetic field (this field has circular force lines). The E-discharge is characterized by easier excitation over a wider range of power and pressure than the H-discharge.

3.1. HF EDLs working principle

The schematic diagram of a HFEDL is shown in Fig. I.9 [**20,21].** The HFEDL vessel is made of glass or quartz and filled with a working element and a buffer gas (usually a noble gas with approximately 2Torr). The lamp contains a bulb (1) and a short side arm containing the working element (2). The lamp bulb is located in a HF generator(approximately 100MHz) coil (3) to induce an inductively coupled electrodeless discharge. The side arm can be thermostatted (4) to control the pressure of the metal

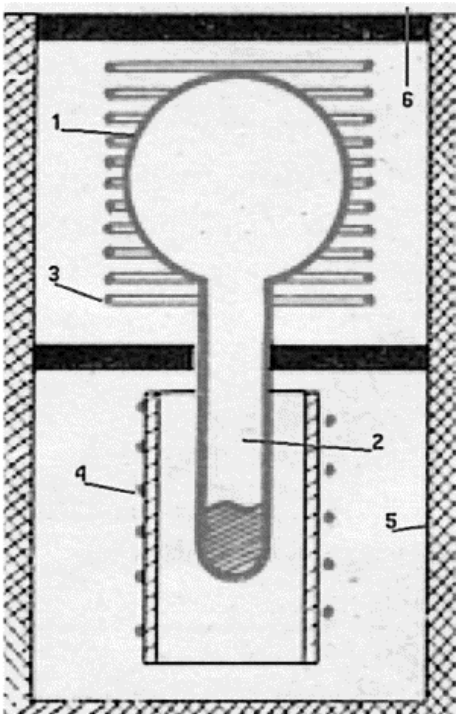

Fig. I.9 Schematic diagram of a HFEDL.

vapour in the lamp. The lamp is thermally insulated with glass or ceramic to maintain a higher temperature around the lamp vessel (5).

The radiation from the lamp is transmitted through a window (6).

The lamps can be manufactured in different forms to suit specific applications. In Fig.I.10 spherical, cylindrical, dumbbell and capillary electrodeless lamp examples are shown[**22].** Dumbbell form like lamp consists of three parts: (i) spherical; (ii) capillary; (iii) cylindrical.

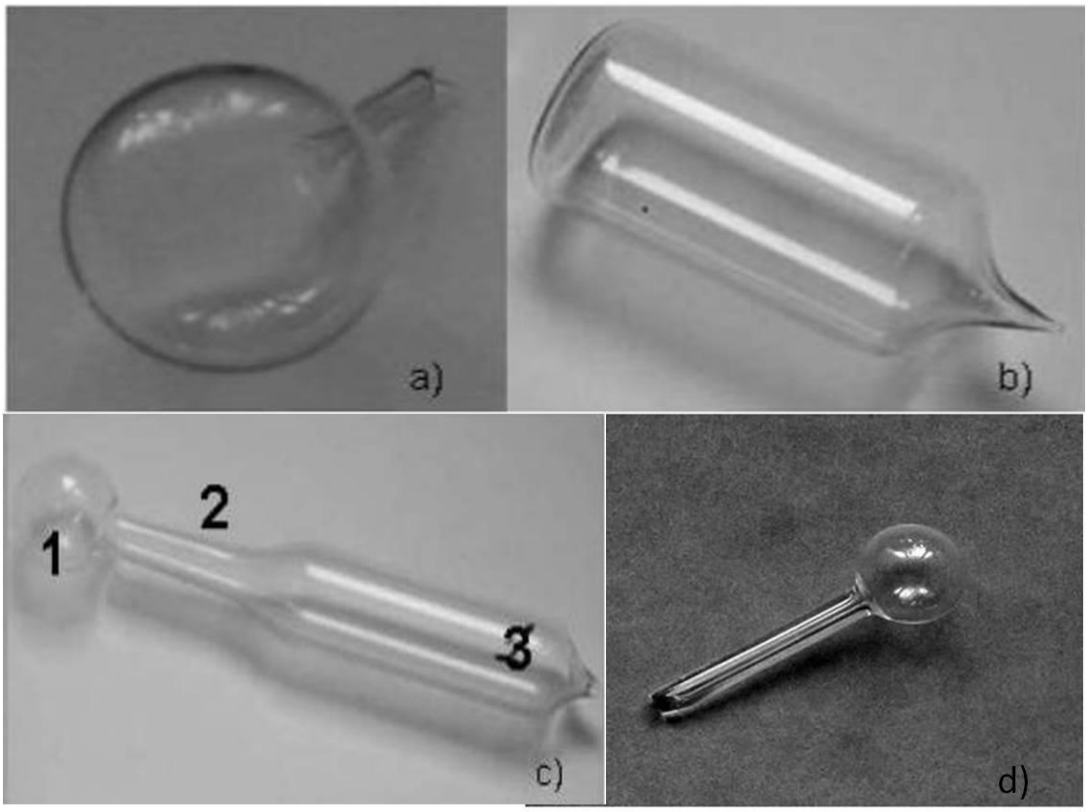

Fig. I.10 Some possible forms of HFELs: a) spherical; b) cylindrical; c) dumbbell; d) capillary. Dumbbell like form lamp consists of three parts: 1) spherical; 2) capillary; 3) cylindrical.

The dumbbell form like (Fig. I.10(c)) and capillary(Fig. I.10(d)) lamps were investigated in this work. The radius of spherical part of dumbbell like lamp(Fig. I.10(c)) is 10mm, and radius of capillary part is 2mm.The length of the capillary of lamp (I.10(d)) is of 2 cm and the discharge size was of 500μm in radius.

3.2. Mercury HFEDLs

Hg HFEDLs have found successful application in food and environment analysis, surgery UV- illumination, optical magnitometry, isotope separation etc. This thesis is connected with investigation of the HFEDLs filled with mercury, both, with natural mixture and separate isotopes

Natural mercury contains 7 stable isotopes (196,198,199,200,201,202,204) and it causes quite complicated spectral line structure. For example, widely used line of 253.7nm (level structure see in **Appendix 6**) wavelength has 5 summary components of similar intensity due to isotope and hyperfine-structure shifts. Zeeman spectrogram of natural mercury resonance line is shown in Fig.I.11 **[Pr.3]**

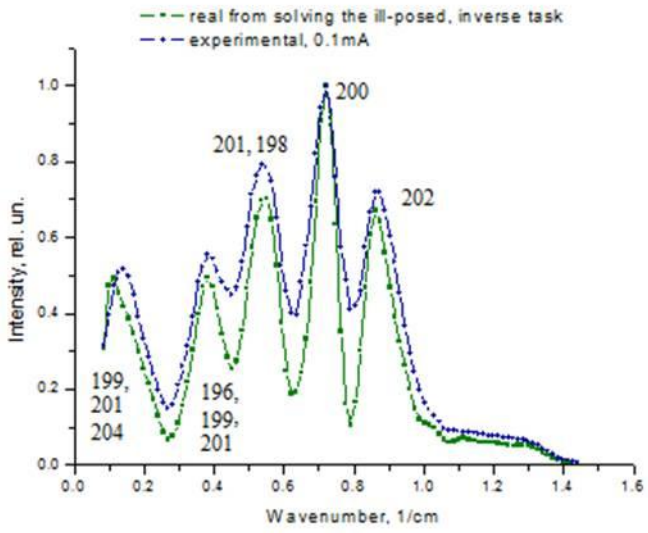

Fig.I.11 measured 253,7 nm line profiles emitted from HFEDL filled with natural mixture

Careful investigation of the spectral line profiles can give information about such plasma parameters as temperature, concentration and distribution of the emitting and absorbing atoms, optical density, collisional parameters.

Information about mercury 253.7 and 184.9 nm resonance lines is also important in fluorescent lamp technology where mercury/argon discharge is used.

Data about 184.9 nm resonance line structure in dependence on the cold spot temperature can be used not only for the lamp diagnostics but also for the validation of

different type of calculations and models, considering radiation trapping [**23,24**]. The radiation trapping effect plays an important role in light source devices using resonance radiation and it is important for the calculation of radiation efficiency and luminous output.

4. Inverse ill-posed tasks

Inverse tasks [**25,26,27**] frequently encountered in various fields of science: spectroscopy[**28,29,30**], computer tomography [**31,32**], image's processing[**33,34],** signal's recovery**[35,36],** geophysics[**37,38**], astrophysics [**39**], plazma diagnostics[**40**]. These tasks always are incorrect**[41,42,43].**The properties of the well posed problems [**44,45]:**

1. Existence of the solution.
2. Uniqueness of the solution.
3. Continuous dependence of the solution on the data.

The problem is ill posed, if, at least, one of properties is not satisfied. In case of inverse tasks the third condition is wrong: small experimental uncertainties can cause large deviations in the solution.

4.1. Ill-posed tasks in the spectroscopy

The measured (experimental) spectral line $f(\nu)$ is a convolution of the real line profile $y\left(\nu^{'}\right)$of the emitted spectral line and instrumental function $A\left(\nu,\nu^{'}\right)$ It can be described by Fredholm integral equation of the first kind **[3,46]:**

$$\int_a^b A(\nu,\nu^{'})y(\nu^{'})d\nu^{'} = f(\nu), \quad c \le \nu \le d, \tag{I.36}$$

where: a, b and c, d the limits of the real and measured (experimental) profiles accordingly. Usually they are chosen such, that a=c and b=d.

In general the problem (I.36) can be written as an operator equation:

$$Ay = f \quad , \tag{I.37}$$

which connects the function $f \in G_2$, in our case the measured spectral profile at frequencies ν with unknown function $y \in G_1$ - in our case the real profile and A^* – the continuous operator, with domain of values - G_2 and definition domain - G_1.

$G_1$and G_2 are some metric spaces. Formally, the solution of the equation (I.36) can be written:

$$y = A^{-1} f \quad , \tag{I.38}$$

where A^{-1} – the inverse operator .

But, according Hadamard [**47**], an inverse problem is well - posed, if the solution:

1) exists for any $f \in G_2$

2) is only one in G_1 ;

3) continuously depends from $f \in G_2$ i.e. the solution must be stable against the changes of the right side part.

For our case, the third condition is wrong, because small experimental uncertainties can cause large deviations in the solution. Therefore Eq.I.38 is wrong in this case.

The task of obtaining of the real spectral line is called by reduction to the ideal device or the classic Rayleigh reduction problem, in spectroscopy.

There are some special methods of the real line profile $y(\nu')$ obtaining, because the direct solution of Eq.I.36 is impossible.

5. Methods of the real shape of the spectral line obtaining

In general, for obtaining the real shape of the spectral line, two main direction of solution exist: there are modelling **[48**] of the spectral line profiles and the real shape obtaining by means of ill-posed inverse task solution.

The theories of the solution of the ill-posed problems are reviewed and compared in the literature. For example: iterative methods of regularization have been discussed in

[**49,50, 51**,**52**]**.** The quasi-solutions method by Ivanov [**46, 52, 53],** cross validation method **[54],**

Fourier transform[**55,56,57**], as well Tikhonov regularization method[**46,47,52, 53,57,58,59,60, 61,62, 63**] and the methods where the statistical (or probabilistic) approach is used- the statistical regularization methods in [**52,57,46,64,65,66**] .

Taking into account, realization time, stability and accuracy of solution, quantity of addition information, we can see that the Tikhonov regularization algorithm is one of the more effective methods of ill-posed inverse task solution. Using minimum of the *a priori* information, we get stable, accurate solution of the inverse ill-posed task.

The calculation were performed using Tikhonov regularization algorithm and compared with results obtained by means of a non-linear multi-parameter chi-square fit[**48**] in this work.

The main ideas of these methods are written below.

5.1. Modeling of the spectral line profiles

The mathematical model is described in the paper [**48**] in detail. This model includes the basic factors causing the spectral line broadening in a low-pressure discharge: natural, Doppler, resonance and collisional. These effects are accounted by means of the Voigt profile which is a convolution of the Doppler and Lorentz profiles. Normally, the Doppler width $\Delta\nu_{D,}$ and Lorentz width, $\Delta\nu_{L,}$ are used as the parameters characterizing the Voigt profile.

For a quantitative description of self-absorption, the approximations of the radiation source are used: i) the approximation of a uniformly excited source; ii) source with spatially separated emitting and absorbing atoms; iii) model suggested by Cowan and Dieke **[67,68**]:

$$I\left(\nu-\nu_0\right)=I_0P\left(\nu-\nu_0\right)e^{-\mu}\sum_{j=0}^{\infty}\frac{n!\mu^{2j}}{\left(2j+n\right)!}\ , \qquad \text{(I.39)}$$

where *n* is the integer characterizing the homogeneity of the radiation source and

$$\mu = \kappa_0 l \frac{P(\nu - \nu_0)}{P(0)} \ , \qquad \text{(I.40)}$$

where $P(\nu-\nu_0)$ is the line profile of radiation in a unity volume, $k_o l$ is the optical density at the centre of the line.

The resulting profile is a convolution of the self-absorbed Voigt profile and the instrumental function.

The real spectral line profiles, estimated using described above method, were used for the comparison with the results obtained by means of Tikhonov regularization method. Below are mentioned some advantages and disadvantages of the both methods.

The disadvantage of the line profile modelling method is that the functions of the line profiles have to be known before and we can apply it manly for the symmetric lines. For the using the Tikhonov's regularization method, the only parameter what we have to know is the instrumental function. The advantage of the modelling is that we can it apply also for the fit of the width of the instrumental function if the type of the instrumental function is known.

5.2. Tikhonov regularization method

Tikhonov's regularization algorithm is one of the most useful tools for solving the task where small experimental uncertainties can cause large deviations in the solution [**63, 69,[P1]].**

Tikhonov proved that an initial, ill-posed task(Eq.I.36) can be transformed to a task of the minimum searching[**70**] of the smoothing functional:

$$M_\alpha\left[y, \tilde{f}\right] = \inf_{y \in Y} M_\alpha\left[y, \tilde{f}\right], \qquad \text{(I.41)}$$

Assuming, that values of the right side and kernel of integral equation (I.36) are known with accuracy:

$$\left.\begin{aligned} \left\| \tilde{f} - f \right\|_F \le \delta; \\ \left\| \tilde{A} - A \right\| \le \xi \end{aligned}\right\} \tag{I.42}$$

where δ is error of right part of (I.36) or error of experimental $f(\nu)$ profile , ξ is error of kernel of (I.36) or error of instrumental function $A\left(\nu,\nu'\right)$.

Smoothing functional $M_\alpha\left[y,\tilde{f}\right]$ so called Tikhonov's functional, is given in form:

$$M_\alpha\left[y,\tilde{f}\right] = \left\|\tilde{A}y - \tilde{f}\right\|_F^2 + \alpha\Omega[y], \tag{I.43}$$

where $\alpha > 0$ -regularization's parameter; number-$\left\|\tilde{A}y - \tilde{f}\right\|_F^2$ - discrepancy.

Stabilizing functional Ω is described by following expression:

$$\Omega[y] = \|y\|_Y^2 \tag{I.44}$$

As the result of minimization of functional(I.43) [**71**] in case when $y \in W_2^1$ and $\tilde{f} \in L_2$ and taking into account norm definitions in these spaces:

$$\left.\begin{aligned} \|y\|_{W_2^1} = \sqrt{\int_a^b y^2\left(\nu'\right)d\nu' + \int_a^b \left(y'\left(\nu'\right)\right)^2 d\nu'} \\ \left\|\tilde{f}\right\|_{L_2} = \sqrt{\int_c^d \tilde{f}^{\,2}(\nu)d\nu} \end{aligned}\right\} \tag{I.45}$$

instead of ill-posed first kind integral equation (I.36), we get the second kind integral equation:

$$\alpha\left(y_\alpha(t) - q y_\alpha''(t)\right) + \int_a^b k\left(t,\nu'\right) y_\alpha\left(\nu'\right)d\nu' = F(t) \quad t \in [a,b], \tag{I.46}$$

where:

$$k\left(t,\nu^{'}\right)=k\left(\nu^{'},t\right)=\int_{c}^{d}\tilde{A}\left(\nu,t\right)\tilde{A}\left(\nu,\nu^{'}\right)d\nu;$$
$$F\left(t\right)=\int_{c}^{d}\tilde{A}\left(\nu,t\right)\tilde{f}\left(\nu\right)d\nu. \qquad \text{(I.47)}$$

Changed integrals in (I.46) to finite sums we obtain the system of lineal equations:

$$\sum_{i=1}^{N}b_i\left(\sum_{m=1}^{N}b_m\tilde{A}_{mk}\tilde{A}_{mi}\right)y_i+\alpha y_k=\sum_{m=1}^{N}b_m\tilde{A}_{mk}\tilde{f}_m,\quad k=\overline{1,N} \qquad \text{(I.48)}$$

or matrix equation

$$\left(\tilde{A}^{*}\tilde{A}+\alpha E\right)Y=\tilde{A}^{*}\tilde{f} \qquad \text{(I.49)}$$

where, где A_{ij} – elements of N xN size matrix A, which approximates kernel $K(x,x')$; f_i – vectors– column with initial dates ; y_i –vector – column of solution, b_i.- the coefficients of quadrature formula .

6. Methods of the parameter of regularization determination

Choosing of the regularization parameter α, which establishes the correspondence between the requirement of the stability of solution and reliability of the solution, is the main difficulty of the regularization methods applying in practice. The finding of the regularisation parameter is crucial for all regularisation methods. The inaccurate determination of the regularization parameter leads to major errors in the solution.

For it obtaining were developed some methods **[57,72,73,74,75]** There are discrepancy, cross-validation, asymptotical, maximum of probability, modeling or model tasks, selection etc methods. Some authors use the quasi optimally criterion**[76]** and adaptive discretization method**[77]** also.

For obtaining the optimal regularization parameter two independent methods were used in this work. There are: i) method of the discrepancy minimization **[52,78]** combined with method of selection**[46]** and ii) method proposed by Kojdecky in work **[79].**

6.1 Combination of the minimization of the discrepancy and selection methods

The regularization parameter α was determined using method of the minimization of the discrepancy [**52**]:

$$\left\| \tilde{A}y_\alpha - \tilde{f} \right\|_{L_2}^2 = \min_\alpha \left\| \tilde{A}y_\alpha - \tilde{f} \right\|_{L_2}^2 , \qquad \text{(I.50)}$$

where, according equation (I.43): measured (experimental) spectral line profile $\tilde{f}(\nu)$, real line profile $y\left(\nu^{'}\right)$, instrumental function $\tilde{A}\left(\nu,\nu^{'}\right)$.

The main idea of this method is: the *a* is taken to satisfy to Eq.(I.50) . Where, L_2 – space of square integrable functions. The norm definition in this space, we can see above, in (I.45)

The initial value of *a* , for further solution, was chosen according the selection method [**46**]. The main idea of this method is to find the value of y_α for reliable values of *a.* The final choice is based on priory information about solution, basically visually.

6.2 Kojdecki method

The regularization parameter was obtained by another independed method for the reliability of the results. This method is based on the knowledge of the errors of experimental data- δ and ξ - error of kernel of equation (I.36) accordingly.

According method proposed by Kojdecki [**79**], regularization parameter α is root of equation:

$$\alpha^q \left\| \tilde{A}^* \tilde{A} y_\alpha - \tilde{A}^* \tilde{f} \right\| = \beta \, \| \tilde{A} \| \left(\xi + \eta \left\| y_\alpha \right\| \right) \qquad \text{(I.51)}$$

or assumed matrix equation(I.49):

$$\alpha^{q+1} \left\| y_\alpha \right\| = \beta \, \| \tilde{A} \| \left(\delta + \xi \left\| y_\alpha \right\| \right) \qquad \text{(I.52)}$$

.

In this work α was obtained from (I.52) in supposition, that error of kernel, in cases when instrumental function was given by formula, is equal of zero, (ξ=0). The coefficients were chosen as q=0 and β=1.

II. Work methods and results

Introduction

The investigation of the mercury electrodeless lamps of different form was performed in this work. The lamps for the investigation were manufactured at the LU Institute of Atomic Physics and Spectrsocopy. The investigation consists of : 1) model profile separating from instrumental function by means of ill-posed tasks solution; 2)measurements, 3) measured spectral line profiles form recovery by means of ill-posed inverse tasks solution; 4)following analysis and comparison with results obtained by another independent method.

For practical realization of solution of ill-posed problem, for the real spectral line profiles reconstruction the following software were developed.

The main program was written in MathCad13[**80,81],** [**Appendix1**]. The program [**82,83,84**] [**Appendix2**] in Delphi 7 was developed for checking of the reliability of the results, obtained by first program, also. The another numerical algorithms **[85,86]** were used for regularization parameter obtaining. The numerical algorithm of conjugate gradient was used in Math Cad and numerical algorithm of Brent and dichotomy method were used in Delphi. Regularization parameter α is determined by using minimization of the discrepancy (Eq. I.50)(realization in MathCad) and method, when α is root of equation I.52 (realization in MathCad; Delphi). All calculations in this work were performed for zero order of regularization (q=0). The mathematical model is described in [parts: 4.1; 5.2; 6]

Both programs, for the real form of the spectral line profile obtaining, operating principal is shown in the block scheme (B.s.1) which can be seen bellow.

The input of the data and it interpolation must be done on the first stage of the numerical solution for both, the instrumental function and experimental data. As well, the instrumental function can be set, as equation and as experimental data array.

After it, according to the mathematical model (Eq.I.36; Eq.I.41-Eq.I.49) instead of initial ill posed problem we get the well posed task, which can be written as system of linear equation(was used trapezium formula) and solved by Gauss method.

On the next steps the value of the parameter of the regularization was obtained and used for the finite solution getting. The results can be saved for future analyzing, as data array or/and graph.

B.s.1. Block scheme of programs of ill-posed inverse task solution.

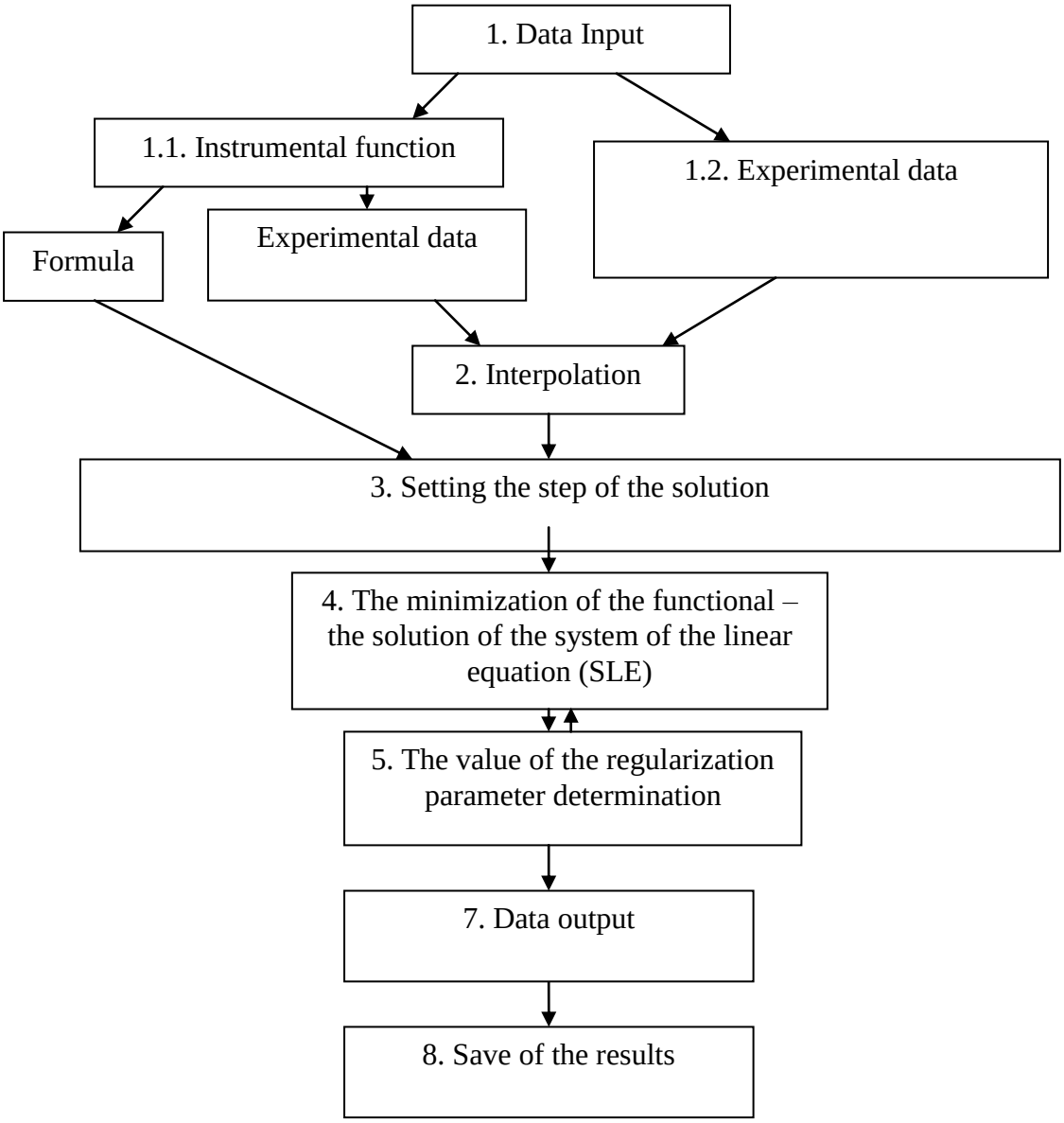

The supporting programs for temperature and FWHM estimation (Delphi)[**Appendix3**], self-absorption estimation (MathCAD) [**Appendix4**] were developed also.

1. Model tasks [Pr.2] ,[Pr.7] ,[A.2], [A.3], [A8]

The reliability of the solution method using Tikhonov regularization algorithm was verified by means of solving model tasks. The test was performed in three stages. First of all several "real profiles" were generated using non-linear multi-parameter modeling with different values of the variable parameters: Doppler broadening, Δ_D, Lorentz broadening, Δ_L, optical density in the line centre, $k_o l$, homogeneity of the radiation source, n. Thus the "real profiles" – the self-absorbed Voigt profile and Voigt profile without self absorption are created. The values of the parameters were chosen so, that the 'experimental' model profiles were maximally close to real spectral profiles, emitted from microsizes light sources. The "experimental profiles" are generated performing a convolution of these "real profiles" with the instrumental function (Gauss or Airy function) with a given value of the full width at half of maximum- FWHM (Δ_{Instr}) . At the end the several sets of "experimental" errors with different variances were generated and overlapped.

In the second stage, the real profiles deconvoluted from the instrumental function by means of solution of ill-posed inverse problem, were obtained.

In the third stage, the deconvoluted real profiles were compared with the initial "experimental profiles". The influences to result were observed for:

1) different ratio of FWHM of 'instrumental function' and FWHM of 'experimental' model profile

2) FWHM and kind of instrumental function,

3) values of the variance of the "experimental" errors,

4) method of estimation of the regularization parameter ,

5) numerical algorithm,

.

Below we can see the examples of the calculations. On the Fig.II.1- FigII.3 we can see comparisons between "modeled -real" profile and "calculated- real" profiles with self

absorption. "Modeled -real" profile was generated with following parameters: Doppler width (FWHM), $\Delta\nu_D$=0.03cm^{-1}, and Lorentz width, $\Delta\nu_L$=0.01cm^{-1}, instrumental function, Gauss profile, $\Delta\nu_{Instr.}$=0.06cm^{-1}, optical density in the line centre, $k_o l$=4, homogeneity of the radiation source, n=13. The "experimental" errors were: variance1=0.01(Fig.II.1), variance2=0.02,(Fig II.2) variance3=0.05(Fig. II.3) accordingly .

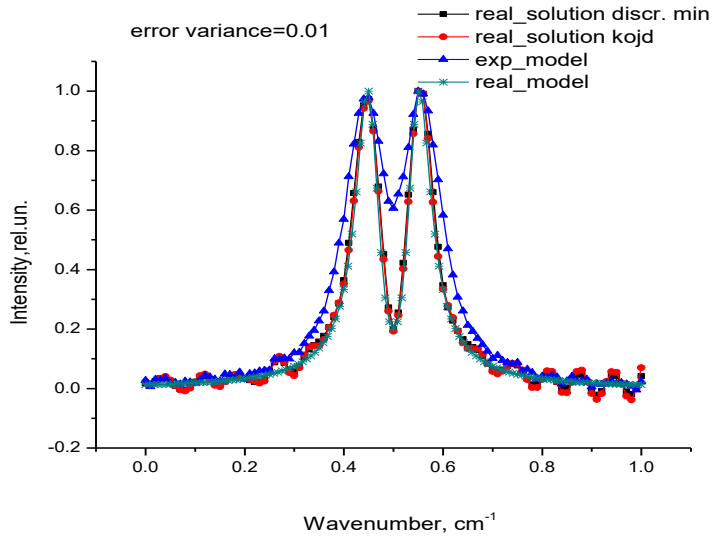

Figure II. 1. Comparison between "Real modeled" profile: modeled by means of non-linear multi-parameter modelling (green line) and "Real solution" profiles: obtained by means of solution ill-posed inverse problem(regularization parameter was obtained:1) from Eq.I.50(black line); 2) from Eq.I.52(red line)). "Experimental" errors-variance 0.01.

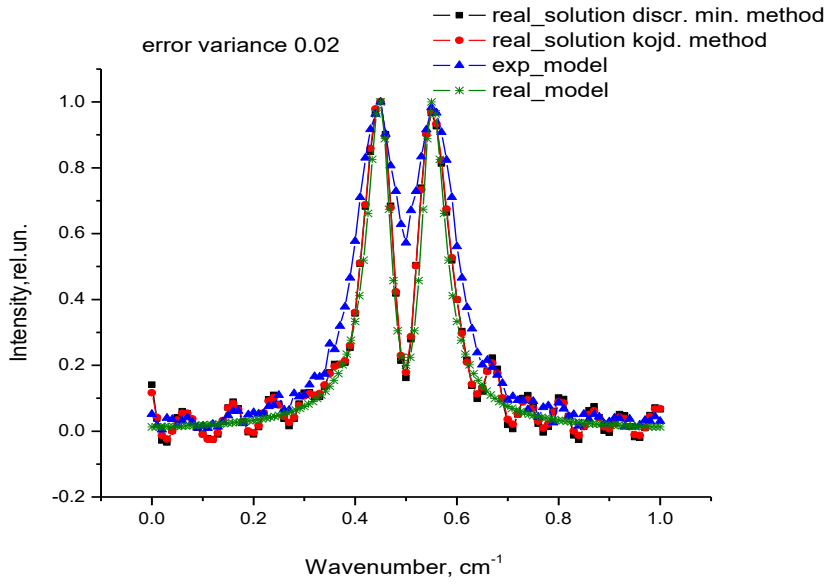

Figure II. 2. Comparison between "Real modeled" profile : modeled by means of non-linear multi-parameter modeling(green line) and "Real solution" profile: obtained by means of solution ill-posed inverse problem(regularization parameter was obtained:1) from Eq.I.50(black line); 2) from Eq.I.52(red line)). "Experimental" errors-variance 0.02.

Two independent methods were used to obtain regularization parameter: 1 method- discrepancy minimization method(Eq.I.50), 2 method- using equation (I.52) .

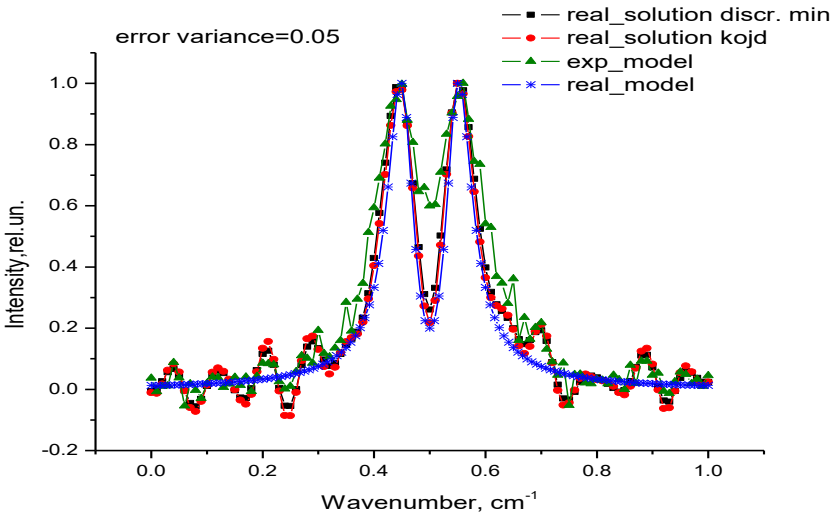

Figure II.3. Comparison between "Real modeled" profile : modeled by means of non-linear multi-parameter modeling(blue line) and "Real solution" profile: obtained by means of solution ill-posed inverse problem(regularization parameter was obtained:1) from Eq.I.50(black line); 2) from Eq.I.52(red line)). "Experimental" errors-variance 0.05.

On the Figs. II.4 - II.7 we can see comparisons between "modeled -real" profile and "calculated- real" profiles without self absorption.

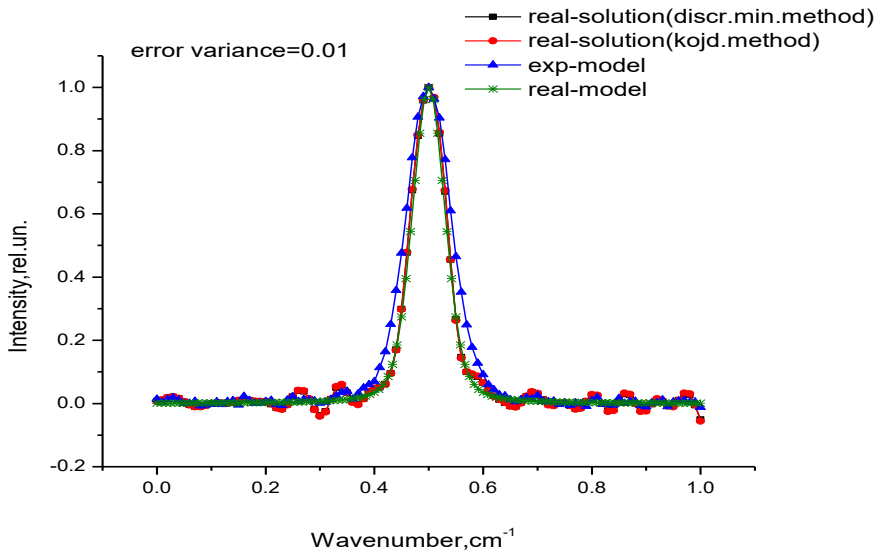

Figure II. 4 Comparison between "Real modeled" profile : modeled by means of non-linear multi-parameter modeling(green line) and "Real solution" profile: obtained by means of solution ill-posed inverse problem(regularization parameter was obtained:1) from Eq.I.50(black line); 2) from Eq.I.52(red line)). "Experimental" errors-variance 0.01.

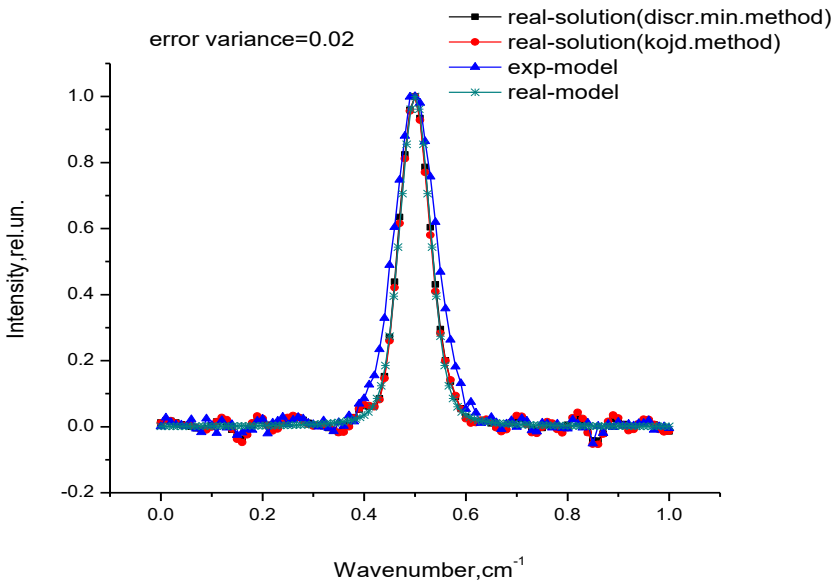

Figure II.5. Comparison between "Real modeled" profile : modeled by means of non-linear multi-parameter modeling(green line) and "Real solution" profile: obtained by means of solution ill-posed inverse problem(regularization parameter was obtained:1) from Eq.I.50(black line); 2) from Eq.I.52(red line)). "Experimental" errors-variance 0.02.

"Modeled -real" profile was generated with following parameters: Doppler width (FWHM), $\Delta\nu_D$=0.03cm^{-1}, and Lorentz width, $\Delta\nu_L$=0.01cm^{-1}, instrumental function, Gauss profile, $\Delta\nu_{Instr.}$=0.06cm^{-1}, without self absorption.

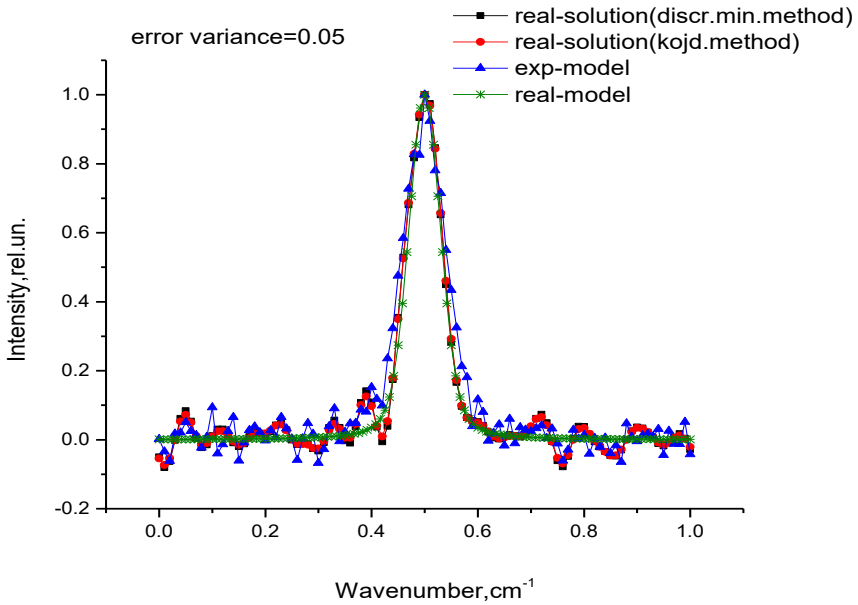

Figure II.6. Comparison between "Real modeled" profile : modeled by means of non-linear multi-parameter modeling(green line) and "Real solution" profile: obtained by means of solution ill-posed inverse problem(regularization parameter was obtained:1) from Eq.I.50(black line); 2) from Eq.I.52(red line)). "Experimental" errors-variance 0.05.

The “experimental” errors were: variance1=0.01(Fig II.4), variance2=0.02(Fig II.5), variance3=0.05(Fig II.6), variance4=0.1 (Fig II.7).

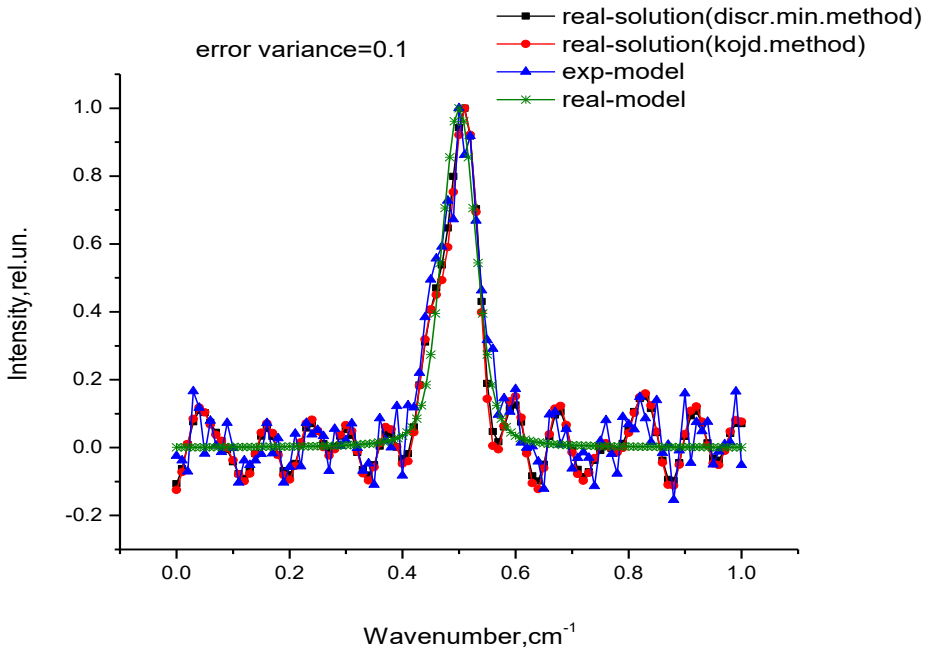

Figure II.7. Comparison between "Real modeled" profile : modeled by means of non-linear multi-parameter modeling(green line) and "Real solution" profile: obtained by means of solution ill-posed inverse problem(regularization parameter was obtained:1) from Eq.I.50(black line); 2) from Eq.I.52(red line))."Experimental" errors-variance 0.1.

As we can see above (Figs. II.1- II.7), the values of FWHM of modeled "real" profile and of calculated "real" profile coincides quite well. This is true for profiles generated with self absorption (Figs. II.1- II.3), as well for profiles generated without self absorption (Figs. II.4- II.7). But the greater values of variance lead to larger solution instabilities on the wings of profiles.

On the Fig.II.8 we can see comparison between comparisons between "modeled -real" profile and "calculated- real" profiles also. In this case "modeled- real" profile was generated with equal values of Doppler width (FWHM) and Lorentz width $\Delta\nu_D$== $\Delta\nu_L$=0.03cm^{-1} and without the "experimental errors" .The instrumental function, Gauss profile, $\Delta\nu_{Instr.}$=0.06cm^{-1}. The density in the line centre, $k_o l$=4, homogeneity of the radiation source, n=13. As we can see in case, when modeled profile was generated without

"experimental" errors, modeled "real" profile and calculated "real" profile coincides perfectly.

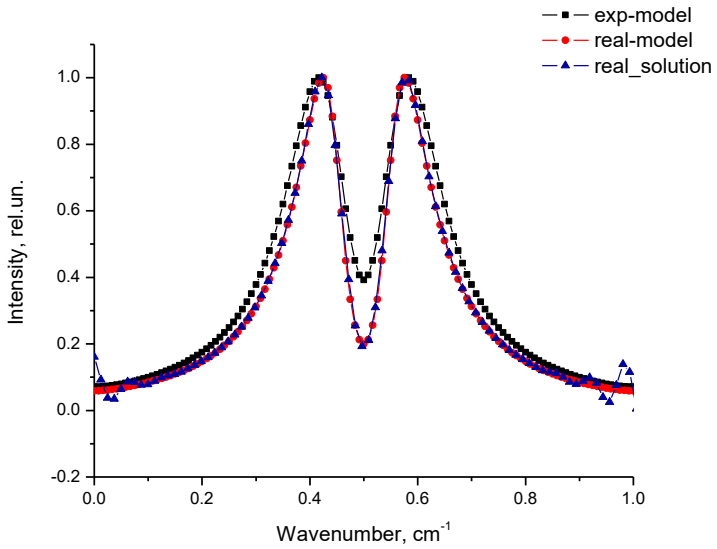

Figure II.8. Comparison between "Real modeled" profile : modeled by means of non-linear multi-parameter modeling(red line) and "Real solution" profile: obtained by means of solution ill-posed inverse problem(regularization parameter was obtained Eq.I.50(blue line).

On the Fig. II.9 we can see we can see comparison between comparisons between "modeled -real" profile and "calculated- real" profiles.

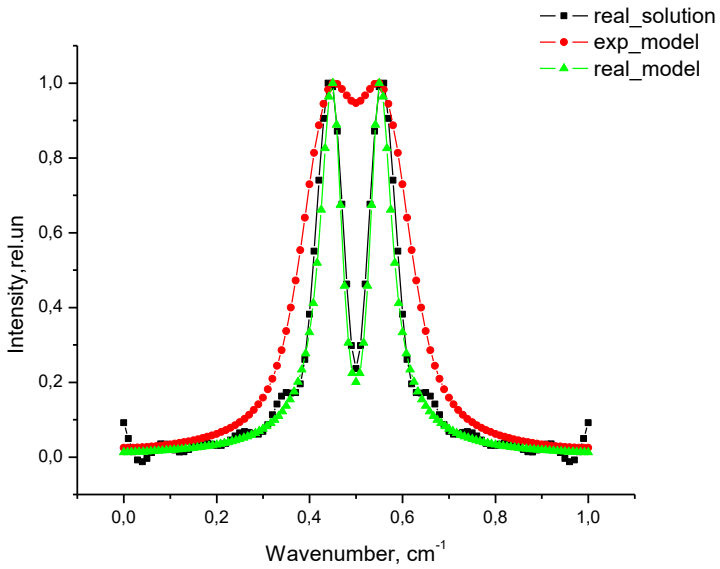

Figure II.9. Comparison between "Real modeled" profile : modeled by means of non-linear multi-parameter modeling(green line) and "Real solution" profile: obtained by means of solution ill-posed inverse problem(regularization parameter was obtained from Eq.I.50(black line).

In this case the instrumental function, Gauss profile, $\Delta\nu_{Instr.}=0.1cm^{-1}$, which is significantly more than in previous cases. The "modeled- real" profile was generated with Doppler width (FWHM), $\Delta\nu_D=0.03cm^{-1}$, and Lorentz width, $\Delta\nu_L=0.01cm^{-1}$ and without the "experimental errors" .The density in the line centre, $k_o l=4$, homogeneity of the radiation source, n=13.

As we can see on Fig.II.9., such wide instrumental function leads to unstable solution and to difference in values of self absorption in cases of modeled "real" profile and calculated "real" profile.

"Real calculated" profiles on Figs. II.8- II.9 were obtained using discrepancy minimization method(Eq.I.50) for regularization parameter determination. On Figs. II.1- II.9 instrumental function was given as equation.

On the Fig. II.10 the solutions were obtained using two different programs(written in mathCad and Delphi) and different numerical algorithms were used.

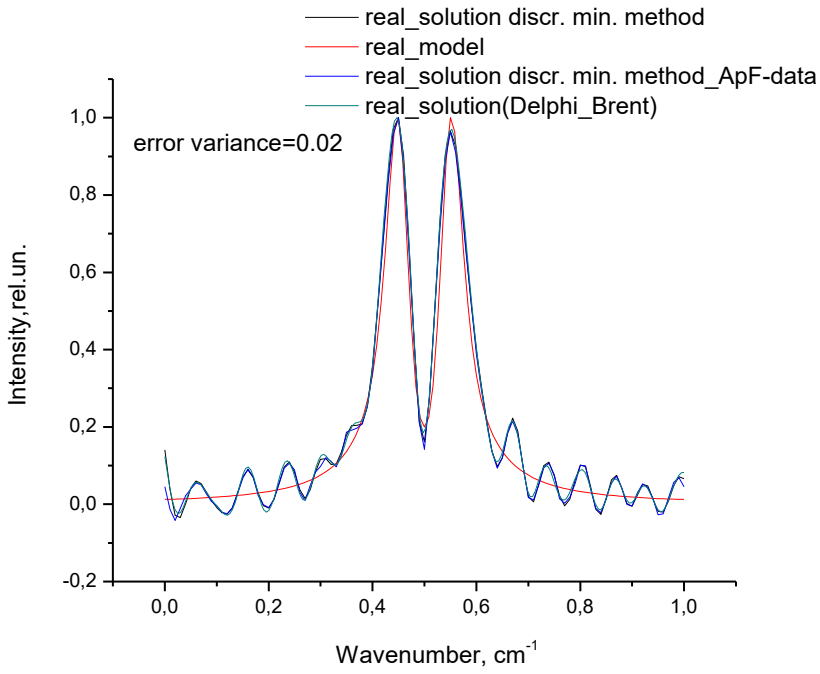

Figure II.10 Comparison between "Real modeled" profile : modeled by means of non-linear multi-parameter modeling(red line) and "Real solution" profile: obtained by means of solution ill-posed inverse problem(regularization parameter was obtained:1) from Eq.I.50(black line- instrumental function analytical equation; blue line- data array-realization in MathCad); 2) from Eq.I.52(green line)- realization in Delphi)."Experimental" errors-variance 0.02.

There are numerical algorithm of conjugate gradient (Math Cad; (Eq.I.50) for regularization parameter determination) and numerical algorithm of Brent (Delphi; (Eq.I.52) for regularization parameter determination). As well, the instrumental function was given as experimental data array and as analytical expression.

On the Fig.II.11 the solutions were obtained for “Experimental” profile, which was generated with larger “Experimental error” value. The error variance is 0.05 in this case.

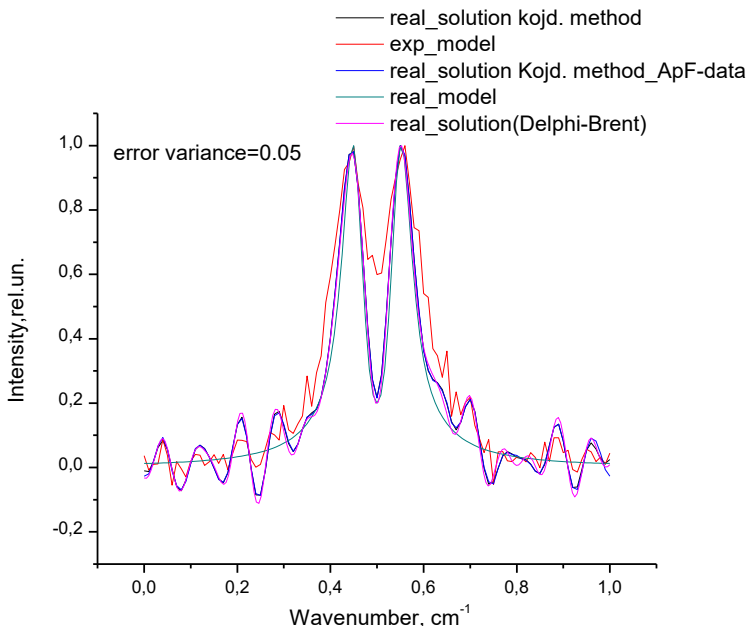

Figure II.11 Comparison between "Real modeled" profile : modeled by means of non-linear multi-parameter modeling(red line) and "Real solution" profile: obtained by means of solution ill-posed inverse problem(regularization parameter was obtained:1) from Eq.I.52(black line- instrumental function analytical equation; blue line- data array-realization in MathCad; pink line - realization in Delphi)."Experimental" errors-variance 0.05.

On the Figs. II.12 - II.15 we can see results obtained for cases when was used absolutely different instrumental function- Airy function(Eq.I.30). The instrumental function was given as data array , for regularization parameter determination Eq.I.50 was used. The mirrors refraction coefficients are: 0.6, 0.7, 08 and 0.9 accordingly. "Experimental" profile was generated without errors.

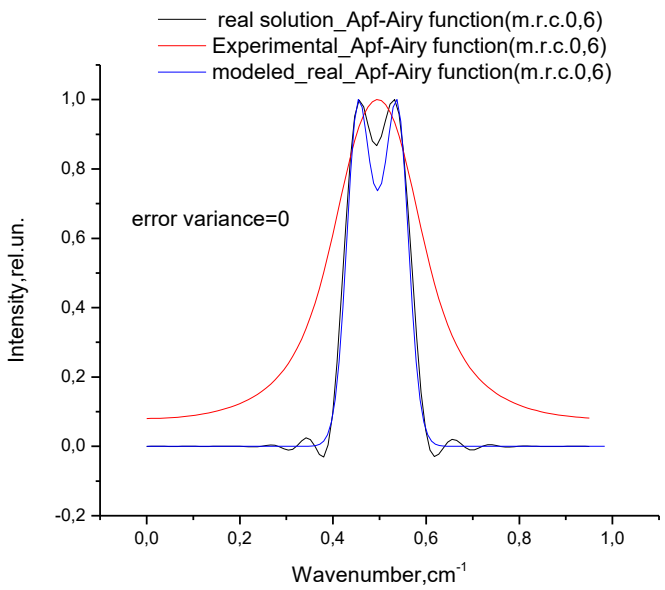

Figure II.12 Comparison between "Real modeled" profile : modeled by means of non-linear multi-parameter modeling(blue line) and "Real solution" profile: obtained by means of solution ill-posed inverse problem(regularization parameter was obtained from Eq.I.50(black line).Mirrors refraction coefficient is 60%. Instrumental function is Airy function.

As we can see (Fig.II.12) too wide instrumental function(mirrors refraction coefficient is 60%) leads to the solution errors.

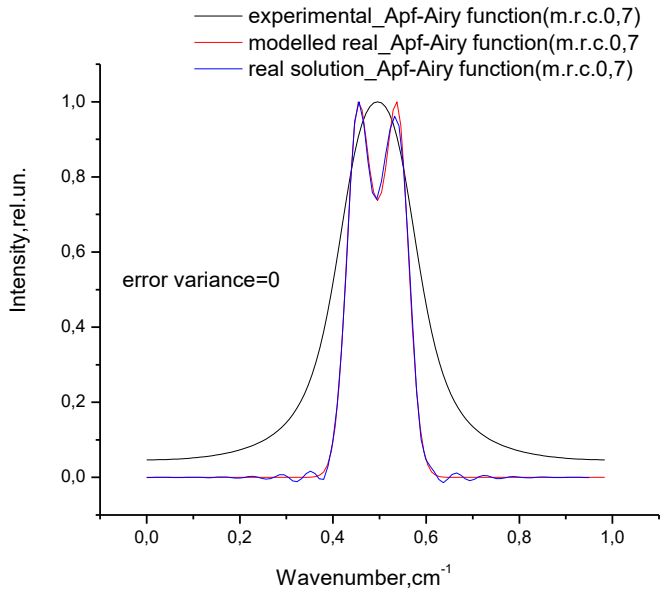

Figure II.13. Comparison between "Real modeled" profile : modeled by means of non-linear multi-parameter modeling(red line) and "Real solution" profile: obtained by means of solution ill-posed inverse problem(regularization parameter was obtained from Eq.I.50(blue line). Mirrors refraction coefficient is 70%. Instrumental function is Airy function.

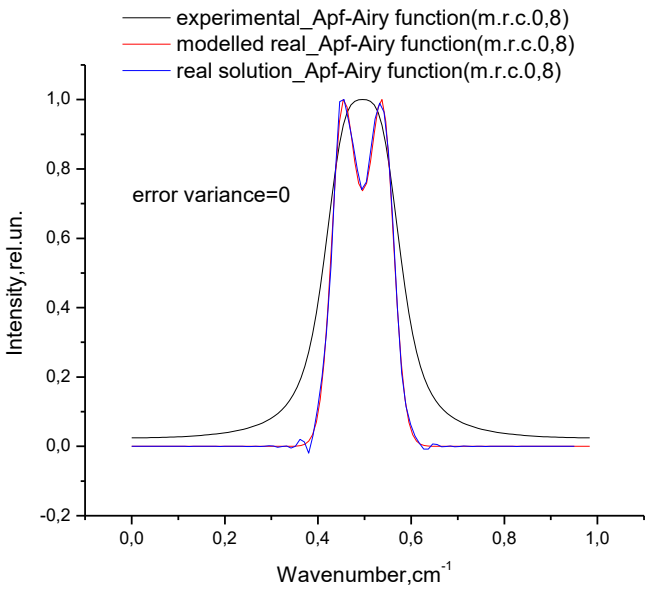

Figure II.14. Comparison between "Real modeled" profile : modeled by means of non-linear multi-parameter modeling(red line) and "Real solution" profile: obtained by means of solution ill-posed inverse problem(regularization parameter was obtained from Eq.I.50(blue line). Mirrors refraction coefficient is 80%. Instrumental function is Airy function.

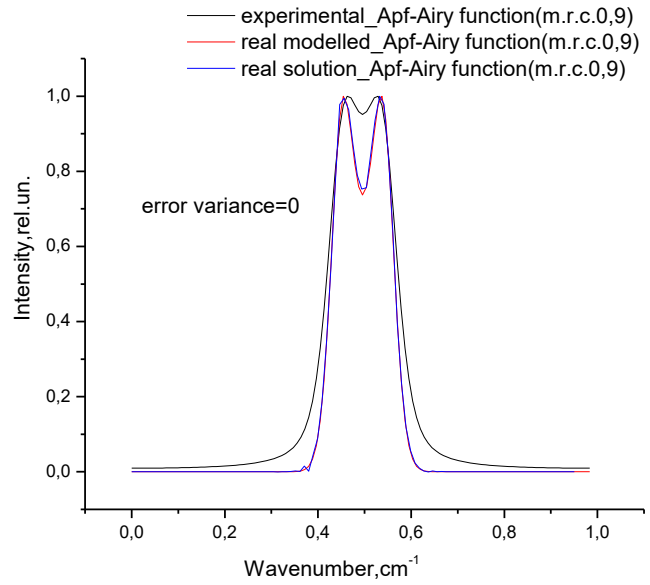

Figure II.15. Comparison between "Real modeled" profile : modeled by means of non-linear multi-parameter modeling(red line) and "Real solution" profile: obtained by means of solution ill-posed inverse problem(regularization parameter was obtained from Eq.I.50(blue line). Mirrors refraction coefficient is 90%. Instrumental function is Airy function.

1.1 Analysis and validation of the results of modeling

Below (Table 1) we can see correlation matrix (Spearman coefficient) [**87**], obtained in IBM SPSS Statistics 22 for case when "modeled -real" profile was generated with following parameters: Doppler width (FWHM), $\Delta\nu_D$=0.03cm^{-1}, and Lorentz width, $\Delta\nu_L$=0.01cm^{-1}, instrumental function, Gauss profile, $\Delta\nu I_{nstr}$.=0.06cm^{-1}, optical density in the line centre, $k_o l$=4, homogeneity of the radiation source, n=13. The "experimental" errors were: variance1=0.01, variance2=0.02, variance3=0.05. Two independed methods were used to obtain the regularization parameter: 1 method-discrepancy minimization method (Eq.I.50), 2 method- using equation (Eq.I.52).

As we can see, significant correlations (probability that agreement between results is randomness, $p<0.001$) between values, obtained by both method and between values of each of methods and values of "real-modeled" profile were obtained.

Table 1. Correlation matrix (Spearman's rho) -modeled profiles with self-absorption

Spearman's rho		variance0_01_2met.	variance0_02_2met.	variance0_05_2met.	real-modeled
variance0_01_1met.	Correlation Coefficient	,993**	,803**	,803**	,714**
	Sig. (2-tailed)	,000	,000	,000	,000
	N	101	101	101	101
variance0_02_1met.	Correlation Coefficient	,789**	,996**	,631**	,644**
	Sig. (2-tailed)	,000	,000	,000	,000
	N	101	101	101	101
variance0_05_1met.	Correlation Coefficient	,809**	,679**	,992**	,660**
	Sig. (2-tailed)	,000	,000	,000	,000
	N	101	101	101	101
real-modeled	Correlation Coefficient	,702**	,661**	,636**	1,000
	Sig. (2-tailed)	,000	,000	,000	.
	N	101	101	101	101

**. Correlation is significant at the 0.01 level (2-tailed).

In following case (Table 2) "modeled -real" profile was generated with following parameters: Doppler width (FWHM), $\Delta\nu_D$=0.03cm^{-1}, and Lorentz width, $\Delta\nu_L$=0.01cm^{-1}, instrumental function, Gauss profile, $\Delta\nu_{Instr.}$=0.06cm^{-1}, without self absorption. The "experimental" errors were: variance1=0.01, variance2=0.02, variance3=0.05, variance4=0.1. Two independed methods were used to obtain the regularization parameter: 1 method-discrepancy minimization method (Eq.I.50), 2 method- using equation (Eq.I.52).

As we can see on Table2, significant correlations between values, obtained by both method ($p<0.001$) and between values of each of methods and values of "real-modeled" profile ($p<=0.01$) were obtained.

Table 2. Correlation matrix (Spearman's rho)- modeled profiles without self-absorption

Spearman's rho		variance0_01_2met.	variance0_02_2met.	variance0_05_2met.	variance0_1_2met.	real-modeled
variance0_01_1met.	Correlation Coefficient	,999**	,544**	,551**	.297**	,435**
	Sig. (2-tailed)	,000	,000	,000	.003	,000
	N	101	101	101	101	101
variance0_02_1met.	Correlation Coefficient	,570**	,981**	,574**	.281**	,417**
	Sig. (2-tailed)	,000	,000	,000	.004	,000
	N	101	101	101	101	101
variance0_05_1met.	Correlation Coefficient	,533**	,520**	,992**	.356**	,437**
	Sig. (2-tailed)	,000	,000	,000	,000	,000
	N	101	101	101	101	101
variance0_1_1met.	Correlation Coefficient	,342**	,281**	,398**	.991**	,272**
	Sig. (2-tailed)	,000	,004	,000	.000	,006
	N	101	101	101	101	101
real-modeled	Correlation Coefficient	,427**	,393**	,447**	.254	1,000
	Sig. (2-tailed)	,000	,000	,000	.010	.
	N	101	101	101	101	101

**. Correlation is significant at the 0.01 level (2-tailed). *. Correlation is significant at the 0.05 level (2-tailed).

The solution of the model examples shows that this method can be used for real profile restoring for further diagnostic of the HFEDL if the following conditions can be performed is satisfied the following conditions:

- normal level of the noise. The variance of data must be less than 0.1;

- the ratio between instrumental function and measured profile can be less or equal of 2.

There are significant correlation between values, obtained by means of method1(discrepancy minimization method(Eq.I.50)) and method 2 (Eq.I.52). As we can see on Table 1(case with self- absorption), the correlation coefficients are: 0.993, 0.996, 0.992 in cases, when variances of modeled data are 0.01, 0.02, and 0.05 accordingly. We can see the significant correlation between values, obtained by two independent methods in case when modeled profile was without self-absorption too (Table 2). In this case the correlation coefficients are 0.999, 0.981, 0.992, 0.991 in cases, when variances of modeled data are 0.01, 0.02, 0.05, 0.1 accordingly.

As well significant correlation is observing between values of calculated "real" profiles and modeled "real" profiles. In case of modeled profile with self-absorption, the correlation coefficients are 0.714(method 1) and 0.702(method 2) for case when variance of modeled data is 0.01; 0.644(method 1) and 0.661(method 2) in case when variance is 0.02; 0.660(method 1) and 0.636(method 2),variance of modeled data is 0.05. In case of modeled profile without self-absorption, the correlation coefficients are 0.435(method 1) and 0.427(method 2) for case when variance of modeled data is 0.01; 0.417(method 1) and 0.393(method 2) in case when variance is 0.02; 0.437(method 1) and 0.447(method 2),variance of modeled data is 0.05; 0.272(method 1) and 0.254(method 2), variance of modeled data is 0.1.

As we can see above, „calculated real" profiles coincide with „modelled real" profiles quite well. Errors adding to the "experimental" profiles leads to the waves on the wings in the solution, but the physical values, which are necessary for further calculations: FWHM of profiles and dip of self-absorption coincide with "calculated- real" very well. This is true for both cases, when the instrumental function was used as formula and as data array.

The value of FWHM (case without self-absorption, instrumental function-Gauss function) is 0.07448±0.0036 (the confidences interval ,using Z criterion). The absolute errors of FWHM in this cases are: 0.057% (error variance 0), 2.14%(error variance 0.02) and 13.5% (error variance 0.05). The absolute error of mean value of FWHM is 6.4%.

The absolute errors of the dips of self-absorption (instrumental function- Airy function) are 14%, 0.53%, 0.43% and 1.53% when mirrors refraction coefficients are 60%, 70%, 80%, 90% accordingly.

The solution of the model examples by means of both programs shows good results. Obtained results show little dependence from used numerical algorithm. As well, changing the instrumental function doesn't influence the program. It gives the correct results in cases, when Gauss function was used as instrumental function as well as when Airy function was used.

2. Deconvolution of the Hg profiles, measured by means of the Fabry-Perot interferometer [P.2], [Pr.4] [A5]

Experiment

The dumbbell like HFEDL(Fig.I.10(c)), investigated in this case, was filled with mercury of a high isotopic abundance (99.3% of 202 isotope) and argon as a buffer gas.

The lamp was placed into an induction coil (Fig.II.16) and an inductive coupled discharge was excited by means of a high frequency electromagnetic field of about 100MHz frequency. Spectral line profiles, emitted from the spherical part of HFEDL were collected from it with two different argon pressures of 2 and 10 Torr, in dependence on the discharge current (80-190 mA) at the mercury cold spot temperature value of 20 C, which corresponds to the mercury vapour pressure of 0.0013Torr**[Appendix 5]**. Changing the generator current, changes the discharge power. Line profiles were recorded by means of a high-resolution scanning Fabry-Perot interferometer, using mirrors with a dielectric coating and a 0.4 cm spacer between them, giving the free

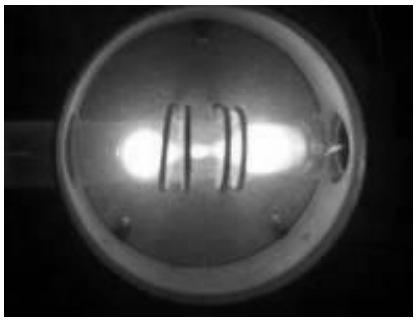

Fig.II.16. The Hg HFEDL

spectral range of 1.25 $cm^{-1}$and effective refraction coefficient value of 0.8. All calculations were made for the Hg 253.7 nm line ($6^3 P_1 - 6^1 S_0$ transition [**Appendix 6**]) using program written in MathCAD [**Appendix Nr1**].

The procedure of the obtaining of the real spectral lines shapes

The measured profiles were processed in two stages, before temperature estimation. First of all, the deconvolution procedure or solving of this ill-posed inverse problem (Eq.I.36) was performed to obtain the real spectral line shape, by means of the Tikhonov's regularization method. After procedure of deconvolution the influence of the self-absorption was taken into account (Eq. I.7)

In Fig.II.17 we can see the influence of the instrumental function and self-absorption to the FWHM of the measured spectral line profiles. In case of the 253,7 nm line, emitted from the HFEDL with 10 Torr argon, the FWHM of the measured (experimental) spectral lines were in the range of 0.15- 0.20 cm^{-1}, but real FWHM were obtained to be in the range of 0.1 – 0.15 cm^{-1} after deconvolution and in the range of 0,048 – 0,066 cm^{-1} taking into account absorption influence.

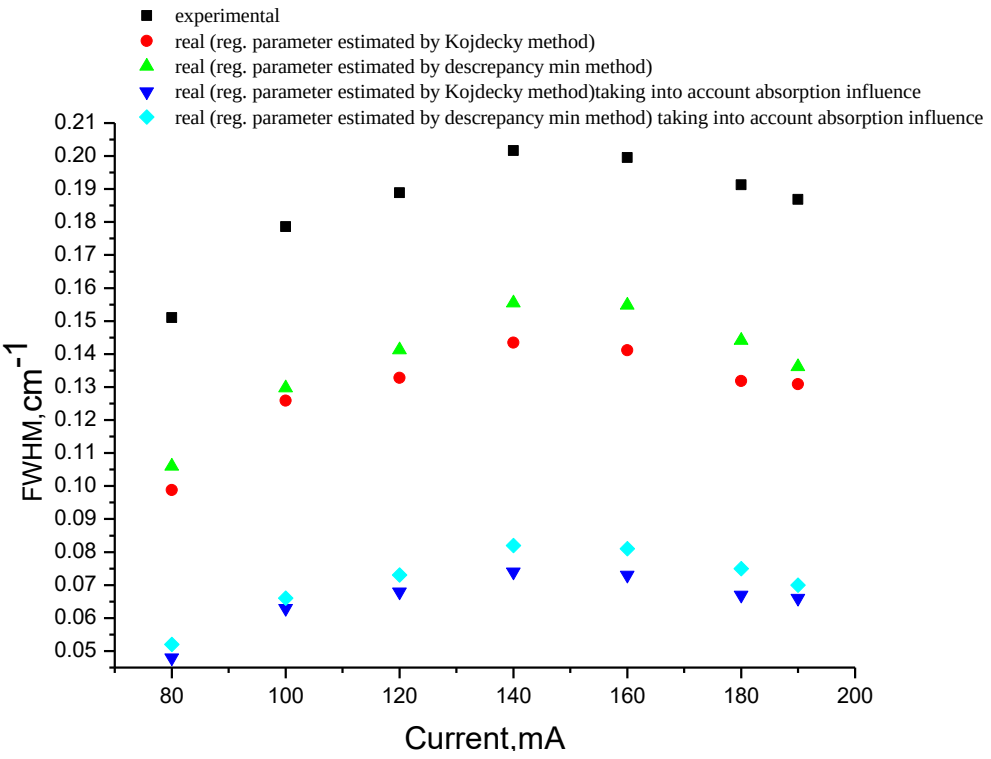

Fig..II.17 The FWHM of experimentally registered Hg 253.7nm line profile (black points) and the FWHM of the results after deconvolution by means of ill-posed inverse task solution, using two ways to determinate regularization parameter: by Koidecki method Eq.I.52 (red points) and using method of discrepancy minimization Eq.I.50 (green points) in dependence on the generator current. The Ar pressure is 10 Torr .

There is a clearly expressed maximum of the FWHM dependence from generator current at 140mA.

The results of the dependences of the optical density as a function from the discharge current for this lamp are shown in Fig.II.18 In this case the optical density is in range of 7.938-11.642 (regularization parameter was by (Eq.I.50)) and of 9,362-12.494 (regularization parameter was determined by (Eq.I.52)).

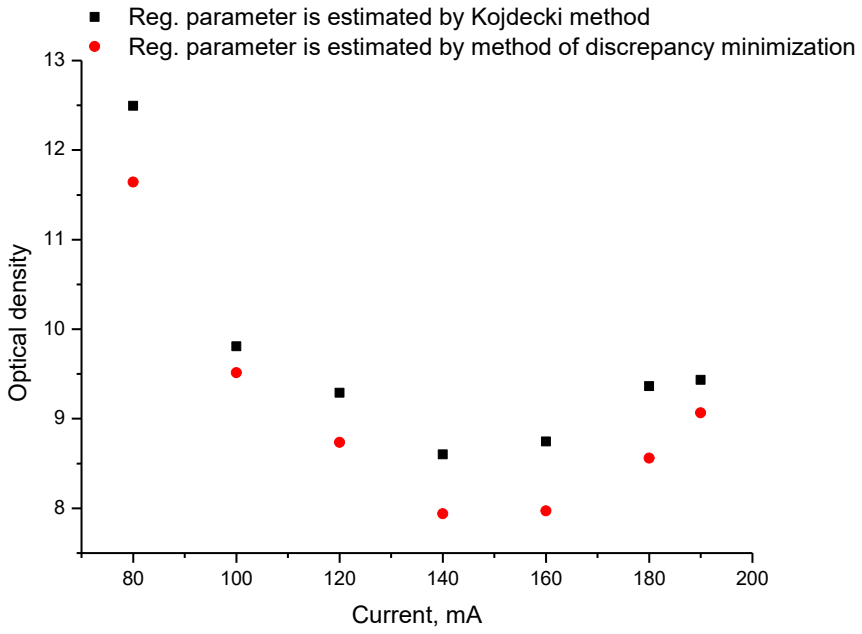

Fig.II.18 The optical density dependence on the generator current. The Ar pressure is 10 Torr . The optical density obtained for lines deconvoluted by means of ill-posed inverse task solution, using two ways to determinate regularization parameter: by Koidecki method Eq.I.52 (black points) and using method of discrepancy minimization Eq.I.50 (red points).

As we can see the results obtained used two methods to obtain the parameter of regularization: minimization of discrepancy Eq.I.50 and by method where it is assumed, that the regularization parameter is the root of the Eq.I.52, agree well.

Examples of the experimental dependence of the FWHM from the generator current and the influence of the instrumental function and self-absorption to it in case of the 253,7 nm line emission from the HFEDL with 2 Torr argon are shown in Fig.II.19.

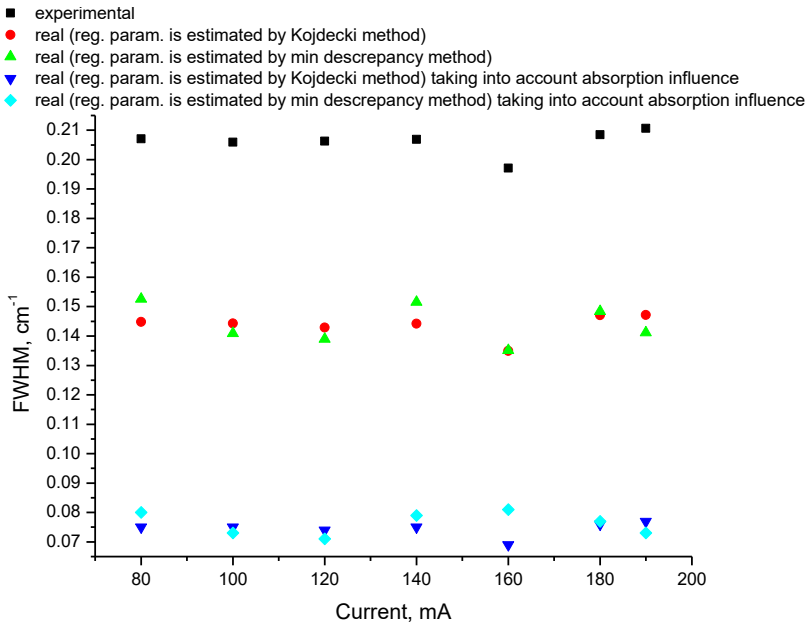

Fig.II.19 The FWHM of experimentally registered 253.7nm line profile (black points) and the full width at half of maximum of the results after deconvolution by means of ill-posed inverse task solution, using two ways to determinate regularization parameter: by Koidecki method Eq.I.52 (red and blue points) and using method of discrepancy minimization Eq.I.50 (green and light blue points). in dependence on the generator current. The Ar pressure is 2 Torr .

In case of argon pressure at 2 Torr the FWHM of the experimental as well as the obtained real profiles are practically independent from the generator current. The estimated FWHM of the real profiles in average is broader by argon pressure 2 Torr in Hg HFEDL: about 0.14 cm^{-1} and about 0.07 cm^{-1} taking into account absorption.

The optical density is in range of 7.964-9.136 (regularization parameter was determined by method of discrepancy minimization) and of 8,391-9.147 (regularization parameter was determined by (Eq.I.52)) (Fig.II.20)

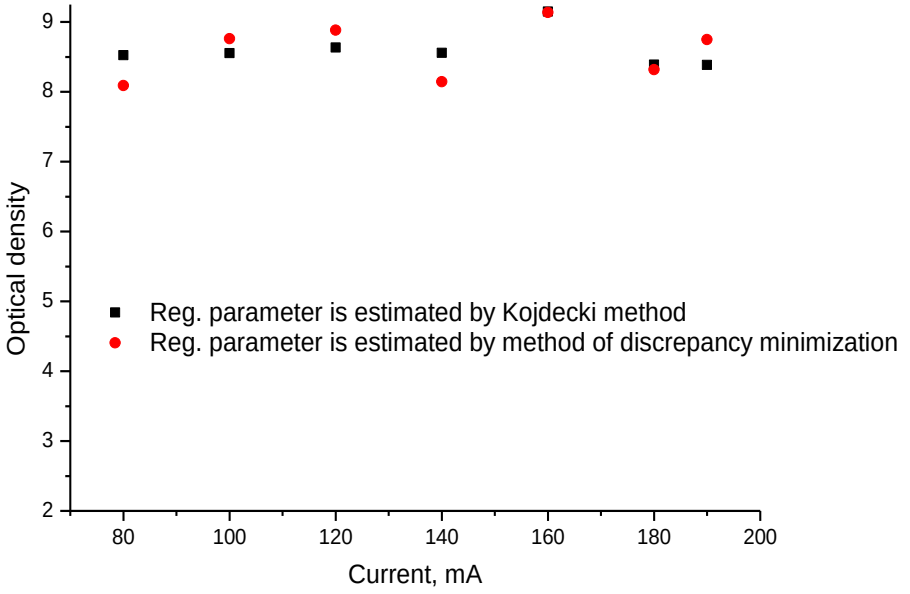

Fig.II.20. The dependence of the optical density from the generator current. The Ar pressure is 2 Torr . The optical density obtained for lines deconvoluted by means of ill-posed inverse task solution, using two ways to determinate regularization parameter: by Koidecki method Eq.I.52 (black points) and using method of discrepancy minimization Eq.I.50 (red points).

The tendencies of clear maximum appearance in the dependence FWHM from discharge current at the Ar pressure 10 Torr and independence from discharge current at 2 Torr agree well with the results obtained by Revalde et all [**88**] In that case the estimated FWHM of Hg 253,7 nm spectral line was obtained by another method – the mathematical modeling, described in [**88,89**].

Discharge temperature estimation

Temperatures of the radiating atoms, estimated from the Doppler broadening (Eq.I.5) of the deconvoluted real spectral lines profiles, taking into account influence of the absorption are shown in Figs. II.21-II.22.

In Fig.II.21 are shown the dependences of the temperatures from the discharge current for case when Ar pressure was 10 Torr. Clear maximum of dependence can be seen by 140-150 mA. The temperature varies from approximately 600-1700 K as a function of discharge generator current.

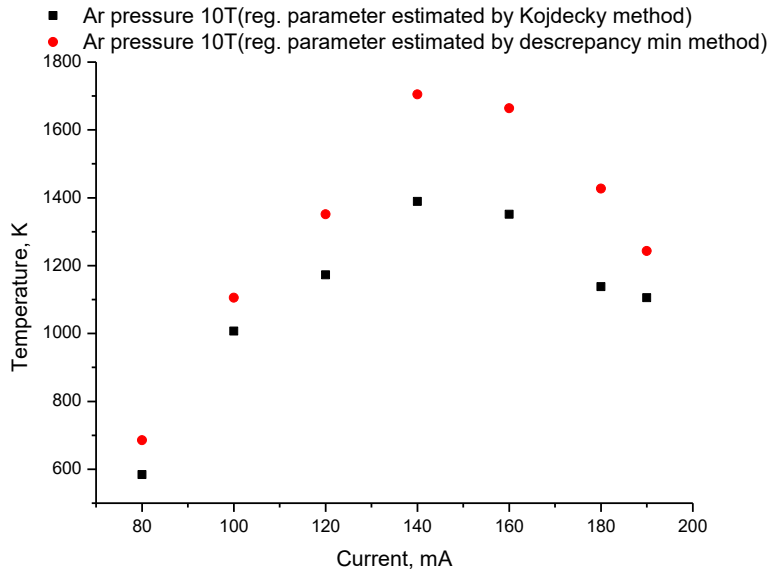

Fig.II.21. The dependences of the temperatures from the discharge current for case when Ar pressure was 10Torr.

The results of the dependences of the temperatures as a function from the discharge current for the lamp with Ar pressure of 2 Torr are shown in Fig.II.22. The temperature of the radiating atoms is in the range of 1400-1500 K.

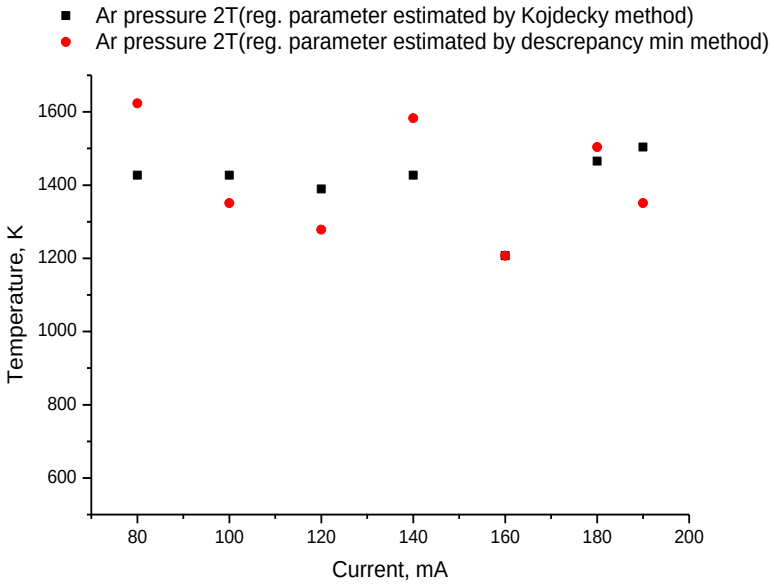

Fig II.22. The dependences of the temperatures from the discharge current. for case when Ar pressure was 2Torr.

3. Deconvolution of the Hg profiles, measured by means of the Zeeman spectrometer[Pr.3], [A4]

3.1. The Hg 253.7 nm spectral line profile deconvolution procedure and discharge temperature estimation

Experimental

In this case microsize capillary HFEDLs were investigated (Fig.I.10(d)). The lamps were filled with mercury of natural abundance or with pure isotope Hg ^{198} or with pure isotope Hg ^{202} and buffer gas argon of about 2 Torr pressure. Lamps were measured by means of a Zeeman scanning spectrometer at the mercury cold spot temperature value at 20 C (p_{Hg}=0.0013Torr).

HFEDL filled with natural Mercury mixture

In Fig.II.24 we can see measured and restored 253,7 nm line profiles emitted from HFEDL filled with natural mixture of Hg isotopes. The lamp was operated with the HF electromagnetic field of about 100 MHz frequency and the discharge current was of 0.1 mA.

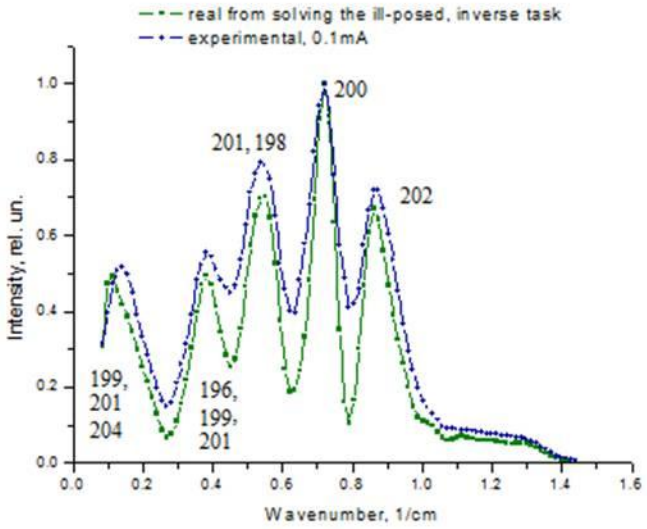

Fig. II.24. The measured(blue line) and deconvoluted (green) line profiles emitted from HFEDL filled with natural mixture of Hg

As we can see, the total width of the 253,7 nm line profile, emitted from the natural Hg lamp, is quite broad- the total width of such line is about 1.1-1.2 cm^{-1}. Thus it cannot be used for ZAAS, because this method needs very narrow spectral line to reach high sensitivity. Therefore we consider mercury lamp filled with only one isotope.

HFEDL filled with isotope Hg ^{198}

On the Fig. II.25. we can see measured line emitted from Hg HFEDL filled with pure isotope Hg ^{198} (92.8%) and buffer gas argon of about 2 Torr pressure.

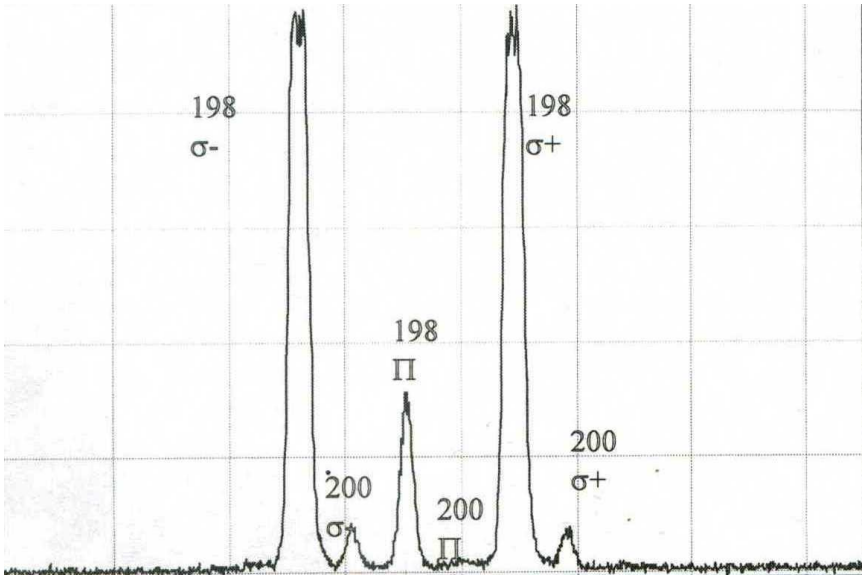

Fig. II.25. The measured line profile emitted from HFEDL filled with pure isotope Hg 198 (92.8%) and buffer gas argon of about 2 Torr pressure.

Results of the deconvolution of the right and left components are shown at Fig. II.26(a) and Fig. II.26(b) accordingly.

In this case parameter of regularization was determined by two ways: minimization of discrepancy (Eq.I.50) and by method proposed by Kojdecki[79] (Eq.I.52). The solution was implemented in MathCad (algorithm of conjugate gradient) and in Delphi algorithm of Brent.

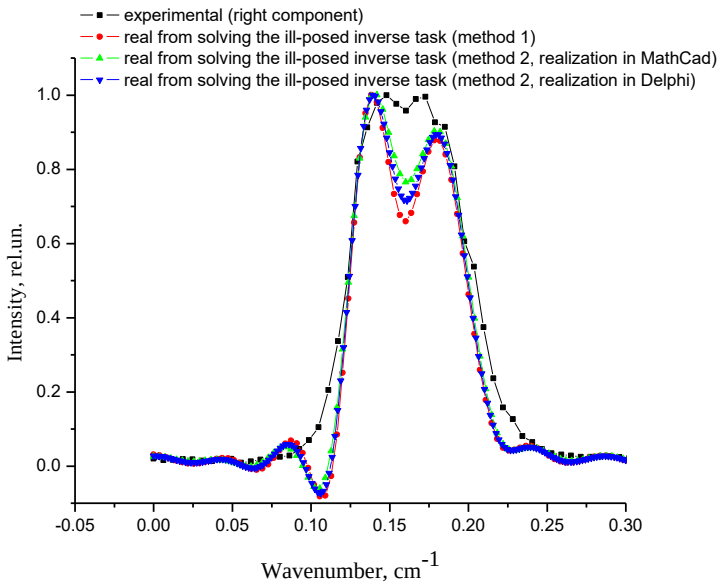

Fig. II.26 (a). Right component: measured (black line) and deconvoluted line profiles (red, green, blue lines) Regularization parameter was obtained 1)from Eq.I.50(realization of solution in MathCad-red line);2) from Eq.I.52(realization in Delphi- blue line , in Math Cad- green) HFEDL filled with pure isotope Hg ^{198} (92.8%) and buffer gas argon of about 2 Torr pressure.

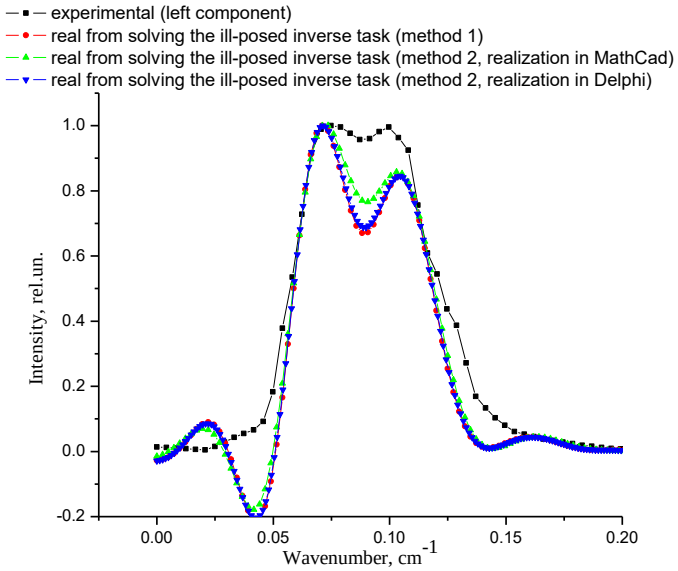

Fig. II.26 (b). Left component: measured (black line) and deconvoluted line profiles (red, green, blue lines) Regularization parameter was obtained 1)from Eq.I.50(realization of solution in MathCad-red line);2) from Eq.I.52(realization in Delphi- blue line , in Math Cad- green) HFEDL filled with pure isotope Hg ^{198} (92.8%) and buffer gas argon of about 2 Torr pressure.

The parameters of regularization determined for both components are shown in the table 3:

Table 3. The parameters of regularization determined for both components, using two different methods and two algorithms for numerical calculation. Accuracy E-7

	Regularization parameter	
Method/algorithm	Right component	Left component
Minimization of discrepancy/ conjugate gradient	1.664E-5	2.068E-5
By Kojdecki(MathCad)/ conjugate gradient	3.745E-5	3.253E-5
By Kojdecki(Delphi)/ algorithm of Brent	2.61318652730945E-5	2.25700219881838E-5

The waves observed in the left side wing of the obtained real spectral line profile in Fig. II.26 are due to the difficulty to stabilise the solution for the given level of errors of experimental data. The experimental profiles, shown in Fig. II.25, are very narrow, with very sharp increase and decrease of signal and this gives quite high level of uncertainty of numerical experimental. Nevertheless, from the obtained lines we can see that the deconvoluted profiles have larger dip in the line centre than the experimental ones. In general good agreement can be observed between the deconvoluted real spectral line profiles using different methods of obtaining the regularisation parameter.

The centre of the spectral line profile is also the most interesting part for the deconvoluted spectral line for AAA, because the dip in the line centre shows that the self-absorption is present.

The mean value of I_{max}/I_0 is 1.31 (standard deviation is 0.079) for calculated profiles instead of 1.04 (standard deviation is 0.002) in case of measured profile. The I_o is the intensity of the spectral line profile at the centre of the line; I_{max} is the intensity at the line maximum.

HFEDL filled with pure isotope Hg 202

On the Fig. II.27 we can see measured line emitted from capillary Hg HFEDL filled with pure isotope Hg 202 (99.8%) and buffer gas argon of about 2Torr pressure as well as real spectral line shapes.

For the comparison **[A.1]** of obtained results were used previous results obtained, by means of non-linear multiparameter chi-square fit**[48].**

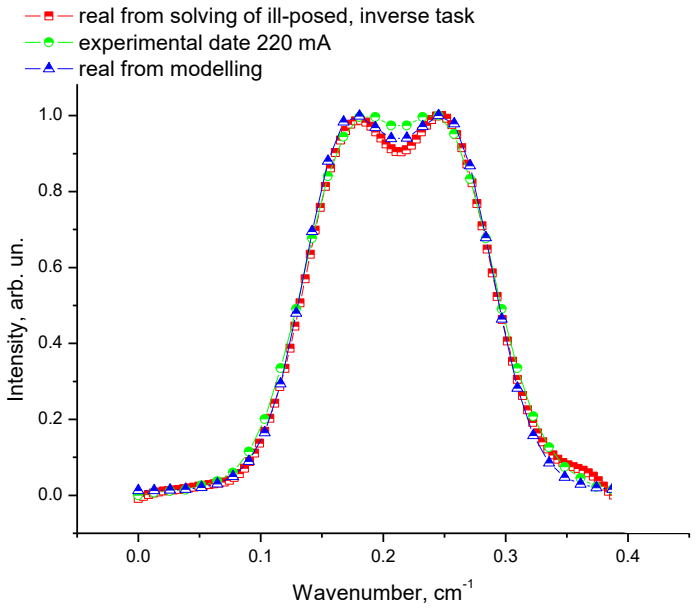

Fig. II.27. The comparison of the determined real profiles of Hg 254 nm line, using both methods: 1) by means of non-linear multi-parameter modeling (blue line) and 2) by means of solution ill-posed inverse problem (regularization parameter was obtained from Eq.I.50(red line). Line emitted from HFEDL containing Hg^{202} (99,8 %) isotope.

As we can see, the results obtained by means of modelling and using solution of ill-posed inverse task agree very well.

3.2. The Hg 184.9nm spectral line profile deconvolution [P.1], [Pr.1]

Experiment

In this case were studied the line profiles 184.9 nm Hg resonance line emitted from a capillary Hg low-pressure high-frequency electrodeless discharge lamp, containing Hg ^{198} isotope. The profiles were registered at different cold spot temperatures of the lamp in the range from 0^{o}C to 23^{o}C (p_{Hg} in [**Appendix 5**])and at different values of the discharge currents by means of a Zeeman scanning spectrometer.

The procedure of the obtaining of the real spectral lines shapes

The examples of the comparison of the experimentally registered 184.9 nm line(6^1P_1 - 6^1S_0 transition [Appendix 5])profile at the cold spot temperature of Hg 23 ^{o}C and 9 ^{o}C with these ones after deconvolution procedure are shown in Figs. II.28 - II.29, accordingly. The Ar pressure in the absorption filter was of 0.5 Torr.

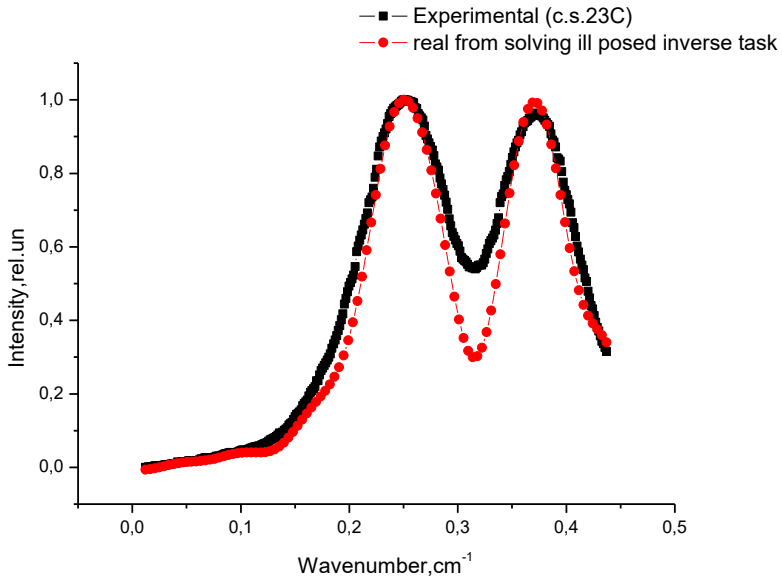

Fig. II.28 .Comparison of the experimentally registered (black line) 184.9 nm Hg resonance line profile with restored one (red line). The cold spot temperature of the mercury HFEDL is 23^{o}C.

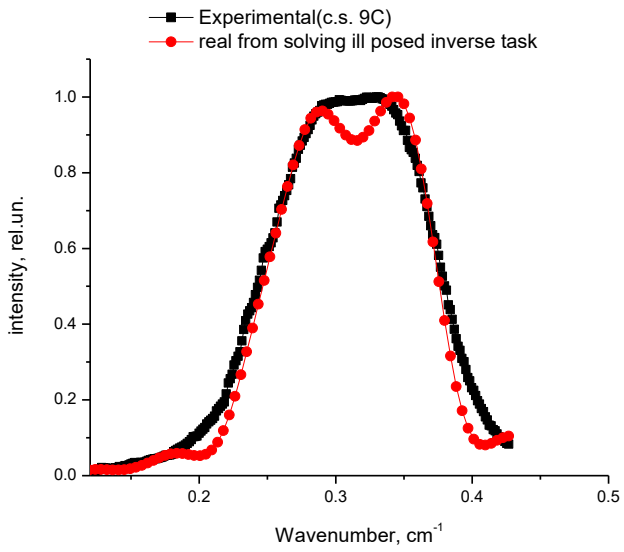

Fig. II.29 .Comparison of the experimentally registered (black line) 184.9 nm Hg resonance line profile with restored one (red line). The cold spot temperature of the mercury HFEDL is 9° C.

The regularization parameter α was obtained using discrepancy minimization method by Eq.I.50. As we can see at Fig. II.30 , the largest influence of the instrumental function can be observed on the depth of the dip in the middle of the line. The small waves on the wings of the line can be explained due to larger errors on the line wings. Even using the regularization cannot stabilise the solution of the inverse task completely by such errors. To avoid the oscillations, more accurate experimental data are necessary.

In Fig.II.30, the comparison of the restored real 184.9 nm line profiles is shown, calculated from 2 different experimental lines, registered by different argon pressure values of 0.5 Tor and 50 Torr in the absorption cell. Since the experimental conditions in the lamp were kept approximately the same, the only difference between both experimentally registered profiles was the width of the instrumental function. Thus, the comparison of the restored real profiles can serve for the validation of the calculation. As we can see, the profiles coincide quite well.

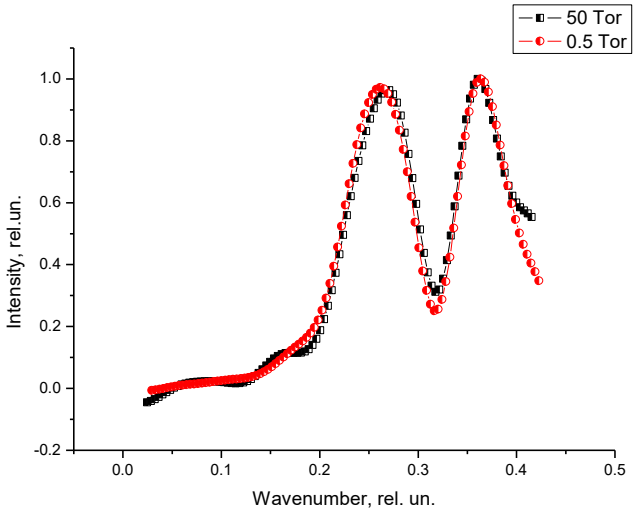

Fig.II.30. The comparison of the restored real 184.9 nm line profiles, calculated from 2 experimental lines registered by different argon pressure values in the absorption cell of 0.5 Tor (red line) and 50 Tor (black line). The experimental conditions in the lamp were nearly the same.

For validation the results were compared with the results obtained by means of a non-linear multi-parameter chi-square fit.

An example of the restored profiles by both methods of the 185 nm Hg line is shown in Fig.II.31. The instrumental function was the absorption profile (Voigt profile) in the absorption filter at the Ar pressure of 0.5 Torr and the room temperature.

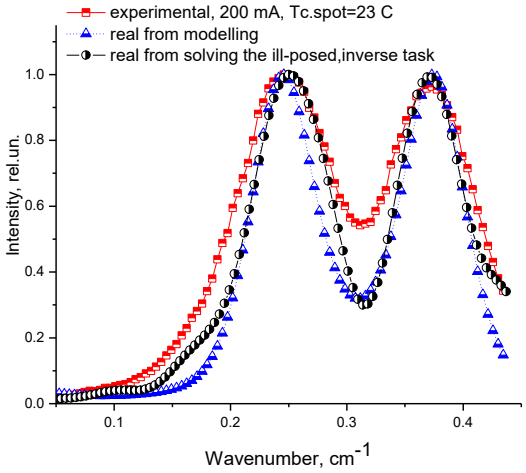

Fig. II.31. The comparison of the determined line profiles applying both methods1) by means of non-linear multi-parameter modeling (blue line) and 2) by means of solution ill-posed inverse problem (regularization parameter was obtained from Eq.I.50(black line)

The good agreement between values of the dip of the self-absorption, obtained used each method was reached.

The obtained qualitative self- absorption dependence on the Hg cold spot temperature is shown in the Fig. II.32. The I_o is the intensity of the spectral line profile at the centre of the line; I_{max} is the intensity at the line maximum. When the spectral line profile is not reversed than the ratio $I_{max}/I_o = 1$. This parameter can serve as a parameter showing the degree of the self-reversal. |

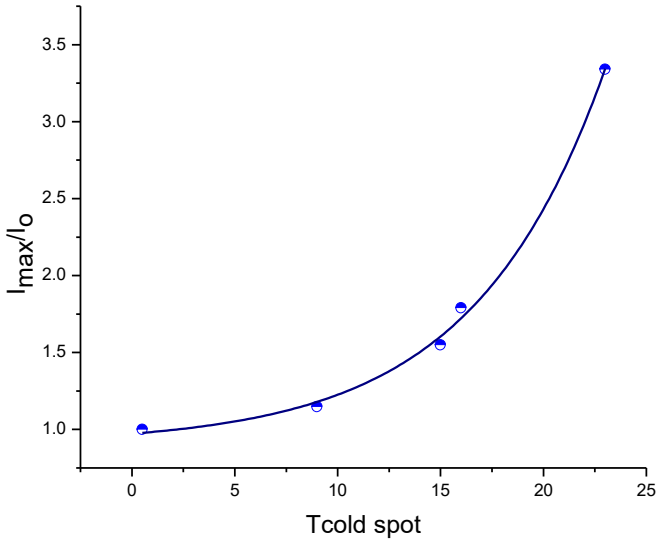

Fig. II.32. The obtained self- absorption (I_{max}/I_0, where I_{max}- intensity at the maximum of the profile and I_0-at the center of the profile) dependence on the Hg cold spot temperature.

At the minimum optical density conditions, by the cold spot temperature of about 0^oC, we can assume that the 184.9 nm line is practically optically thin. The temperature of the radiating atoms, calculated from the fitted Doppler broadening is of 250^o C.

4. The approximation of the instrumental function of the Fourier transform spectrometer [P.4], [A7]

For the defining of the best approximation of the instrumental function of the Fourier transform spectrometer were done the following steps.

First, was used an experimentally measured He spectral line of 632.8 nm wavelength emitted from the single mode He/Ne laser as a data array for instrumental function matrix A in the formula (I.49) for deconvolution without any approximation. The example of the measured line by means of the Fourier transform spectrometer is shown in Fig. II.33.

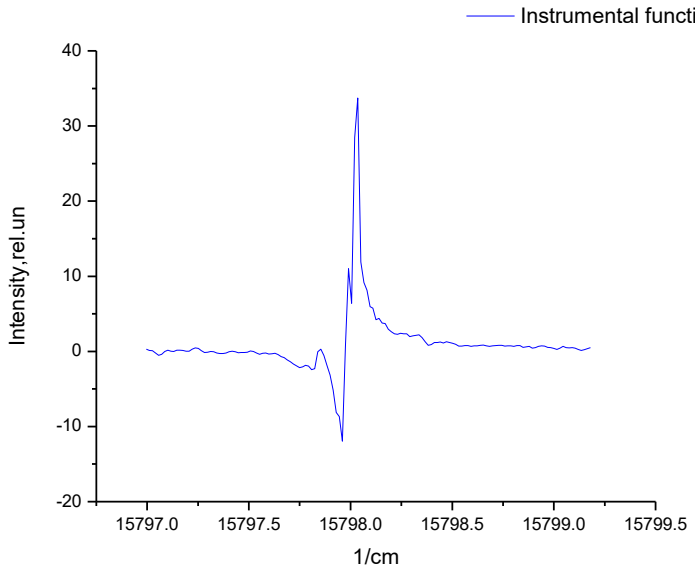

Fig. II.33 - The experimentally measured instrumental function of Fourier transform spectrometer Bruker IFS-125HR.

But it led to false maximums, especially, in the far wings of the profile.

In Figs. II.34 - II.35 the examples of the deconvolution are shown when the instrumental function was taken as a data array.

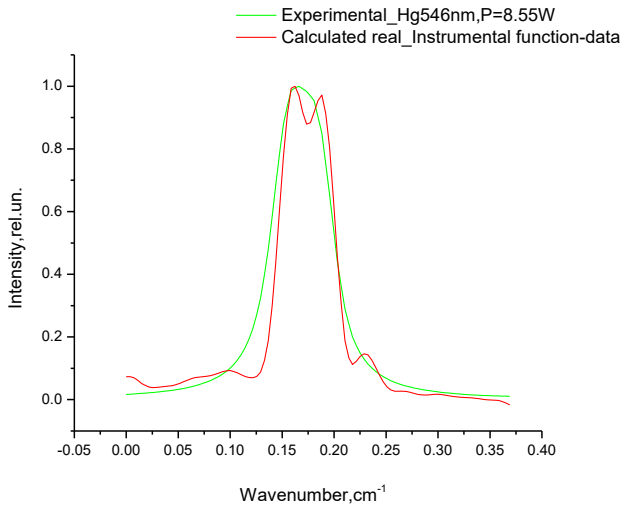

Fig. II.34- The example of the Hg 546.1nm spectral line in the case when instrumental function was taken as a data array. Line was emitted from Hg/Ar lamp without magnetic field. Green line denotes the experimental line and red – the calculated real line.

The results of calculations are demonstrated on the single spectral line and on multiple spectral lines that is our case. On the Fig. II.34 we can see example for the case when measured 546.1 nm Hg line was emitted from Hg/Ar lamp without magnetic field. On the Fig. II.35 we can see case when measured Hg 546.1 nm line was emitted from Hg/Xe lamp in magnetic field and therefore are split due to the Zeeman effect.

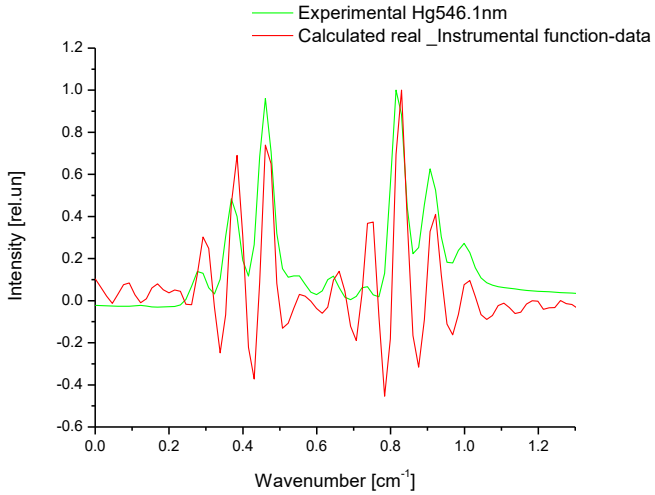

Fig. II.35- The example of the deconvolution for Hg 546.1nm spectral line in the case when instrumental function was taken as a data array. Line was emitted from Hg/Xe lamp in the magnetic field. Lamp was operated horizontally. Green line denotes the experimental line and red – the calculated real line.

As we can see, in the case of direct using the measured data array as an instrumental function A in the matrix equation (I.49) leads to the fraud maximums in the far wings of the profile.

Second step was to test the instrumental function given by the theory of Fourier transform spectrometry [**12**] giving restrictions of the resolution of the device due to the limited optical path difference in the Michelson interferometer inside the Fourier transform spectrometer. This function is known as sinc(x) function(Eq.I.35).

Below we can see the example of the deconvolution when the instrumental function was taken as a function which is described by the equation (Eq.I.35).

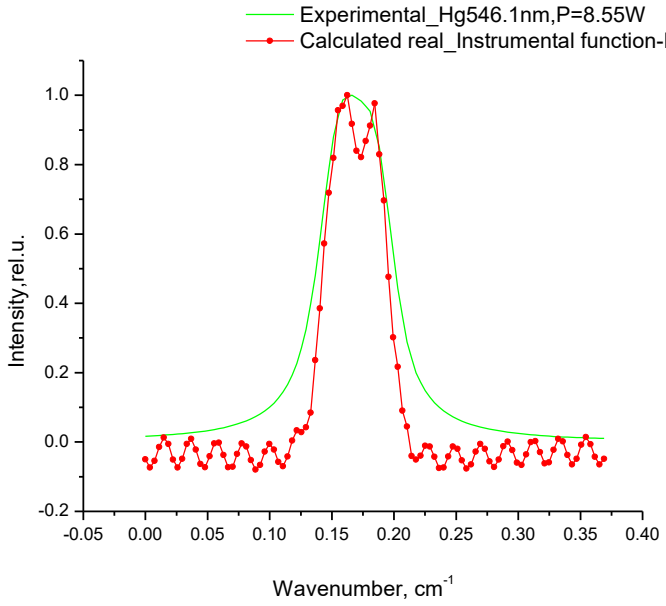

Fig. II.36 - The example of the deconvolution of Hg 546.1nm spectral line in the case when instrumental function was taken as the function, which is described by the equation (Eq.I.35). The line was emitted from the Hg/Ar lamp without magnetic field. Green line denotes the experimental line and red – the calculated real line.

As we can see usage of this function gives a lot of negative values and also false beats in the wings where no real maxima can be present.

Afterwards were performed approximations of the instrumental function trying to fit it with several known peak functions, for example, Voigt, Gauss and Lorentz functions (see part1).

Fig. II.37 shows the respective fitting results for the experimental instrumental function (He laser line). We can see the experimental instrumental function and its approximation with

the Voigt function (fitting parameters are: the FWHM of Gaussian part $\Delta\nu_G$ is of 0,02926cm^{-1}, the FWHM of the Lorentz part $\Delta\nu_L$ is of 0.02926 cm^{-1}; the fit to the Lorentz function (fitting parameters are: $\Delta\nu_L$ is of 0,02862 cm^{-1}), and the fit to the Gauss function (fitting parameters are: the $\Delta\nu_G$ is of 0,03974 cm^{-1}).

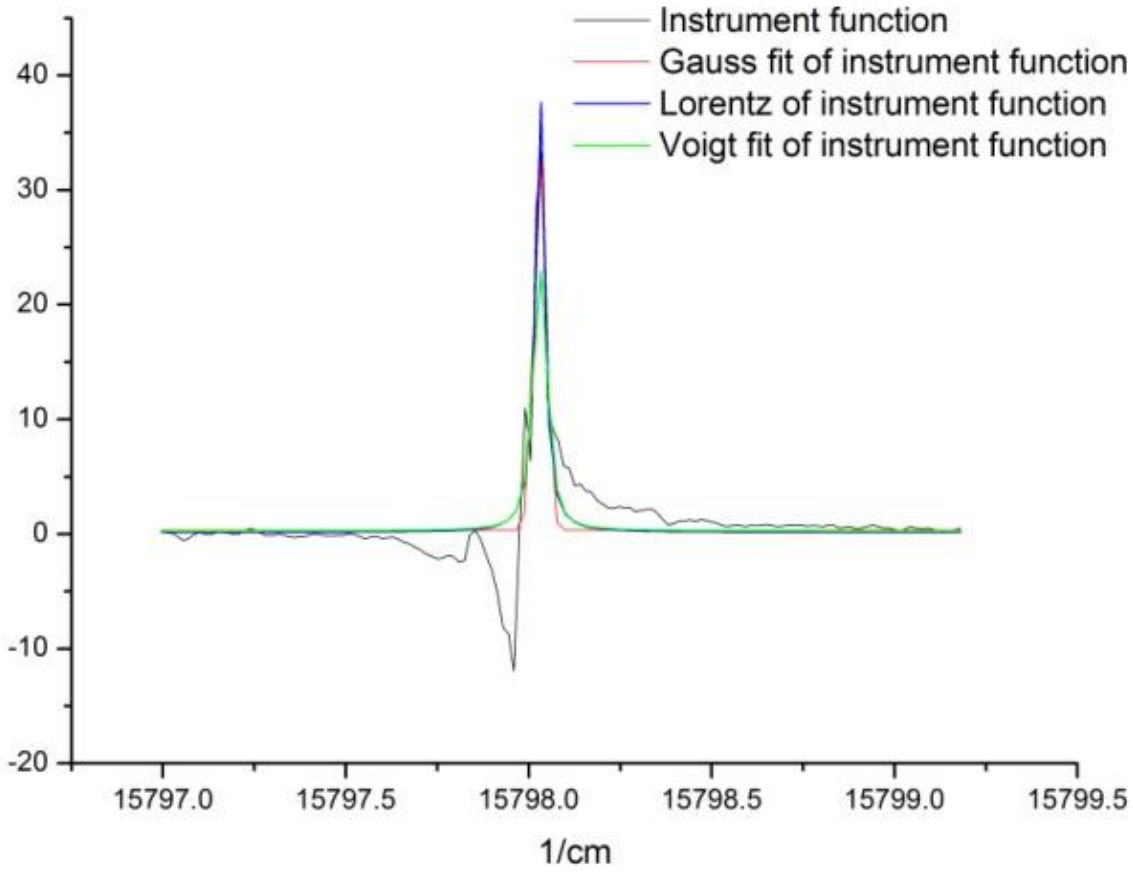

Fig. II.37 - The experimentally measured instrumental function (black line) of the Fourier transform spectrometer Bruker IFS-125HR and its approximation: with the Voigt function (green line); with the Lorentz function (blue line); with the Gauss function (red line).

The best fitting results were obtained for the fitting with the Lorentz function, so was decided to use it for further tests.

In Fig. II.38 the examples of deconvolution are shown when the instrumental function was taken as a data array (blue line), Lorentz function (red line) and as a function described by Eq.I.35 (green line). Fig. II.38 shows the deconvolution example for the measured 546 nm Hg line, emitted from Hg/Ar lamp without magnetic field. The example clearly

demonstrates the case when the self-absorption dip in the centre of spectral line is covered by the instrumental function.

The comparisons in figures below clearly demonstrate that the deconvolution procedure in cases, when instrumental function was taken in a form of raw data, or as a theoretical instrumental function described by equation (Eq.I.35), gave very noisy solutions on the wings of profiles. Also, this test illustrates that the best approximation of instrumental function was its approximation with the Lorentz function.

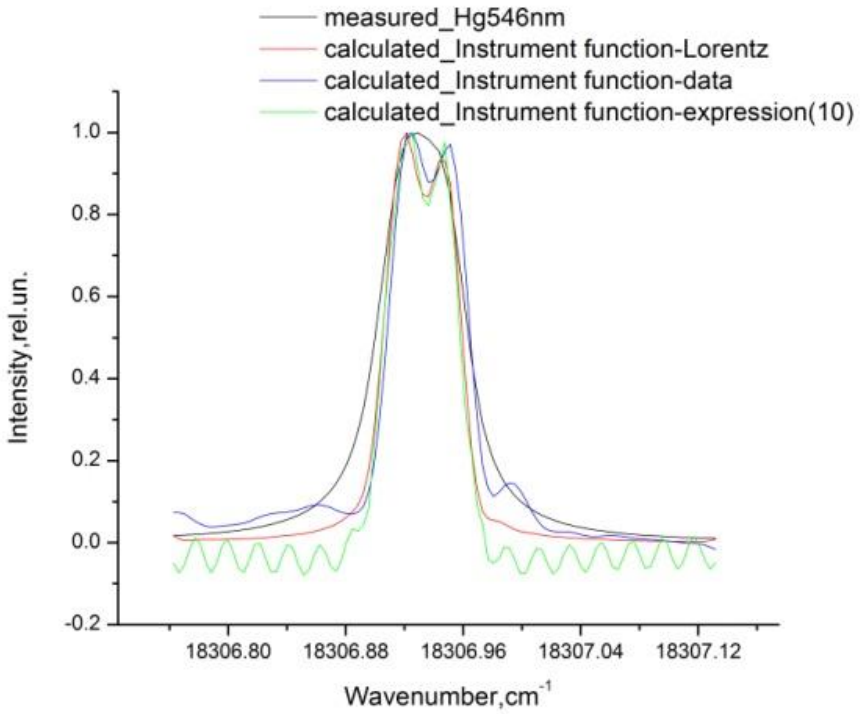

Fig. II.38 The example of the measured Hg 546 nm spectral line (black line) and calculated real lines in the case, when instrumental function was taken as a data array (blue line), Lorentz function (red line) and as a function described by Eq.I.35 (green line). Line was emitted from Hg/Ar lamp without magnetic field.

5. Deconvolution of the Hg visible triplet profiles, measured by means of the Fourier transform spectrometer

For these investigations the HFEDLs with microsize capillary shown in Fig.I.10(d) were used. The discharge is ignited in the capillary part of lamp. The reservoir at the end of lamp

is used as a cold spot to control the metal vapour pressure in lamp [**20**]. In this experiments the mercury isotope pressure was of 0,003 Torr [**90**]. The lamps were filled with mercury isotopes 198 or 202. Xenon, argon, krypton were used as buffer gases. The Hg/Xe lamp was observed in magnetic field also.

Spectral lines, emitted from Hg/Xe, Hg/Ar, Hg/Kr high frequency microsize capillary lamps, were measured using Fourier Transform spectrometer *Bruker IFS-125HR*in the wavelength region 330-2000 nm. In this case, the Hg visible triplet lines with wave lengths: 404,7 nm, 435.8 nm, 546.1 nm(7^3S_1-$6^3P_{0,1,2}$ transition) [**Appendix 6**] were analysed.

5.1. Investigation of the Hg/Xe lamp in the magnetic field [P.3], [Pr.5] [Pr.6], [A6].

In this case the lamp was filled with xenon of 2 Torr partial pressure and mercury isotope 198. The lamps were capacitatively excited using 100 MHz frequency applied to external electrodes. The lamps were operated in three different positions in accordance to the Earth plane, namely, horizontally, vertically with Hg reservoir up, and vertically with Hg reservoir down (Fig. II.39) . The lamps were placed in magnetic field to observe Zeeman splitting, as necessary for their application in Zeeman Atomic Absorption Spectrometry (ZAAS). Magnetic field was perpendicular to the axis of capillary and the direction of observation was parallel to the magnetic field lines.

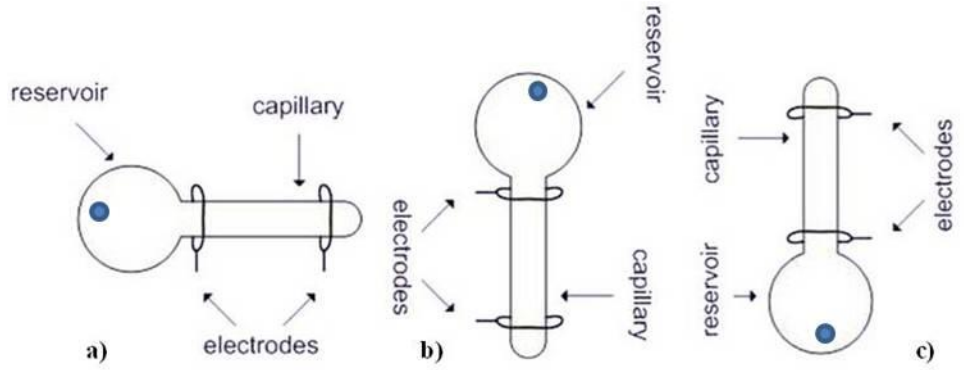

Fig. II.39 - Working position of the Hg/Xe capillary lamp: a) horizontally, b) vertically with the Hg reservoir up, c) vertically Hg reservoir down.

The examples of experimental measurements of the 404.7 nm line in three different working positions are shown in Fig. II.40. As clearly can be seen in Fig. II.40, the most intensive lines were obtained when the lamp was operated vertically, especially with the

reservoir up. The smallest intensity was observed when the lamp was operated horizontally. This effect was observed in the research [**91]**, where the difference between the distributions of atoms in different working positions was found.

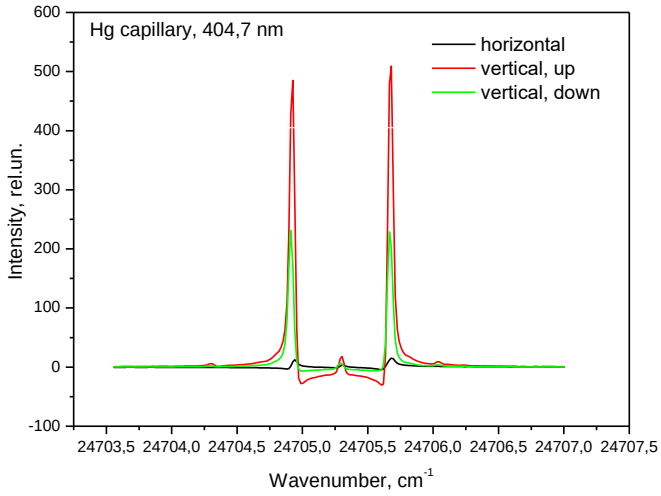

Fig. II.40 - Example of experimentally measured Hg 404.7 nm line. The line was emitted from Hg/Xe capillary light source placed in three different working positions: horizontally (black line), vertically with Hg reservoir up (red line), and vertically with Hg reservoir down (green line).

Figs. II.41(a) and II.41(b) show the results for the vertical lamp operation, with Hg reservoir up and Hg reservoir down, respectively. All experimental lines were normalised for the line shape future calculations in magnetic field. The line is split due to the Zeeman effect into one non-shifted π component and two σ components. The deconvolution was done using two independent methods Eq(I.50) and Eq(I.52) for finding the regularisation parameter.

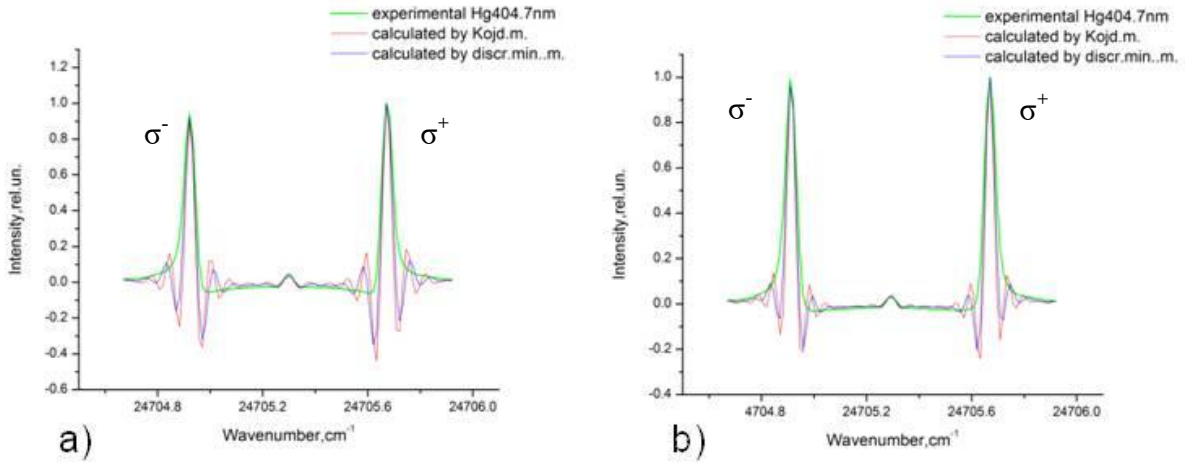

Fig. II.41 Measured and deconvoluted Hg 404.7 nm profiles: green line – experimental profile; blue and red lines – calculated real profiles, obtained using discrepancy minimization method for the getting of the regularisation parameter, and method when α is root of Eq(I.46), respectively. a) Lamp was operated vertically with Hg reservoir up. b) Lamp was operated vertically with Hg reservoir down.

After the deconvolution was performed Gauss fit to the calculated real lines.
In the Table 4 we can see the values of the full width at half of maximum (FWHM) of the Gauss profile. The values are shown for the Hg 404.7nm emission line for vertical position of the lamp. The results of the solutions are shown for both methods of finding the regularisation parameter.

Table 4.
The results of the deconvolution: the FWHM of the calculated real line shapes from the Gauss fit to the calculated real profiles for the Hg 404.7nm emission line for both vertical positions of the lamp.

FWHM(cm^{-1}) after Gauss fit	σ^-	σ^+	Lamp position
Experimental	0.05020	0.04746	Vertically, with Hg reservoir up
Real calculated (discr.min.met.)	0.03541	0.03437	
Real calculated (Kojdecki met.)	0.02893	0.02826	
Experimental	0.05072	0.05036	Vertically, with Hg reservoir down
Real calculated (discr.min.met.)	0.03518	0.03539	
Real calculated (Kojdecki met.)	0.02873	0.02903	

Both methods give credible results. However, we can observe that the Kojdecki method gives smaller values of the FWHM of the calculated real line shape than discrepancy method. It can be explained by the fact that the method proposed by Kojdecki strongly depends on errors of measurements and instrumental function. For application of the discrepancy minimization method it is necessary to know only the instrumental function. We can also observe that the signal for the horizontal lamp position is very weak (see Fig. II.40); therefore, the results of calculations for this working position were not taken into account for temperature estimation.

The average calculated temperature value (see Eq.I.5) of radiating atoms is of (650±126)K, which is in good agreement with our initial calculations **[Pr.5]**. The relative error is 19%. No clear evidence of the temperature changes in different working positions was found.

5.2. Investigation of the Hg lamp with different buffer gases (Ar, Xe, Kr) without magnetic field [Pr.8]

In this case the lamp was filled with argon of 2 Torr partial pressure and mercury isotope 198. The Hg 404nm, 435nm and 546nm line profiles (7^3S_1-$6_3P_{0,1,2}$ transition **[Appendix 6]**) were measured for further calculations, by means of Fourier Transform spectrometer. The example of experimental measurement of the 546.1 nm line (power 8.55W) is shown in Fig. II.42.

On the Figs. II.43 - II.45 the FWHM of the measured and calculated real profile dependency from the power can be seen. On Fig.II.43 can be seen the Hg 404.7nm line, on Figs. II.44 - II.45, 435.8nm and 546.1nm lines accordingly.

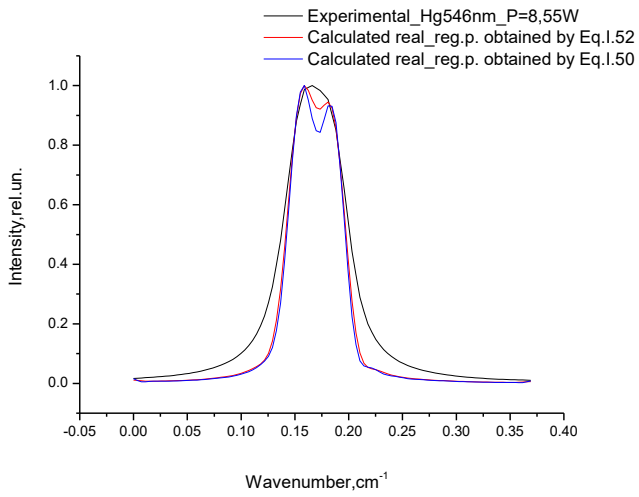

Fig. II.42 Example of measured and deconvoluted Hg 546.1 nm profiles: black line – experimental profile; blue and red lines – calculated real profiles, obtained using discrepancy minimization method Eq(I.50) for the getting of the regularisation parameter, and method when α is root of Eq(I.52), respectively.

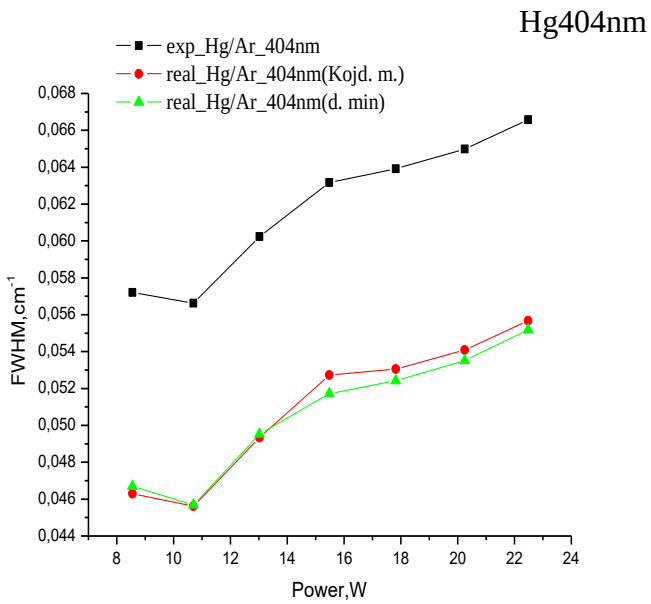

Fig. II.43 FWHM of measured and deconvoluted Hg 404.7 nm profiles: black line – experimental profile; green and red lines – calculated real profiles, obtained using discrepancy minimization method Eq(I.50) for the getting of the regularisation parameter, and method when α is root of Eq(I.52), respectively.

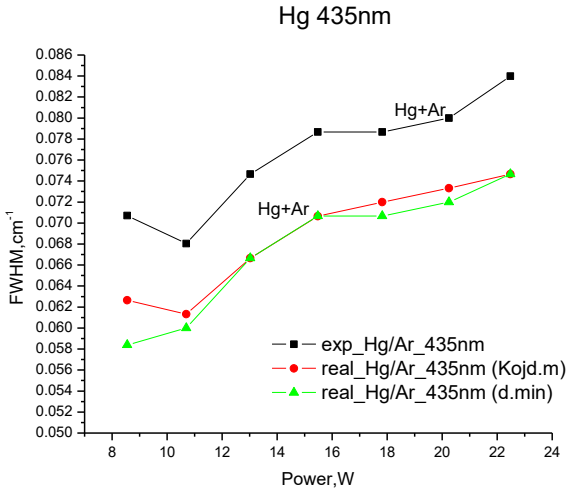

Fig. II.44 FWHM of measured and deconvoluted Hg 435.8 nm profiles: black line – experimental profile; green and red lines – calculated real profiles, obtained using discrepancy minimization method Eq(I.50) for the getting of the regularisation parameter, and method when α is root of Eq(I.52), respectively.

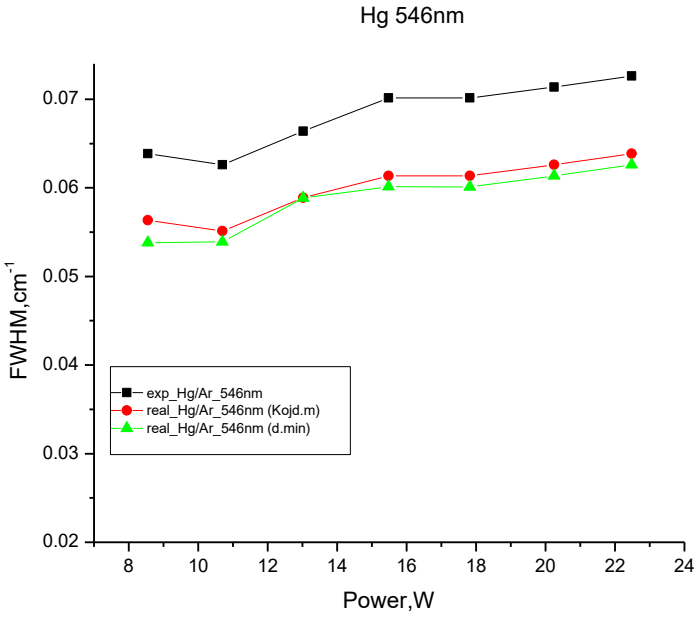

Fig II.45 .FWHM of measured and deconvoluted Hg 546.1 nm profiles: black line – experimental profile; green and red lines – calculated real profiles, obtained using discrepancy minimization method Eq(I.50) for the getting of the regularisation parameter, and method when α is root of Eq(I.52), respectively.

As can be seen on Figs. II.43 - II.45, the instrumental function significantly effects on the line width.

Below, the results of the deconvolution procedure for the Hg 546.1 nm visible triplet line can be seen. The line was emitted from Hg lamps with different buffer gases. For cases, when as buffer gaseswere used Kr and Xe, the Hg 202 isotope was used. In the case for Ar as the buffer gas, Hg 198 isotope was used. Figs. II.47- II.48 show the comparison of the results in cases, when as buffer gas Ar or Xe(Fig II.47) and Ar or Kr(Fig. II.48)were used. The results are given for two methods of finding the regularization parameter α: the Kojdecki method [**79**] and minimum of discrepancy method [**52**]. Both methods give similar results. It is interesting to observe that the line, emitted from the 198 isotope lamp, after deconvolution is self-absorbed.

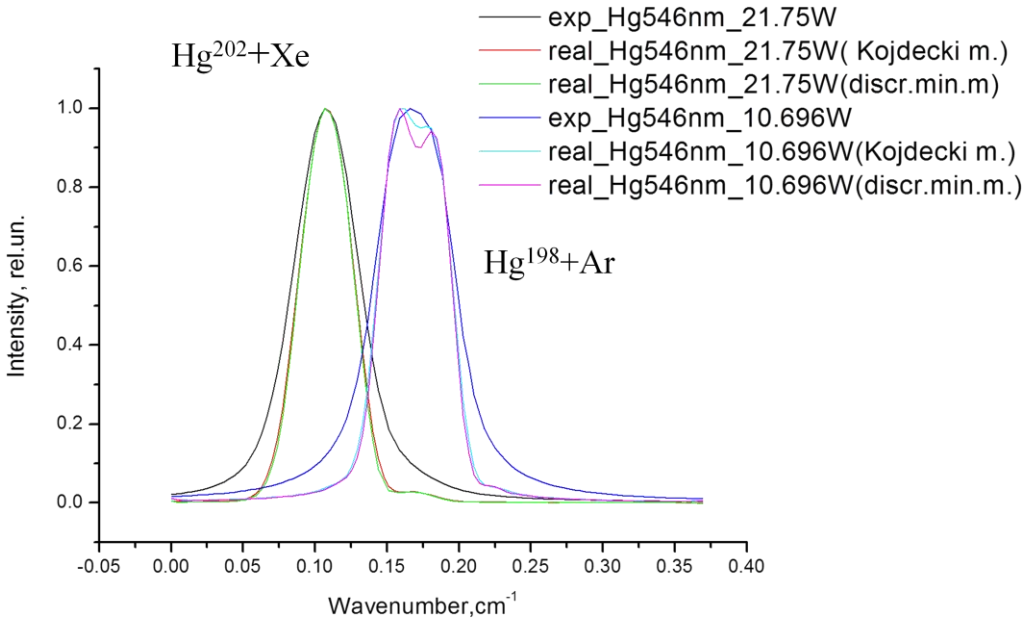

Fig. II.46 Example of measured and deconvoluted profiles of Hg 546nm; as buffer gas was used Ar (experimental profile- blue line; calculated real: light blue line(Eq.I.50); pink line (Eq.I.52)) and Xe(experimental profile- black line; calculated real: green line(Eq.I.50); red line (Eq.I.52)).

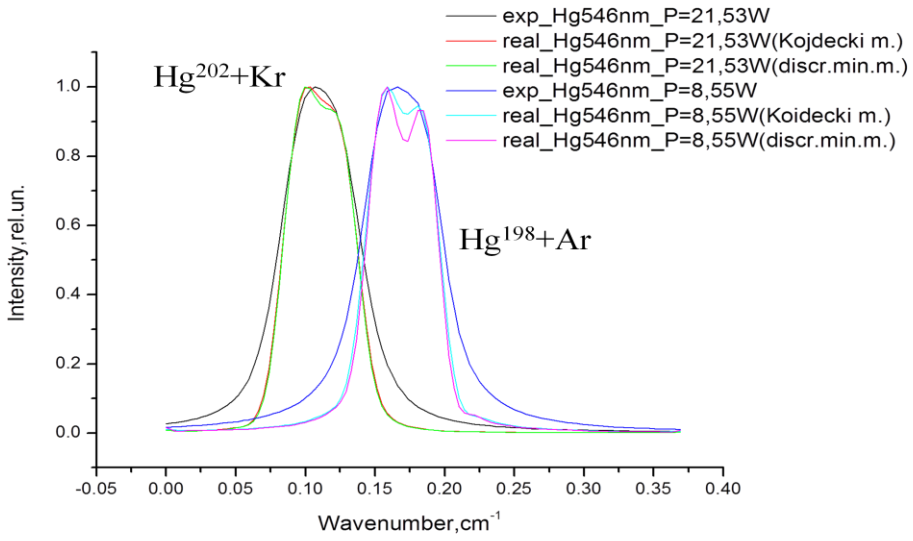

Fig. II.47 Example of measured and deconvoluted profiles of Hg 546nm; as buffer gas was used Ar (experimental profile- blue line; calculated real: light blue line(Eq.I.50); pink line (Eq.I.52)) and Kr(experimental profile- black line; calculated real: green line(Eq.I.50); red line (Eq.I.52)).

The obtained real FWHM for all the registered lines is shown in FigII.48. It is clearly demonstrated that the neglecting instrumental function can lead to large error in the full width calculations. Clear dependence of the FWHM of the type of buffer gas can be observed – the heavier the buffer gas, the colder the plasma. Adding Kr or Xe instead of Ar decreases FWHM and consequently decreases temperature.

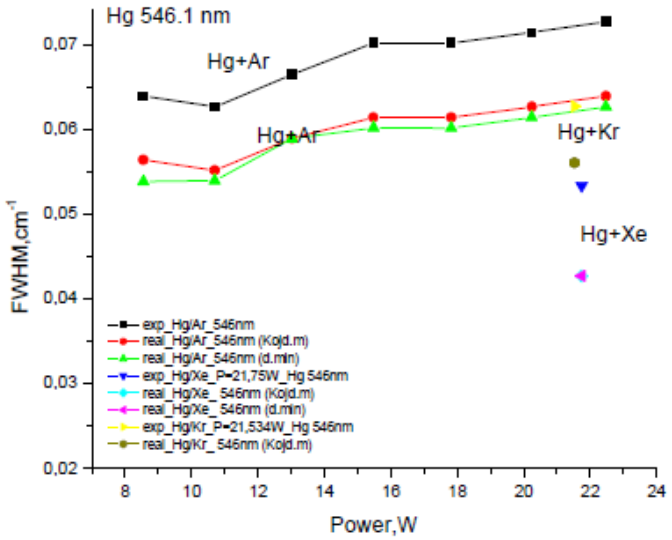

Fig. II.48 FWHM in dependence from the discharge power, calculated from the deconvoluted line shapes of Hg line 546.1 nm emitted from the Hg/Ar, Hg/Kr, Hg/Xe discharge plasmas

III. Concluding considerations

1. The new method of the diagnostic of the low temperature plasma in case of high-frequency electrodeless discharge lamps (HFEDLs) by means of the ill posed inverse task solution - the real spectral line deconvolution from experimental ones emitted from low temperatures plasma sources- was elaborated based on the Tikhonov's regularization principle. Two different methods for finding the regularization parameter were implemented. The elaborated method was tested on model tasks and on the examples of different type of microsize high frequency electrodeless lamps containing low temperature mercury discharge plasma. The spectral line profiles were measured by Zeeman spectrometer, Fabry-Perot interferometer, Fourier transform spectrometer. The specific instrumental functions for each of apparatus were used for restoring real line profile.

2. First time was developed new software for this method realization for different spectrometers: Zeeman spectrometer , Fabry-Perot interferometer, Fourier transform spectrometer with their instrumental function as analytical functions or as experimental data arrays.

3. To obtain the limits of the credibility, the solution of the model task was performed:

- with different ratio between instrumental function and measured profile [**Pr.2;**A2,Pr.7];
- with different level of noise[A3, Pr.7].

4. The solution of the model examples shows that this method can be used for the narrow spectral profiles restoring if the following conditions can be performed[Pr.7]:

- normal level of the noise. The variance of data must be less than 0.1;
- the ratio between instrumental function and measured profile can be less or equal of 2.

5. First time the new method was used for the diagnostics of the microsize Hg high-frequency electrodeless lamps for their application in atomic absorption spectrometry.

6. The new diagnostic method was tested using experimental spectral line shapes without and with presence of magnetic field.

7. First time with this method, for high frequency electrodeless lamps(Hg^{198}), were obtained the results for the mercury resonance 184.9 nm line profile, 6^1S_0-6^1P_1transitions:

- line measured by means of Zeeman spectrometer : [**P1**; **Pr.1;**A1]

8. First time with this method, for high frequency electrodeless lamps(Hg^{202})were obtained the results for the mercury resonance 253.7 nm line profiles, 6^1S_0-6^3P_1transitions:

- line measured by means of Fabry-Perot interferometer [**P2**; A5]- dumbbell like lamp;
- line measured by means of Zeeman spectrometer**: [Pr.3; Pr.4;**A1;A4]- microsize capillary lamp.

9. First time with this method, for microsize capilary high frequency electrodeless lamps (Hg^{202}, Hg^{198}), were obtained the results for the mercury visible triplet (with the wave lengths Hg 404,7 nm, 435.8 nm, 546.1 nm respectively) 7^3S_1-$6^3P_{0,1,2}$ transitions

a) lines measured by means of Fourier transform spectrometer in magnetic field[**P3, Pr.5;Pr.6;**A6;A7];

b) lines measured by means of Fourier transform spectrometer without magnetic field.

10. For the validation of the method, some results were compared with the results obtained by modelling of the spectral line profiles [**P1; Pr1;** A1**;**]. The results obtained by the method developed in this work are in good agreement with results obtained by the method of spectral line modelling. That gives possibility to perform the solution by method presented above when another method has restriction (limitations). The disadvantage of the line profile modelling method is that the functions of the line profiles have to be known

before and it is applicable manly for the symmetric lines. For the usage of described in this work method of diagnostics of low temperature plazma in case of HFEDL, that based on the Tikhonov's regularization algorithm, the only parameter what we have to know *a priori* is - the instrumental function. Both methods can be used for bigger credibility in the difficult cases.

11. It was found out that the neglecting the instrumental function, in the case of low – temperature plasma where typically the instrumental function is on the same order that experimental profile, gives huge error for the FWHM estimation and consequently for discharge temperature estimation. The influence of the type of buffer gas was investigated also.

IV. List of publications[1](Scopus)

[P1] G.Revalde, A.Sholupov, A.Skudra, N.Zorina, **Investigation of Hg resonance 184.9 nm line profile in a low-pressure mercury-argon discharge**, JQSRT, 107 (2007) 164–172

[P2] N. Zorina, **Deconvolution of the spectral line profiles for the plasma temperature estimation**, Nuclear Inst. and Methods in Physics Research A 623 (2010) p. 763-765 (doi:10.1016/j.nima.2010.02.085)

[P3] G. Revalde, N. Zorina, A. Skudra, Z. Gavare, **Deconvolution of the line spectra of microsize light sources in the magnetic field**, Romanian Reports in Physics, Vol. 66, No. 4, P. 1099–1109, 2014

I agree that the research results reported in above mentioned publications are used in this work.

_____/G.Revalde/

[1]Coresponding author of [P1] – Gita Revalde;

Corresponding author of [P2] – author of this work N.Zorina;

Corresponding authors of [P3] – author of this work N.Zorina and G.Revalde.

V. List of proceedings

[Pr.1] G.Revalde, S.Sholupov, A.Skudra, N.Zorina, **Study of Hg resonance 185 nm line profile**, Proceedings of XXVII International Conference on Phenomena in Ionized Gases,July 17 – 22, 2005, The Netherlands, Eindhoven, N. 08 – 192

[Pr.2] N. Zorina, G. Revalde, A. Skudra**, Calculation of the real spectral line shape by solving the ill-posed inverse problem**, Proceedings of XXVIII International Conference on Phenomena in Ionized Gases, Czech Republic, Prague, July 15 – 20 ,2007, 543 - 545.

[Pr.3] N. Zorina, G. Revalde, R. Disch, **Deconvolution of the mercury 253.7 nm spectral line shape for the use in absorption spectroscopy**, *Proc.* ***SPIE*** 7142, Sixth International Conference on Advanced Optical Materials and Devices (AOMD-6), 71420J (December 02, 2008); doi:10.1117/12.815460 **(Scopus)**

[Pr.4] N. Zorina, G. Revalde, A. Skudra, **Discharge plasma diagnostics by means of spectral line profile studies**, The 20th European Conference on the Atomic and Molecular Physics of Ionized Gases, P.2.37, 13-17 July 2010, Novi Sad, Serbia

[Pr.5] G. Revalde, N. Zorina, J. Skudra, A. Skudra, **Diagnostics of capillary light sources by means of line shape measurements and modeling**, IOP Publishing, Journal of Physics Conference Series Volume 397, Number 1, 2012 , pp. 12070-12073(4), (DOI:10.1088/1742-6596/397/1/012070) **(Scopus)**

[Pr.6] G. Revalde, N. Zorina, A. Skudra, **Deconvolution of multiple spectral lines shapes by means of Tikhonov's regularization method**, in Imaging and Applied Optics, OSA Technical Digest (Fourier Transform Spectroscopy, FTS 2013; Arlington, VA; United States; 23 June 2013 through 24 June 2013) (**Optical Society of America**, 2013), paper JTu4A.12. (http://dx.doi.org/10.1364/AOPT.2013.JTu4A.12) **(Scopus)**

[Pr.7] N. Zorina, G. Revalde, A. Skudra, **Validation of the solution method using Tikhonov regularization algorithm for spectral line diagnostics of microsize plasma**, *Proc.* ***SPIE*** 9421, Eighth International Conference on Advanced Optical Materials and Devices (AOMD-8), 94210H (October 22, 2014); doi:10.1117/12.2083842**(Scopus)**

[Pr.8] G. Revalde, N. Zorina, A. Skudra, **Line Shape Measurement and Modelling for Plasma Diagnostics**, IOP Publishing, J. Phys.: Conf. Ser. Vol.548 (2014)012034 (doi:10.1088/1742-6596/548/1/012034) **(Scopus)**

VI. List of abstracts

[A1] N. Zorina, G. Revalde, A. Skudra, S. Sholupov, **Recovering of mercury 185 nm and 254 nm resonance line profiles**, Abstracts of 18th European Conference on Atomic and Molecular Physics of Ionised Gases, July 12 – 16 (2006), Lecce, Italy, pp. 323. – 324 http://users.ba.cnr.it/pfambrico/_downloads/BookESCAMPIG18.pdf

[A2] N. Zorina, G. Revalde, A. Skudra, **Calculation of the real spectral line shape by solving the ill-posed inverse problem**, Abstracts of XXVIII International Conference on Phenomena in Ionized Gases, Czech Republic, Prague, July 15 – 20 (2007) 48

[A3] N.Zorina, G.Revalde, A.Skudra, **Ill-posed inverse problem solving using two methods of choosing of regularization parameter**, Abstracts of 19th European Conference on Atomic and Molecular Physics of Ionised Gases (ESCAMPIG -2008), Granada, Spain, 15 – 19 July (2008), 3-99 (http://www.escampig2008.csic.es/PosterSessions/286.pdf)

[A4] N. Zorina, G. Revalde, R. Disch, **Deconvolution of the Mercury 253.7 nm Spectral line shape for the use in Absorption Spectroscopy**, Abstracts of the 6th International Conference "Advanced Optical Materials and Devices" (AOMD-6), Riga, Latvia, 24 – 27 August (2008), p.62.

[A5] N. Zorina G. Revalde,A. Skudra, **Deconvolution of the spectral line profiles for plasma temperature estimation**, 1st International Conference on "Frontiers in DiagnosticTechnologies", Roma, Italy, November 25-27, 2009 , Abstract ID 63

[A6] Gita Revalde, Janis Skudra , Natalia Zorina, Egils Bogans, **Diagnostics of Capillary Light Sources by Means of Line Shape Measurements and Modeling,** ICSLS-21 International Conference on Spectral Line Shapes, Saint-Peterburg, Russia, June 3-9, 2012, p 87

[A7] G. Revalde, Z. Gavare, N. Zorina, A. Skudra, **Diagnostics of microsize light sources in magnetic field**, In abstracts of 16th International Conference on Plasma Physics and Applications (CPPA 2013), Magurele, Bucharest, Romania, June 20-25, 2013, p.81

[A8] N. Zorina, G. Revalde, A. Skudra, **Validation of the solution method using Tikhonov regularization algorithm for spectral line diagnostics of microsize plasma**, Abstracts of the 8th International Conference "Advanced Optical Materials and Devices" (AOMD-8, Riga, Latvia, 24 – 27 August (2014), p.65.

VII. References

1. S.A. Kazantsev, V.I. Khutorshchikov, G.H. Guthöhrlein, L. Windholz, **Practical Spectroscopy of HF Discharges**, Plenum Press, New York, p. 337,(1998);
2. J.F. Waymouth, **LTE and Near –LTE Lightening Plasmas**, IEEE Trans. On Plasma Science 19, pp.1003-1012, (1991);
3. Ganeev A, Gavare Z, Khutorshikov V I, Khutorchikov S V,Revalde G, Skudra A, Smirnova GM, Stankov, **High-frequency electrodeless discharge lamps for atomic absorption spectrometry,** Spectrochimica Acta Part B 58,pp. 879–8891 (2003) ;
4. V. Lebedeva , **The technique of the optic spectroscopy** ,Moscow: Moscow university, pp.353,(1977);
5. **Inductively Coupled Plasma Spectrometry and its Applications**, Edited by Steve J. Hill School of Earth, Ocean and Environmental Sciences University of Plymouth Plymouth, UK 2007 by Blackwell Publishing Ltd;
6. E. Frish, **Spectroscopy of the gas discharge plasma**, Nauka, Leningrad, 9-11(1970);
7. W. Demtroeder, **Laser Spectroscopy**, third ed, Springer, p. 70, (2003);
8. J.M. Luque, M.D. Calzada, M. Saez, **A new procedure for obtaining the Voigt function dependent, upon the complex error function**, Journal of Quantitative Spectroscopy & Radiative Transfer 94, 151–161, (2005);
9. G.D. Rostona, F.S. Obaid, **Exact analytical formula for Voigt spectral line profile**, Journal of Quantitative Spectroscopy & Radiative Transfer 94, 255–263, (2005);
10. H.O. Di Rocco, **The exact expression of the Voigt profile function**, Journal of Quantitative Spectroscopy & Radiative Transfer 92, 231–237,(2005);
11. G.Revalde, D.Berzina, V.Lhevkovski, L.Luizova, S.Putnina, P.Reppo, et al., **The automatic spectrometric complex for spectral line profile measurements**, J Appl Spectrsc, 56, 681–686 ,(1992);
12. V.Revalds, **Spektrālie aparāti**, University of Latvia, part 3, (1977),
13. O. Vasiljev, A. Kotkin, D. Stoljarov, D. Chopornjak, R.Umorhodzhajev , **High-frequency electrodeless light sources**, Riga, Latvia: Acta Universitatis Latviensis,p. 105(1992);
14. A.A. Ganeyev, S.E. Sholupov, M.N. Slyadnev, **Zeeman modulation polarization spectrometry as a version of atomic-absorption analysis:potentials and limitations**, J Anal Chem 51:788,(1995);
15. P. Griffiths and J. de Haseth, **Fourier transform infrared spectrometry**, Wiley & Sons, (1986);
16. B.N.Tarasevich, **Bases infrared Fourier transform spectroscopy**,Moskow State University,2012 (http://www.chem.msu.su/rus/teaching/tarasevich/Tarasevich_FT-IR_basic.pdf)
17. G. Revalde,_, N. Denisova, Z. Gavare, A. Skudra, **Diagnostics of capillary mercury–argon high-frequency electrodeless discharge using line shapes**,Journal of Quantitative Spectroscopy & Radiative Transfer, 94, 311–324,(2005);

18. G.U. Babat, **Electrodeless discharges and some allied problems**, J. Inst. Elec. Eng. Lond. 84, 27–37(1947);
19. Annemie Bogaerts, Erik Neyts, Renaat Gijbels, Joost van der Mullen, **Gas discharge plasmas and their applications**, Spectrochimica Acta Part B 57 , 609–658,(2002);
20. W. Bell, A.L. Bloom, **Electrodeless discharge method and apparatus**, US Patent 2975330, (1961);
21. G. Revalde, J. Silinsh, J. Spigulis and A. Skudra, **High-frequency electrodeless light sources for application**, *SPIE* Proc 4318, pp. 78–83,(2000)
22. Atis Skudra, Gita Revalde, Zanda Gavare, **Natalia Zorina**, **Study of Inductive Coupled Hydrogen and Argon Plasma Interaction with SiO2 Glass**, Plasma Process. Polym., 6, S183–S186,(2009);
23. M. Baeva, D.Reiter, **Monte Carlo simulation of radiation trapping in Hg–Ar fluorescent discharge lamps**, Plasma Chem Plasma Process 23(2),(2003);
24. K. Rajaraman, M.J.Kushner, **A Monte Carlo simulation of radiation trapping in electrodeless gas discharge lamps**, J Phys D, 37:1780, (2004);
25. A. Bukhgeim, M.Lavrentjev, **Introduction to the theory of Inverse Problems**, Novosibirsk: Nauka (1988);
26. C.W. Groetsch, **Inverse problems in the mathematical sciences**, Providence,AMS, (1993);
27. H.W. Engl, M. Hanke, A. Neubauer, **Regularization of inverse problems**, Dordrecht, Kluwer, (1996)
28. N.Preobrazensky, A. Sidelnikov, **Optimization of the spectroscopic measurements on the basis of regularization methods**, Journal of Applied Spectroscopy, V. XXXV, 4, 592-599, (1981) ;
29. M. Glazov, T. Bolohova, **The solution of the Rayleigh reduction problem by using various modifications of the method of regularization**, Optics and Spectroscopy, V.67, 3, 533-537, (1989);
30. I.Konchikov, G.Kuramshina, Yu.Pentin, A. Yagola, **Inverse problems of vibrational spectroscopy**, Moscow: Moscow Univ., (1993);
31. V.S. Sizikov, M.J. Marusina, S.V. Ivanov, T.B .Kolobuhova, D.B. Nikolaev, D.Y. Sokolov, E.V. Homutnikova, **Direct and inverse problems of synthesis of magnetic field in MRI**, Science & Technology newsletter, Issue 3, Physical processes, systems and technology of Precision Mechanics, St. Petersburg State Institute of Fine Mechanics and Optics (Technical University), St.Petersburg , p.209-214,(2001);
32. V. Pikalov, N. Preobrazensky, **Reconstructive tomography in the gas dynamics and plasma physics**, Novosibirsk:Nauka, (1987)
33. M. Piana and M. Bertero, **Regularized deconvolution of multiple images of the same object**, J. Opt. Soc. Am. A/Vol. 13, No. 7/July,p.1516-1523, (1996);
34. A Bouhamidi, K. Jbilou, **Sylvester Tikhonov-regularization methods in image restoration,** Journal of Computational and Applied Mathematics 206, 86 – 98,(2007);
35. V.Morozov, **Some aspects of the recovery of the signals by the regularization method**, Numerical methods and programming,V.2, 27-33,(2001);
36. G. Vasilenko, **Theory of recovery of the signals**, Moscow, Soviet Radio (1979);

37. K. Parchevsky, V. Parchevsky, **Restoring of instantaneous velocity from the experimental data by means of A.N. Tikhonov regularization**, Sea ecology, , Issue.55,.87-91,(2001)
38. K. Parchevsky, **Using regularizing algorithms for the reconstruction of growth rate from the experimental data,** Ecol. Modelling, 133, № 1-2, 107 – 115, (2000);
39. A.Goncharsky, A.M. Cherepashchuk A.G. Yagola, **Ill-posed problems in astrophysics**,Moskow: Nauka, (1985);
40. N. Preobrazhensky, V. Pikalov, **Unstable problems of the diagnostics of plasma**, Novosibirsk:Nauka, (1982);
41. A. Tikhonov, A. Leonov, A. Yagola, **Nonlinear ill-posed problems**, Moskow: Nauka, (1995) ;
42. V.Ivanov, V.Vasin, V. Tanana, **Theory of linear ill-posed problems and its applications**, Moskow: Nauka, (1978)
43. 43. M.Lavrentjev, V. Romanov, S. Shishatskiy, **Ill-posed problems of mathematical physics and analysis**, Moskow: Nauka, (1980));
44. A. Tikhonov, V.Arsenin, **The solution's methods of the ill- posed problem**, Moscow: Nauka (1979),
45. Yu.P. Petrov,V.S.Sizikov,**Well-Posed,Ill-Posed and Intermediate problems with Applications**, Publisher V.S.P. Intl Science,(2005)
46. V.S. Sizikov, **Stable methods of processing of the results of measurement**, Tutorial. - St.Petersburg "SpetsLit", (1999);
47. V.A.Morozov , **Regular methods of solution of the ill-posed problems,** Moskow: Nauka, p5(1987)
48. A. Skudra, G.Revalde, **Mathematical modeling of the spectral line profiles in the high-frequency discharge** , JQSRT 61, N6, pp 717-728, (1999);
49. A.Bakushinsky, A.Goncharsky, **Iterative methods of solution of the ill-posed problems**, Moskow: Naukа, (1989)
50. O.M. Alifanov, E.A.Artjuhin, Rumjancev, **Extreme methods of the solution of the ill posed tasks**, Moskow:Nauka,(1988);
51. S.F.Giljazov, **The methods of the solution of the lineal ill-posed tasks**,Moskow:The university of Moskow, 54,**(**1987);
52. F. Verlan, V.S Sizikov, **The integral equations: the methods, algorithms, program**, Kiev: Naukova Dumka (1986);
53. V.A. Morozov, **Algorithmic basis of the methods of solution of ill-posed problems**, Numerical methods and programming,V.4, 130-141,(2003);
54. B.A. Mair, F.H. Ruyngart **A cross-validation method for first kind integral equations**, J. Comput. Control IV, 20, pp. 259–267,(1995);
55. Xiang-Tuan Xiong, Chu-Li Fu, Hong-Fang LiJ, **Fourier regularization method of a sideways heat equation for determining surface heat flux**, Math Anal Appl, 317:331–48, (2006);
56. K. Maleknejad, **A comparison of Fourier extrapolation methods for numerical solution of deconvolution**, Applied Mathematics and Computation 183, 533–538, (2006);

57. Yu E.Voskoboynikov, NG Preobrazhensky, AI Sedelnikov , **Mathematical processing of the experiment in the molecular gasdynamics**, Novosibirsk: Nauka, (1984),
58. A. Tikhonov, A. Goncharski, V. Stepanov, A. Jagola , **Numerical solution's methods of the ill-posed problem** ,Moscow: Nauka, (1990);
59. A. Tikhonov, V.Arsenin, **The solution's methods of the ill- posed problem**, Moscow: Nauka (1979);
60. C.W Groetsch, **The theory of Tikhonov regularization for Fredholm equations of the first kind**, London: Pitman (1984).
61. A.N. Tihonov, **The regularization of the ill-posed problems**, DAN USSR, V.153, N 1, (1963);
62. A. Tihonov, A. Goncharskij, V. Stepanov, A. Jagola , **Regularizing algorithms and priori information**, Moskow:Nauka, (1983) ;
63. M. P. Rajan, **An efficient discretization scheme for solving ill-posed problems**, J. Math. Anal. Appl. 313, 654–677,(2006);
64. N.G. Preobtazhenskij, B.Z.Tambovcev, **Excluding of the corruption of apparatus, of the spectral lines by means of the statistical regularization method**, V.XXXV, Issue5, Optics and Spectroscopy, 946-953,(1973);
65. V.F.Turchin, L.S.Turovtseva, **The recovery of the optical spectra, and other non-negative functions by means of a method of statistical regularization**, V.XXXVI, Issue 2, Optics and Spectroscopy, 280-287, (1974);
66. V.Turchin, V.Kozlov, M. Markevich, **The usage of the methods of the mathematical statistics for solving ill-posed problems**, Uspekhi-fizicheskikh-nauk, V. 102, №3, 345-386,(1970);
67. N.G.Preobrazhenskii ,**Spectroscopy of Optical Thick Plasma**, Novosibirsk: Nauka, p. 177,(1971);
68. R. D Cowan, G. H Dieke, **Self-Absorption of Spectrum**, Lines.Rev. Mod. Phys2 ,418,(1948);
69. G.M. Petrov, **A simple algorithm for spectral line deconvolution**, Journal of Quantitative Spectroscopy &Radiative Transfer 72, 281–287, (2002);
70. L.A Lyusternik, S.L Sobolev, **Elements of the functional analysis**, Moskow:Nauka, (1965);
71. S.L Sobolev, **Some applications of the functional analysis in the mathematical physics**, Moskow:Nauka,(1988);
72. Hyoung Gil Choi1, Anand N. Thite, David J. Thompson, **Comparison of methods for parameter selection in Tikhonov regularization with application to inverse force determination**, Journal of Sound and Vibration 304, 894–917,(2007);
73. V. Sizikov, **The methods of the discrepancy in the solution of the ill-posed problems**, Computational Mathematics and Mathematical Physics Journal, V. 43. № 9. p. 1294–1312,(2003);
74. H.W .Engl, **Discrepancy principles for Tikhonov regularization of ill-posed problems leading to optimal convergence rates**, J. Optimizet. Theory Appl., V.49, 209-215,(1987);
75. V. Sizikov, **The new version of the a posteriori selection of the regularization parameter in the ill-posed problems**, the International Conference «Inverse and

ill-posed problems of mathematical physics", dedicated to the 75th anniversary of academician M.M.Lavrentev, 20-25 August 2007, Novosibirsk, Russia http://www.math.nsc.ru/conference/ipmp07/abstracts/Section3/SizikovVS.doc

76. F. Bauer,S. Kindermann, **The quasi-optimality criterion for classical inverse problems,**Inverse Problems 24 035002, (20pp), (2008),doi:10.1088/0266-5611/24/3/035002;

77. A. Griesbaum, B. Kaltenbacher, B. Vexler, **Efficient computation of the Tikhonov regularization parameter by goal-oriented adaptive discretization**, Inverse Problems 24 025025 (20pp) (2008), doi:10.1088/0266-5611/24/2/025025;

78. V.A. Morozov, **The discrepancy principle for solution of the incompatible equations by Tikhonov regularization method**, Computational Mathematics and Mathematical Physics Journal, V.13, N 5,(1973);

79. M.A. Kojdecki, **New criterion of regularization parameter choice in Tikhonov's method** , Biuletyn WAT (Biul. Mil. Univ. Technol.), V. 49. № 1 (569),47–126,(2000);

80. D. Kirjanov, **MathCad 13**, St. Petersburg, BHV-Petersburg, (2006);

81. D. Kirjanov, **MathCad 12**, St. Petersburg, BHV-Petersburg, (2005);

82. N. Kuljtin, **Delphi 6. Programming in Object Pascal**, St. Petersburg, BHV-Petersburg, (2001);

83. A. Archangelskiy, **Programming in Delphi 7**, Moskow, Binom, (2003);

84. S. Nemnjugin, **Turbo Pascal**, St. Petersburg, Piter, (2000);

85. N. Bahvalov, **Numerical methods**, Moskow:Nauka, V.1(1973);

86. G. Marchuk, **Methods of the Computational Mathematics**, Moskow:Nauka, (1977);

87. A.Buhl,. P Zofel, **SPSS, Art of information processing**, Moscow, St. Petersburg, Kiev, DiaSoft, (2005);

88. G. Revalde, N.Denisova, Z.Gavare, A.Skudra, **Diagnostics of capillary mercury–argon high-frequency electrodeless discharge using line shapes**, J.Q.S.R.T. 94 ,311–324,(2005);

89. G.Revalde, A Skudra, **Estimation of the spectral line profiles in the high-frequency discharge**, Spectral line shapes Vol.10, 14th ICSLS, 179-182,(1998)

90. **Tables of physical quantities**, handbook, Moscow: Atomizdat, 199(1976);

91. N.Denisova, G.Revalde, A.Skudra, and Ja.Skudra, **Spatial Diagnostics of Hg/Ar and Hg/Xe Discharge Lamps by Means of Tomography**, Jpn. J. Appl. Phys. 50, 08JB03, (2011)

Acknowledgements

I would like to express my deepest gratitude to my supervisors: Dr.phys. Atis Skudra and Dr.phys. Assoc.Prof. Gita Revalde, for their huge support, patience and imparted knowledge. My greatest thanks to all my colleagues at the Institute of Atomic physics and Spectroscopy(University of Latvia) for consultation and moral support and Dr.Phys.M.Tamanis for help with measurements by means of Fourier transform spectrometer.

This work partly supported by ESF project: „Spectrometric techniques for detection of heavy metal contaminants”No. 2009/0210/1DP/1.1.1.2.0/09/APIA/VIAA/100 and by the National Research Programme of Latvia"The next generation of information and communication technologies" (NexIT).

Appendixes

Appendix 1.

Bellow we can see the screenshot of the main program written in Math Cad. The program has three parts. There are measured data entering, it interpolation(b(t)) and instrumental function(A(x)) entering in the first part of the program. The instrumental function can be given as data array also. In this case, instead of formula we enter the data as matrix and do approximation similarly as was done for measured data. The results of the interpolation of the measured data and instrumental function can be seen on the first and second graphs, accordingly.

The solution of the ill-posed inverse task will be done in the second part. The regularization parameter were obtained by means of two methods: discrepancy minimization(I.50) and by Kojdecky method(I.52).

The results are shown and can be saved in the third part.

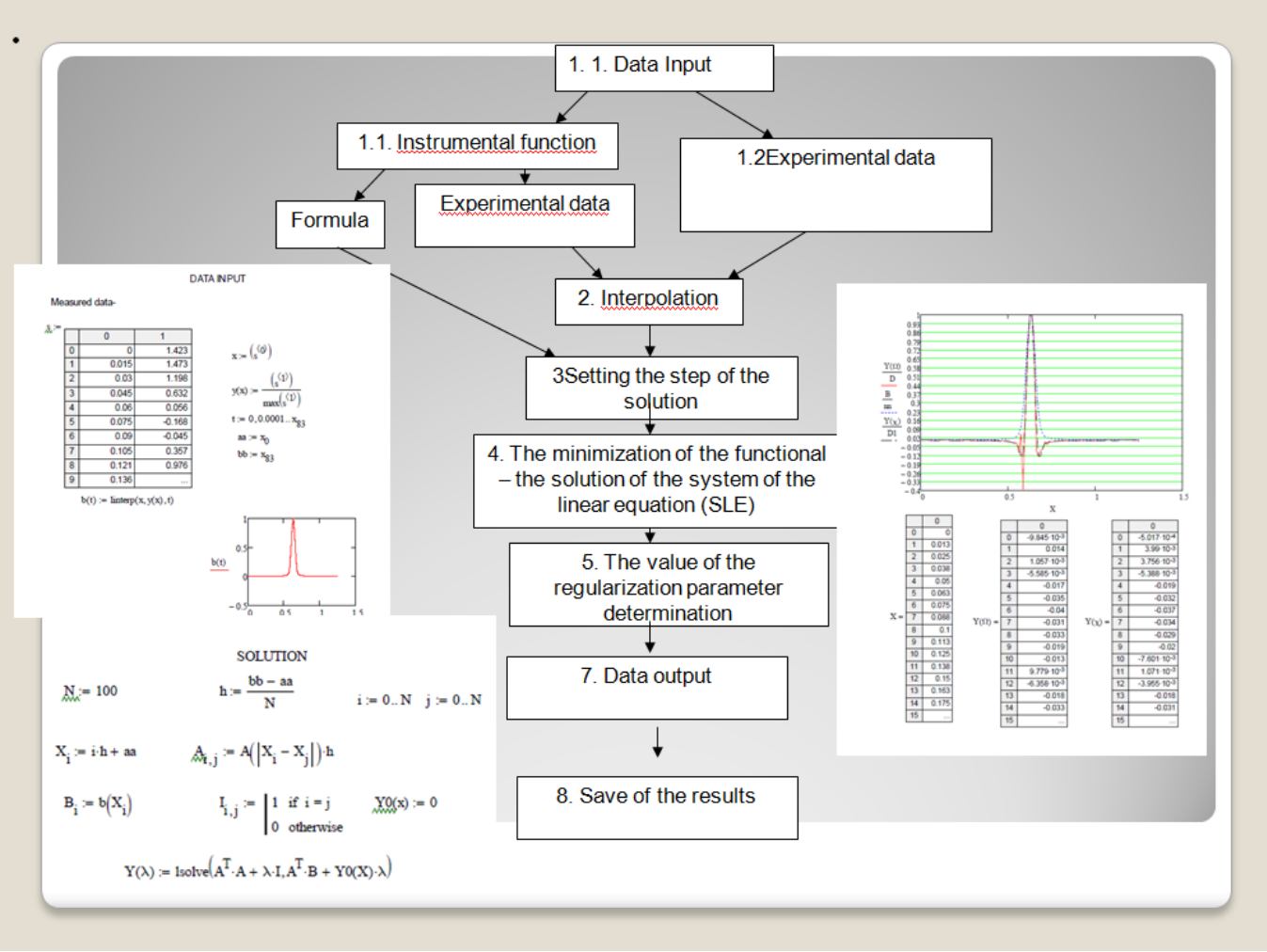

Appendix 2

Bellow we can see the screenshot of the program written in Delphi7. As we can see the program has two parts. There are measured data entering, it interpolation and instrumental function entering in the first part of the program. The solution of the ill-posed inverse task will be done in the second part.

The measured data have to be saved in Microsoft Excel format. First of all we have to open the file with data of measured profile -button "open Excel". The number of row of Excel file we have to write in window on the right side of the button. For future calculation the data must be interpolated-button "interpolate". Measured and interpolated data can be seen on the first graph: red line-measured, green line-interpolated profile. After that we have to choose the type of instrumental function, to write the FWHM of it in the window on the right side and press the button "AF" . If we choose the option –"Data", we have to press button „Open Excel (AF)" and after that only press the button "AF". The measured instrumental function can be seen on the graph with caption: "Measured data".

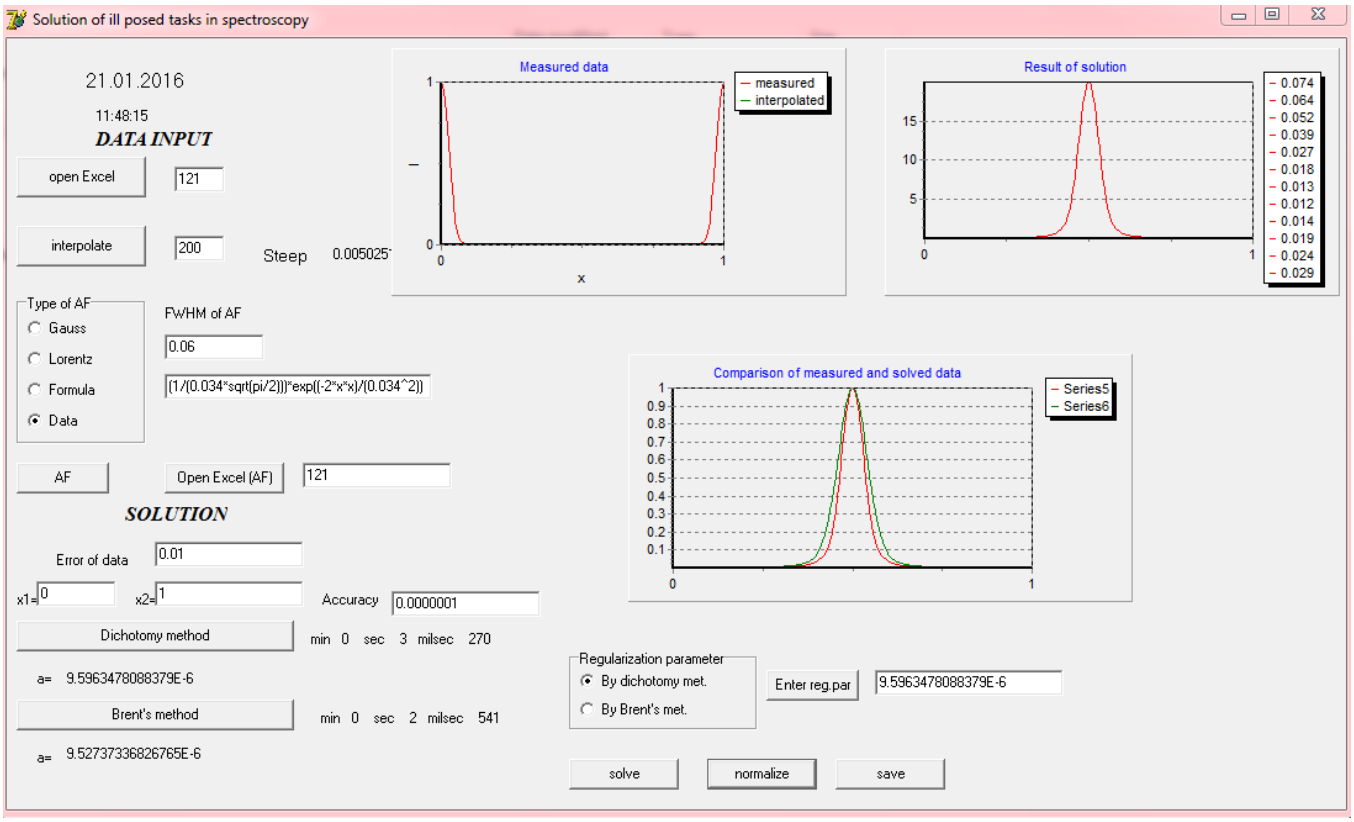

Solution implemented according Eq.II.45 that is why for solution necessary to know the error of the measured data. There are 0.01 in the example above, but of course, it have to be changed to another value in dependence of concrete task. Than have to be entered accuracy of solution (all calculations were performed with the $1*10^{-7}$ accuracy in this work). For regularization parameter obtaining, necessary input value of solution limits and to choose the numerical algorithm. There are two algorithms in the program: dichotomy method and Brent's method. How long the program counts according each of method, can be seen on the right part of the buttons with according title. Then have to be chosen the value of regularization parameter, which will be used in program (in example above, for future calculation was chosen value of regularization parameter, obtained by means of dichotomy algorithm). After button "solve" pressing, the solution was done. The result of solution can be seen on the graph2 and on the graph 3 with comparison with initial data. After pressing "save" button we get the standard window of Microsoft Wiindows for data saving. The data can be saved as text file for future processing.

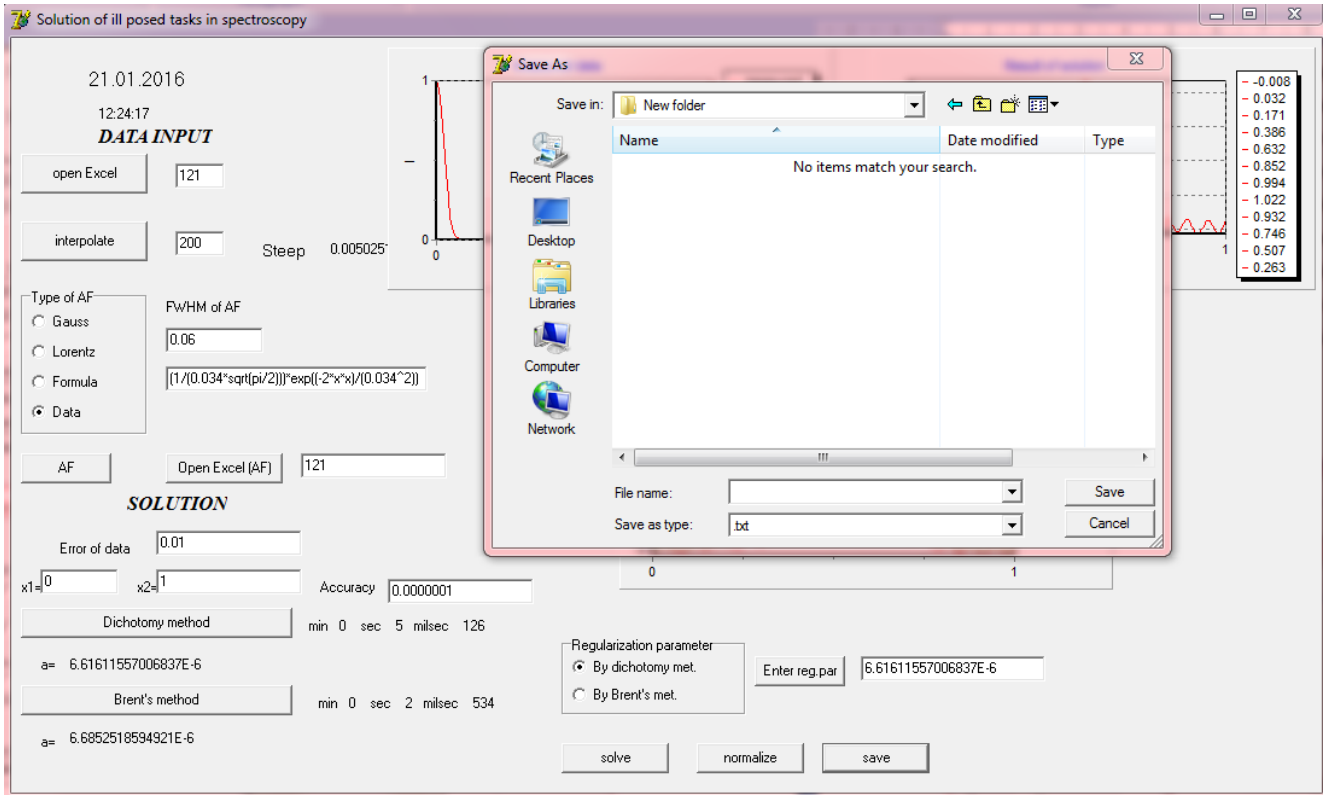

Appendix 3

Bellow we can see the block sheme and screenshot of the program written in Delphi7. This programm is written for temperature or/and FWHM estimation.

If we would like to obtain the temperature of radiating atoms, we have to input the FWHM of measured line in cm^{-1} , length of wave in nm and mass number(M). Atherwise, we have to insert the value of temperature (T,C^0), to obtain the FWHM of line.

Block scheme of program of obtaining of temperature

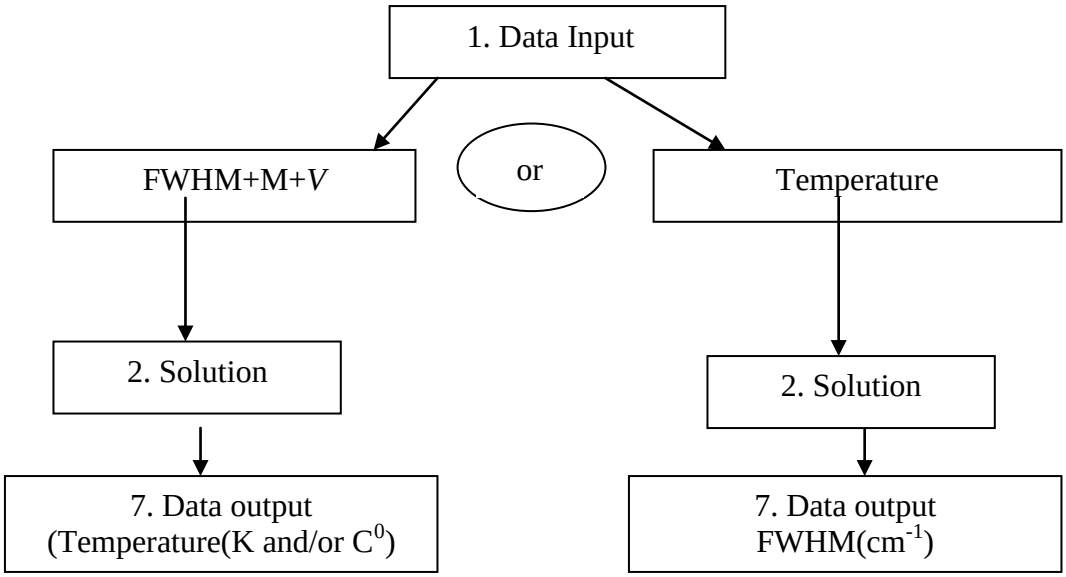

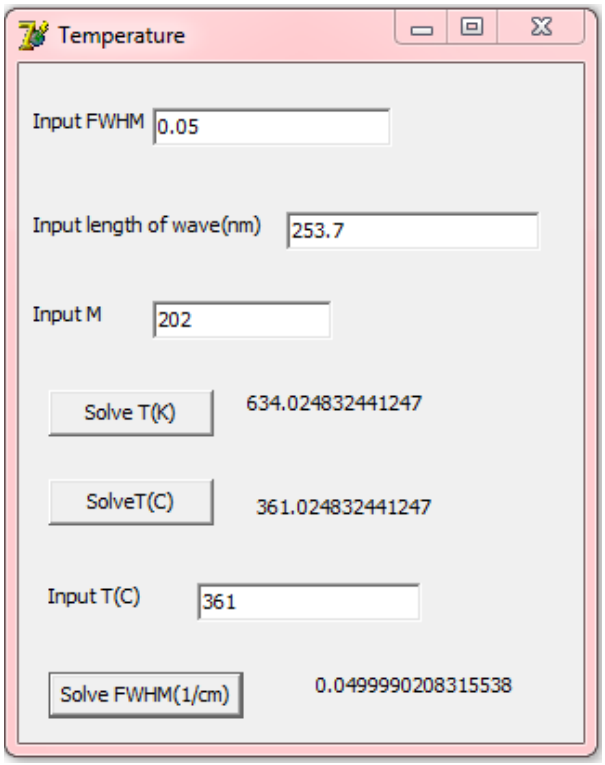

Appendix 4.

Bellow we can see the blockscheme of the program written in Math Cad for obtaining of the value of self absorption of line. First of all we have to input necessery values : wave length, pressure,temperature,oscilator strength, the values of width of line ($\Delta\nu$),etc.(see Eqs.I.7-I.9) After data entering, first of all, can be obtained absorption coefficient and optical density. Using Ladenburg – Levi function we get the values of self absorption of line. At the end we get the values of FWHM, taking into account the influence if self-absorption, and can save the results for further calculations.

Block scheme of program of obtaining of FWHM, taking into account the influence of self-absorption

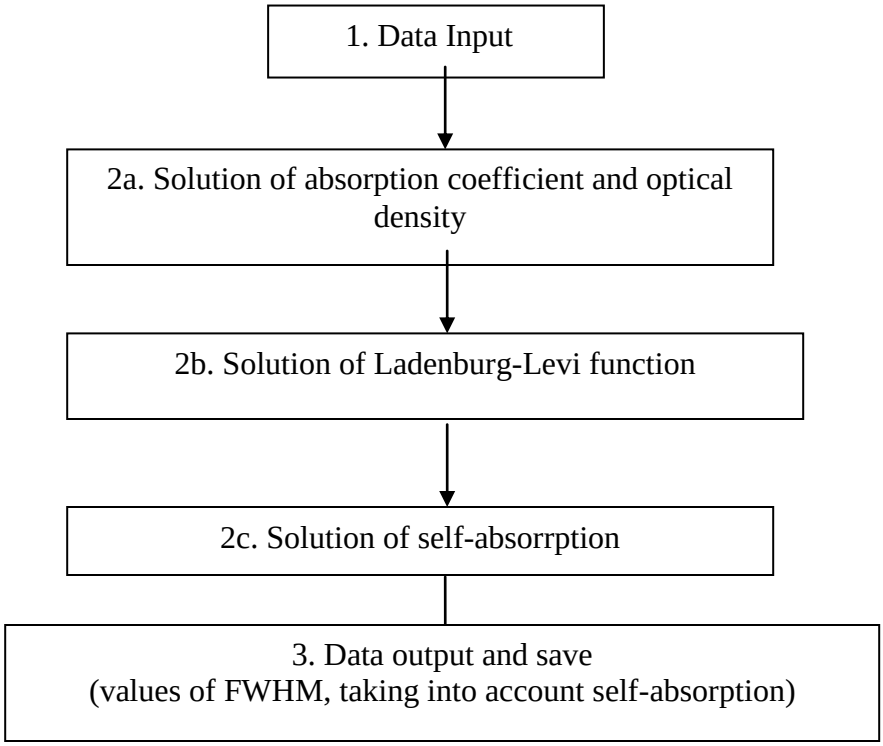

Appendix 5.

Mercury pressure dependence on temperature

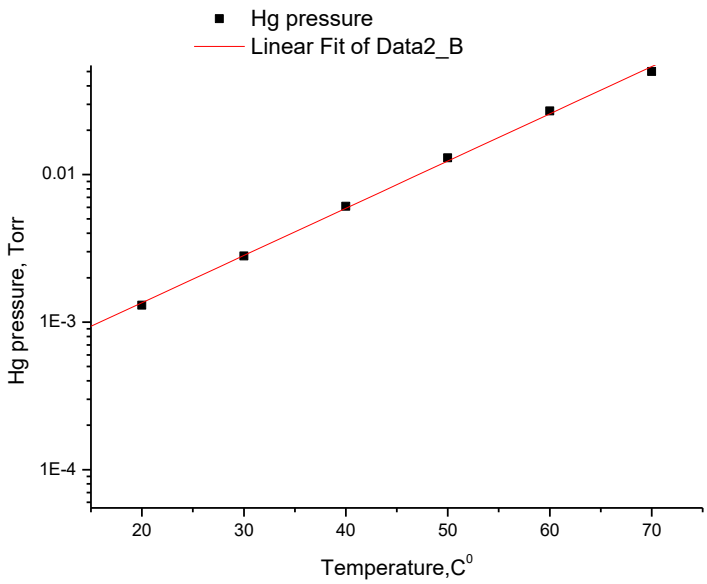

Nesmejanov A.N., **Vapor pressure of the chemical elements,** Moscow, Academy of Sciences of the USSR, (1961)

Appendix 6.

Scheme of mercury

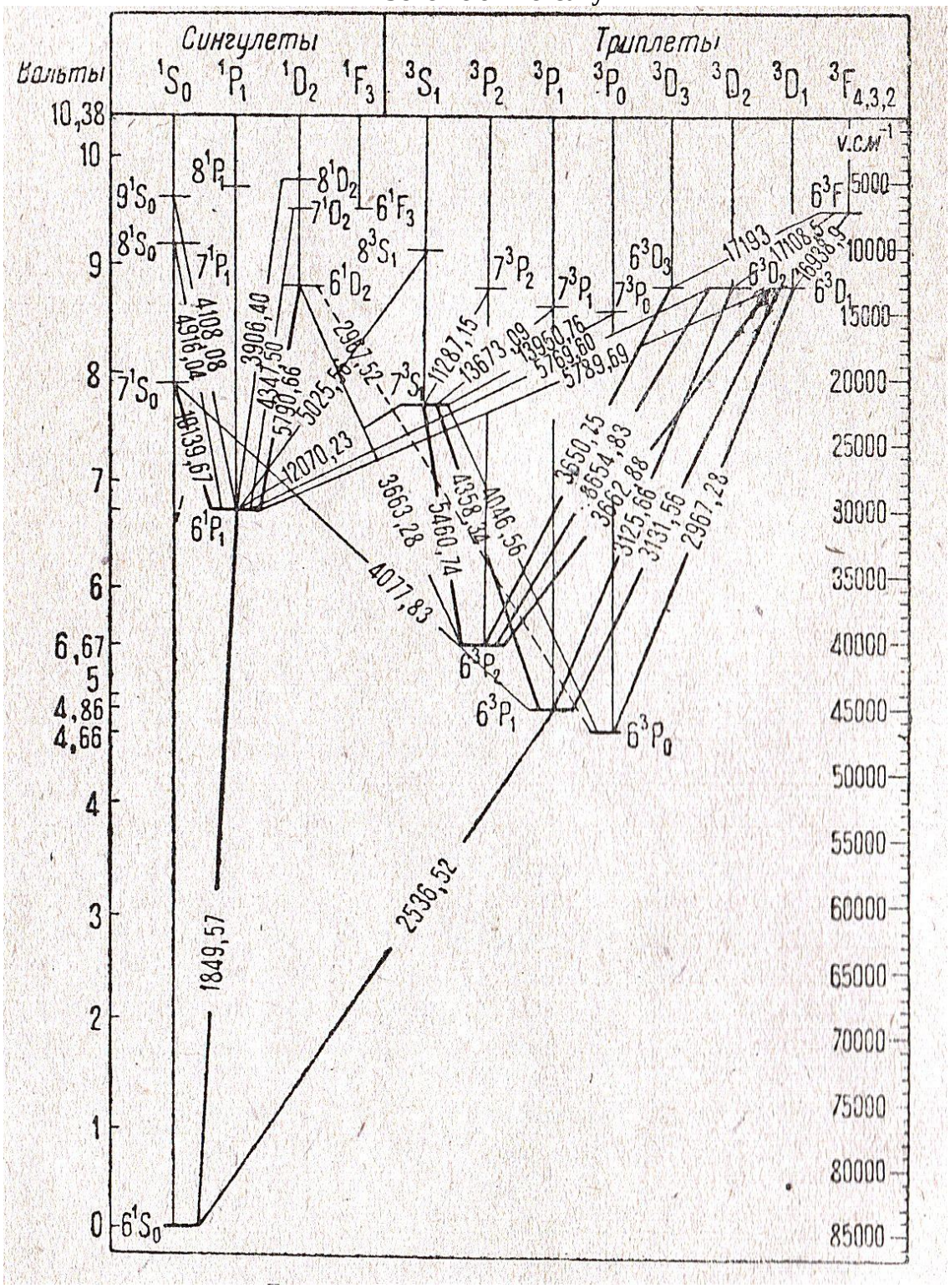

E. Frish, **Spectroscopy of the gas discharge plasma**, Nauka, Leningrad, 9-11(1970)

Publications

P1

Volume 107 Number 1 September 2007 ISSN 0022-4073
website: http://www.elsevier.com/locate/jqsrt

Journal of Quantitative Spectroscopy & Radiative Transfer

ELSEVIER

Journal of Quantitative Spectroscopy & Radiative Transfer 107 (2007) 164–172

Journal of Quantitative Spectroscopy & Radiative Transfer

www.elsevier.com/locate/jqsrt

Investigation of Hg resonance 184.9 nm line profile in a low-pressure mercury–argon discharge

G. Revalde[a,*], A. Skudra[a], N. Zorina[a], S. Sholupov[b]

[a]*Institute of Atomic Physics and Spectroscopy, University of Latvia, Skunu 4, Riga LV-1050, Latvia*
[b]*Chemical Department, University of St. Petersburg, St. Petersburg, Russia*

Received 6 June 2006; received in revised form 12 January 2007; accepted 16 January 2007

Abstract

The line profiles of 184.9 nm Hg resonance line emitted from a Hg low-pressure high-frequency electrodeless discharge lamp, containing Hg 198 isotope, have been measured by means of a Zeeman scanning spectrometer at the mercury cold spot temperature values in the range of 0–23 °C. Two different methods were used to determine the real spectral line profile and to separate the instrument function: (i) solving the ill-posed inverse problem by means of the Tikhonov's regularization method; and (ii) the mathematical modelling by means of a non-linear multi-parameter chi-square fit. The real Hg 184.9 nm spectral line profiles, determined by both methods, are compared. Influence of instrumental function, degree of the self-absorption and temperature of the radiating atoms are obtained.

Keywords: Inverse problem; Deconvolution; Hg 184.9 nm line; Line profile measurement; Zeeman spectroscopy; Regularization

1. Introduction

An experimental study of the emission line profiles is of general interest in connection with diagnostics of different types of plasmas and discharges. Since our work is connected with the development and manufacturing of new performance high-frequency electrodeless discharge lamps (HF-EDLs) [1] containing mercury for their use in scientific devices and lightening, it is crucial to perform different diagnostic methods to obtain the discharge plasma characteristics. Careful investigation of the spectral line profiles can give information about such plasma parameters as temperature, concentration and distribution of the emitting and absorbing atoms, optical density, collisional parameters. Information about mercury 253.7 and 184.9 nm resonance lines is also important in fluorescent lamp technology where mercury/argon discharge is used. Data about 184.9 nm resonance line structure in dependence on the cold spot temperature can be used not only for the lamp diagnostics but also for the validation of different type of calculations and models, considering radiation trapping [2,3]. The radiation trapping effect plays an important role in light source devices using resonance radiation and it is important for the calculation of radiation efficiency and luminous output.

*Corresponding author. Tel.: +371 7047963.
E-mail address: gitar@latnet.lv (G. Revalde).

0022-4073/$ - see front matter © 2007 Elsevier Ltd. All rights reserved.
doi:10.1016/j.jqsrt.2007.01.046

The standard way to measure line profiles is by means of a pressure scanned Fabry–Perot interferometer [4]. In the vacuum–ultraviolet spectra region, the interferometer has to be equipped with special mirrors. An additional difficulty of the 184.9 nm line measurement is the absorption of the radiation by oxygen. Another type of spectrometer based on application of the Zeeman effect, so-called Zeeman spectrometer, offers advantages of a simple experimental set-up [5,6]. Commonly, it has been used to study absorption line profiles. In this work, we have performed the 184.9 nm emission spectral line profile measurements by means of Zeeman scanning spectrometer.

The experimental spectral line is a convolution of the real line profile and instrument function. For many applications, like the usage of light sources in atomic absorption spectrometry, it is important to know the real profile of the spectral line [7]. The instrument function can cover detailed structure of the spectral line, like the dip in the line centre caused by the self-absorption (self-reversal) and characterising the radiation trapping. The subtraction of the instrument function is an ill-posed inverse task where quite small experimental uncertainties can cause large deviations in the solution. Therefore, the solution of such problem is not possible directly [8]. For ill-posed problems in classical sense, the successful usage of the different methods of solution is shown [9]. Some authors use Fourier transform and regularization method [10]. It is well known that Tikhonov regularization is one of the most useful tools for solving the ill-posed problems [11,12].

In the previous papers [13,14], we have demonstrated the possibility to use a multi-parameter non-linear chi-square line fitting to estimate the real spectral line profile for the self-absorbed spectral lines emitted from the HF-EDLs. In this paper, we do also the numerical solving of the inverse ill-posed task using the regularization method suggested by Tichonov [15,16]. The results from both methods are compared. The real mercury 184.9 nm line profile was determined in dependence on the cold spot temperature of the lamp.

2. Experimental

The experimental set-up is shown in Fig. 1. In this work, we have investigated an HF electrodeless light source filled with mercury with high isotopic abundance of Hg 198 (99.9%) and buffer gas argon of 2 Torr pressure. Radiation from the Hg light source passes through a polarizer and modulator. After that the light traverses an absorption filter, which is placed in the variable magnetic field. The absorption filter contains Hg 202 isotope (99.9%) and argon of 0.5 or 50 Torr pressure. A side arm of the filter was thermo-stated using a Peltier element at the temperature of −17 °C to control the Hg vapour pressure. Due to the magnetic field, the absorption line was split into three components—an unshifted π-component and $\sigma+$ and $\sigma-$components. The $\sigma+$ and $\sigma-$components were shifted at a distance being proportional to the magnetic field strength. By scanning of the magnetic field strength, the decrease of the emission line intensity was observed when the emission line coincides with absorption line. Only the $\sigma+$ component of the absorption line was separated and registered. Intensity of the radiation was detected by a photomultiplier tube (PMT). Analytical signal is $S = S_1/S_0$, where S_0 is the continuous current of the PMT and S_1 the signal on the modulation frequency of the polarisation modulator. Polarisation modulator was used to avoid the influence of the light source

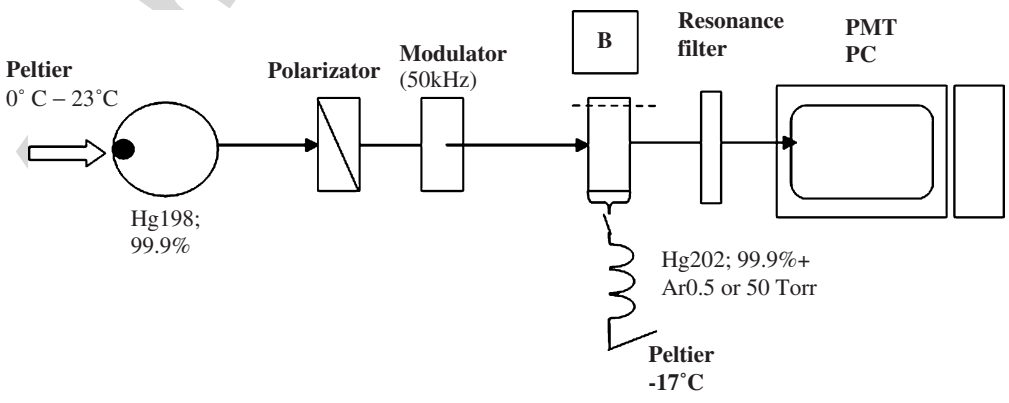

Fig. 1. The experimental set-up.

intensity changes. The registered signal S is $S \approx \Delta Q n l$, where ΔQ is the differential crosssection of the absorption, n the Hg concentration in the filter and l the absorption path length.

The relative shift of the components was 0.47 cm^{-1}/T. The 184.9 nm line profile was registered by different cold spot temperatures of the lamp in the range from about 0 °C to the room temperature of about 23 °C.

3. Theoretical approach

The registered signal $f(v)$ (proportional in our case to the differential cross-section of the absorption ΔQ) is given by a convolution

$$\int_a^b A(v - v')y(v')\,dv' = f(v), \quad c \leqslant v \leqslant d, \tag{1}$$

where $A(v - v')$ is the kernel of the integral—the known instrument function (in our case the absorption profile of the σ_+ component of the Hg); $f(v)$ the experimental distribution function (profile), registered by apparatus; $y(v')$ the unknown real profile of emitted spectral line; a, b the limits of the real profile and c, d the limits of the measured (experimental) profile.

To determine the real spectral line profile $y(v)$, it is necessary to solve the inverse problem (1). The problem (1) is known as the classic Rayleigh reduction problem (or reduction problem to an ideal spectral device) and can be described by the first kind of Fredholm integral equation.

In general, problem (1) can be written as an operator equation:

$$Ay = f, \tag{2}$$

which connects the function $f \in G_2$, in our case the measured spectral profile at frequencies v with unknown function $y \in G_1$ (in our case the real profile of 184.9 nm line of mercury) and A the continuous operator, with domain of values G_2 and definition domain G_1; G_1 and G_2 are some metric spaces. Formally, the solution of Eq. (1) can be written as

$$y = A^{-1}f, \tag{3}$$

where A^{-1} is the inverse operator.

According to Hadamard [9], an inverse problem is well posed, if the solution: (1) exists for any $f \in G_2$; (2) is only one in G_1 and (3) continuously depends on $f \in G_2$, i.e. the solution must be stable against the changes of the right side part. In our case, the third condition is wrong. That is why we did not solve Eq. (2) directly using (3). We implemented the Tikhonov's regularization method in our computations of Eq. (1). The main idea of the regularization consists in the narrowing of the function's class searched for the solution by using some additional *a priori* information. This method is based on a transformation of the initial problem to a problem of minimising of the smoothing functional. The solution is the function that gives the minimum for the smoothing functional (the Tikhonov's functional). The Tikhonov's functional is described by the following expression:

$$M^{\lambda}[y] = \int_c^d \left[\int_a^b A(v - v')y(v')\,dv' - f(v)\right]^2 dv + \lambda\Omega, \tag{4}$$

where Ω the stabilizing functional is

$$\Omega = \int_b^b y^2(v')\,dv', \tag{5}$$

and the regularization parameter $\lambda > 0$.

We performed our calculations using Tikhonov's regularization algorithm written in Mathcad. The solution of the inverse problem was performed in two stages. In the first stage, the problem of the minimum searching of the Tikhonov's functional was solved. The solution of Eq. (4) was implemented as the solution of the linear equation system. So, we have got a regularized solution of the linear equations system, depending on the regularization parameter λ. In the second stage, the regularization parameter λ was determined. The minimum of the function of the linear equations system's discrepancy was searched.

For the validation and comparison, we use also the mathematical modelling to estimate the true profile and fitting the modelled line to an experimental profile by a non-linear multi-parameter chi-square procedure and numerical calculations. The mathematical model is described in the paper [13] in detail. This model includes the basic factors causing the spectral line broadening in a low-pressure discharge: Doppler, natural and collisional. These effects are accounted by means of the Voigt profile.

For a quantitative description of self-absorption, we have to know the excitation function of the source. We use following approximations: (i) the approximation of a uniformly excited source; (ii) source with spatially separated emitting and absorbing atoms and (iii) model suggested by Cowan and Dieke [17,18]:

$$I(\nu-\nu_0) = I_0 P(\nu-\nu_0) e^{-\mu} \sum_{j=0}^{\infty} \frac{n!\mu^{2j}}{(2j+n)!}, \tag{6}$$

where n is an integer characterising the homogeneity of the radiation source and $\mu = k_0 l\,[P(\nu-\nu_0)/P(0)]$, where $P(\nu–\nu_0)$ is the line profile of radiation in a unity volume and $k_0 l$ is the optical density at the centre of the line.

The resulting profile is a convolution of the self-absorbed Voigt profile and the instrument function. The precise values of parameters for the instrument function we can obtain in an independent experiment, so we can estimate the real profile by fitting modelled convolution to an experimental line.

To perform the modelling by both methods, preliminary information about instrument function of the spectrometer is necessary. For the Zeeman spectrometer, the instrument function is the absorption spectral line profile, determined by the Doppler broadening for vapour temperature in the absorption cell, in our case at the room temperature of 20 °C (0.047 cm^{-1}) and collisional broadening described by a Lorentz function. For our calculations, following data were used: the distance between Hg 198 and Hg 202 of 0.308 cm^{-1} [19], the Lorentz broadening for 184.9 nm (in collisions with Ar) of 0.360 cm^{-1} atm^{-1}, and the collisional shift of 0.110 cm^{-1} atm^{-1} [20]. In the case of $p_{Ar} = 0.5$ Torr, the Lorentz broadening is 0.000237 cm^{-1}, but in the case of $p_{Ar} = 50$ Torr, it is 0.0237 cm^{-1}. The resonance broadening of Hg can be neglected due to small vapour pressure at the metal temperature of −17 °C. Thus, the total instrument profile is a Voigt profile, the convolution of the Gauss and Lorentz profiles.

4. Results and discussion

The 184.9 nm line profile was registered at different cold spot temperatures of the lamp in the range from 0 to 23 °C. An example of the experimentally registered 184.9 nm line profile in dependence on the cold spot temperature of Hg is shown in Fig. 2. The Ar pressure in the absorption filter was of 0.5 Torr.

The result of the extraction (deconvolution) of the real profile from the experimental 184.9 nm mercury profile using the Tikhonov's regularization method is shown in Fig. 3.

As we can see, the largest influence of the instrument function can be observed on the depth of the dip in the middle of the line. In Fig. 3 as well as in following figures, small waves (oscillations) on the wings of the deconvoluted line profiles can be seen. They are caused by larger uncertainty of the experimental data on the far line wings. Even using the Tikhonov's method cannot stabilise the solution of the inverse task completely by such relative large errors (about 50%). To avoid the oscillations, more accurate experimental data are necessary.

In Fig. 4, the comparison of the restored real 184.9 nm line profiles is shown, calculated from two different experimental lines, registered by different argon pressure values of 0.5 and 50 Torr in the absorption cell. Since the experimental conditions in the lamp were kept approximately the same, the only difference between both experimentally registered profiles was the width of the instrument function. Thus, the comparison of the restored real profiles can serve for the validation of the calculation. As we can see, the profiles coincide quite well.

The comparison of the real-line shapes, received from the solution of the ill-posed inverse problem and obtained by the non-linear multi-parameter chi-square fit, is shown in Fig. 5. It can be seen that both methods give nearly the same real profiles. It is important that the depth of the dip in the line centre coincide for both real profiles, since it is one of the most important characteristics. Rather good agreement between the

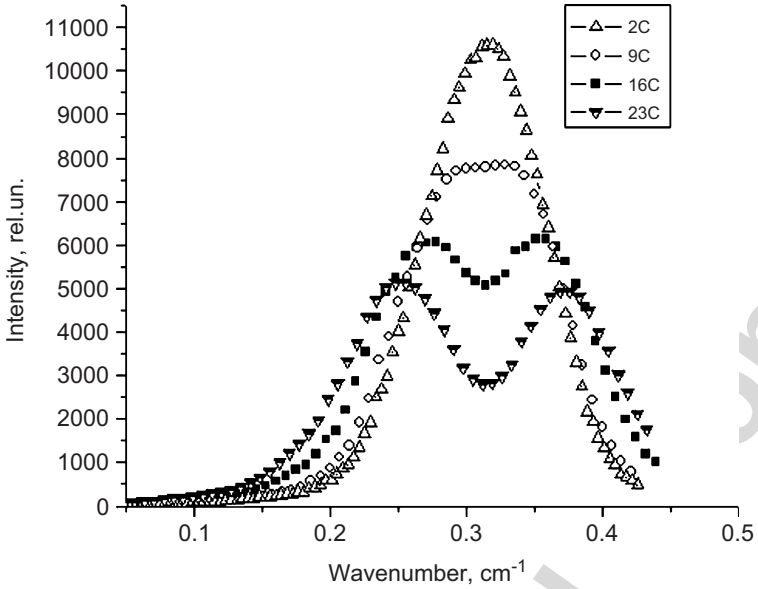

Fig. 2. The experimentally registered profiles of the 184.9 nm Hg resonance line by different cold spot temperatures of the mercury HF-EDL.

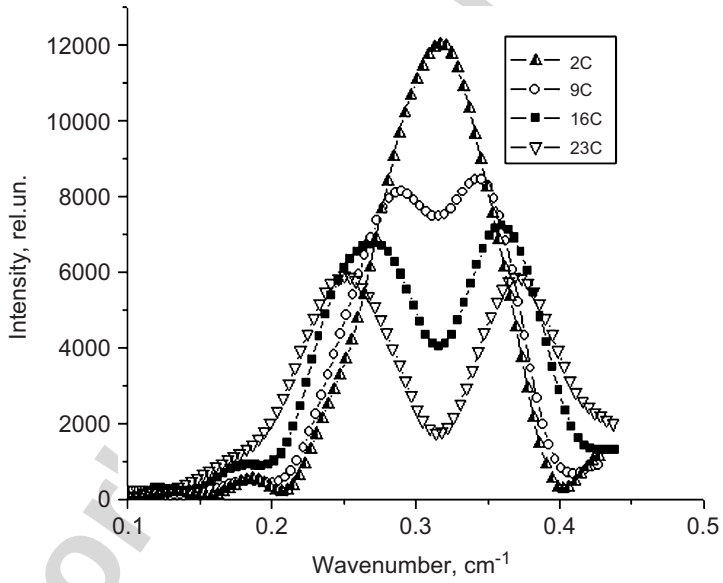

Fig. 3. Restored real 184.9 nm Hg resonance line profiles by different cold spot temperatures of the HF-EDL.

experimental profile (black squares) and the modelled line with instrument function (open circles) is achieved. The divergence of the line shapes far from the line centre can be explained by the inability of the model of Cowan and Dieke (Eq. (6)), used for accounting the self-absorption, to represent the actual distribution of emitters and absorbers in the lamp and also due to the fact that this model does not take account of multiple absorption and re-emission in the surrounding medium [14]. For more accurate fitting of the line wings, it is necessary, therefore, to consider a more complex model.

Despite the problems discussed above about the wings of the obtained real-line profiles, the results can be used to compute the gas temperature, optical density and the influence of the instrument function very well.

Another example of the modelled profiles is shown in Fig. 6. A good coincidence of the experimental and modelled spectral line profiles is also reached here. Knowing of real line profiles allows the further determination of the degree of the optical density of the source.

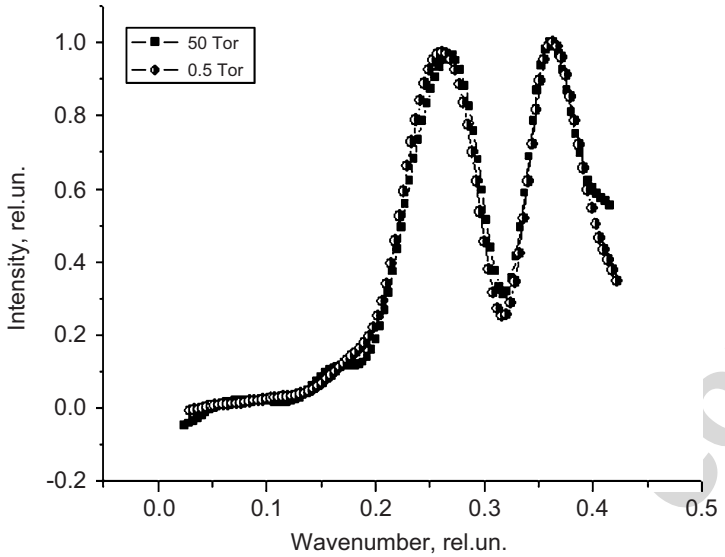

Fig. 4. The comparison of the restored real 184.9 nm line profiles, calculated from two experimental lines registered by different argon pressure values in the absorption cell of 0.5 and 50 Torr. The experimental conditions in the lamp were nearly the same.

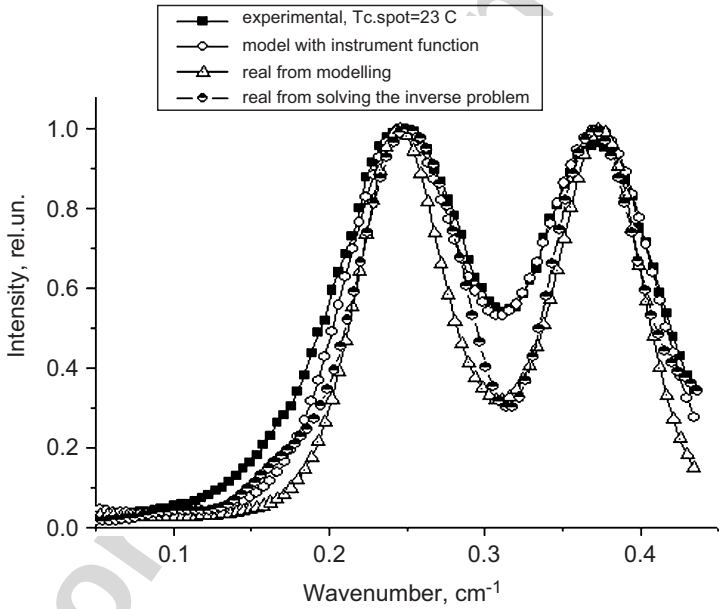

Fig. 5. The comparison of the determined line profiles applying both methods: solving the ill-posed problem using Tikhonov's regularization and the non-linear multi-parameter modelling.

The obtained qualitative self-absorption dependence on the Hg cold spot temperature is shown in Fig. 7: I_0 is the intensity of the spectral line profile at the centre of the line and I_{max} the intensity at the line maximum. When the spectral line profile is not reversed, then the ratio $I_{max}/I_0 = 1$. This parameter can serve as a parameter showing the degree of the self-reversal.

At the minimum optical density conditions, by the cold spot temperature of about 0 °C, we can assume that the 184.9 nm line is, practically, optically thin. By fitting of the deconvoluted real line profile at the minimum optical density conditions to the Voigt function, we can obtain the Doppler broadening and determine the temperature of the radiating atoms (Fig. 8). The temperature of the radiating atoms, calculated from the fitted Doppler broadening, is of 250 ± 40 °C. The magnitude of this value agrees quite well with the previous results

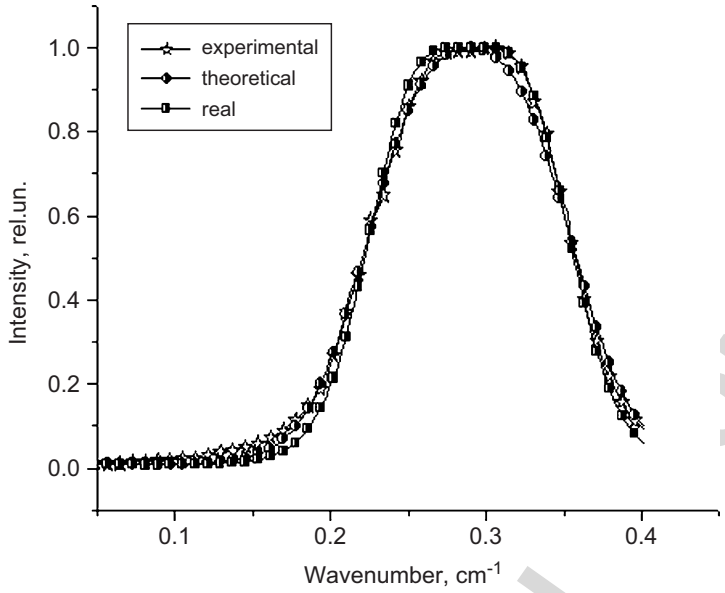

Fig. 6. An example of the modelled 185 nm spectral line for the experimental line at the cold spot temperature of 9 °C and $i = 200$ mA.

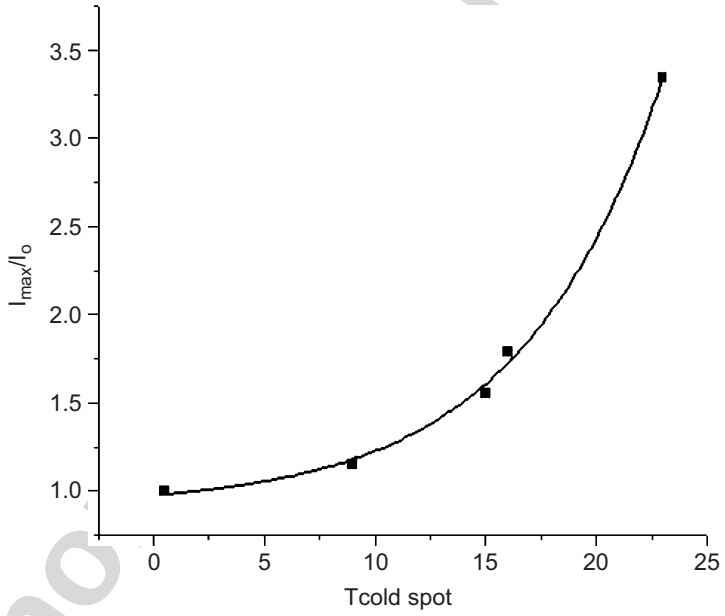

Fig. 7. The obtained self-absorption (I_{max}/I_0, where I_{max} is the intensity at the maximum of the profile and I_0 at the centre of the profile) dependence on the Hg cold spot temperature.

for similar discharge lamps [14]. It was seen in [14] that the gas temperature is dependent on the both the discharge current and argon pressure.

For the comparison of the both methods for the estimation of the real spectral line profile, we can mention that there are some advantages and disadvantages of the both methods. The disadvantage of the line profile modelling method is that the functions of the line profiles have to be known before and we can apply it mainly for the symmetric lines. For using the Tikhonov's regularization method, the only parameter that we have to know is the instrument function. The advantage of the modelling is that we can apply it also for the fit of the width of the instrument function if the type of the instrument function is known.

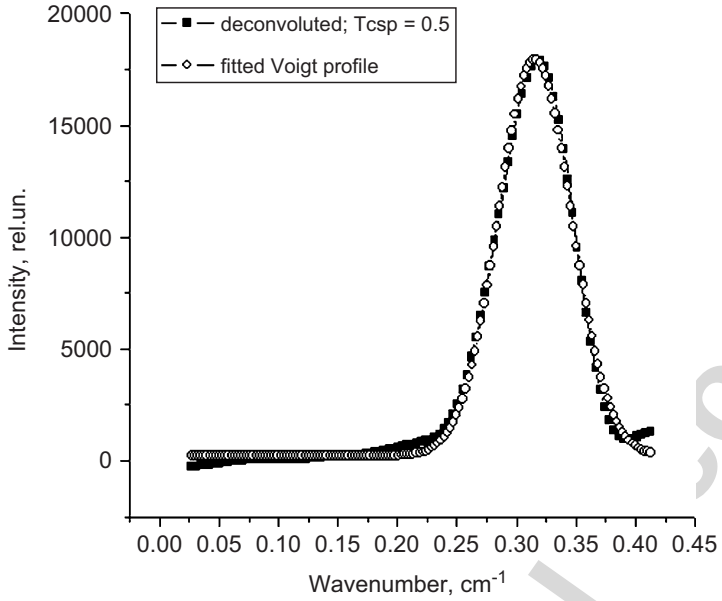

Fig. 8. The fit of the Voigt function to the restored 184.9 nm line profile at the $T_{c.sp.} = -0.5\,^{\circ}C$ for the determination of the temperature of the radiating atoms. The fitting parameters: Gauss width of $0.063\,cm^{-1}$; Lorentz width of $0.016\,cm^{-1}$; $\chi^2 = 0.997$.

5. Summary

The line profiles of 184.9 nm Hg resonance line, emitted from a low-pressure high-frequency electrodeless discharge lamp by different Hg cold spot temperatures, have been measured by means of the Zeeman scanning spectrometer. The line profiles were registered at different instrument functions. The real 184.9 nm Hg line was determined applying two different methods to subtract the instrument function: (i) the solving of the inverse task by the Tikhonov's regularization method and (ii) the multi-parameter chi-square line profile modelling. Good agreement of the real line profile, obtained by the both methods, is observed. The main advantages of the Tikhonov's regularization method are that it is not necessary to make additional assumptions about the real-line profile and it can be applied also for asymmetric line profiles.

The temperature of the radiating atoms was of $250 \pm 40\,^{\circ}C$, estimated from the Doppler broadening of the deconvoluted real-line profile.

Acknowledgements

N. Zorina acknowledges the European social fund for the PhD fellowship.

References

[1] Revalde G, Silinsh J, Spigulis J, Skudra A. High-frequency electrodeless light sources for application. SPIE Proc 2000;4318:78–83.
[2] Baeva M, Reiter D. Monte Carlo simulation of radiation trapping in Hg–Ar fluorescent discharge lamps. Plasma Chem Plasma Process 2003;23(2).
[3] Rajaraman K, Kushner MJ. A Monte Carlo simulation of radiation trapping in electrodeless gas discharge lamps. J Phys D 2004;37:1780.
[4] Revalde G, Berzina D, Lhevkovski V, Luizova L, Putnina S, Reppo P, et al. The automatic spectrometric complex for spectral line profile measurements. J Appl Spectrsc 1992;56:681–6.
[5] Vasiljev O, Kotkin A, Stoljarov D, Chopornjak D, Umorhodzhajev R. High-frequency electrodeless light sources. Riga, Latvia: Acta Universitatis Latviensis; 1992. p. 105.
[6] Ganeyev AA, Sholupov SE, Slyadnev MN. Zeeman modulation polarization spectrometry as a version of atomic-absorption analysis: potentials and limitations. J Anal Chem 1995;51:788.

[7] Ganeev AA, Gavare Z, Khutorshikov VI, Khutorshikov SV, Revalde G, Skudra A, et al. High-frequency electrodeless discharge lamps for atomic absorption. Spectrochem Acta 2003;B58:879–89.
[8] Lebedeva VV. The technique of the optic spectroscopy. Moscow: Moscow University; 1977. p. 354 [appendix].
[9] Verlan F, Sizikov VS. The integral equations: the methods, algorithms, program. Kiev: Naukova Dumka; 1986. p. 223–321.
[10] Xiang-Tuan Xiong, Chu-Li Fu, Hong-Fang LiJ. Fourier regularization method of a sideways heat equation for determining surface heat flux. Math Anal Appl 2006;317:331–48.
[11] Groetsch CW. The theory of Tikhonov regularization for Fredholm equations of the first kind. London: Pitman; 1984.
[12] Rajan MP. An efficient discretization scheme for solving ill-posed problems. J Math Anal Appl 2006;313:654–77.
[13] Skudra A, Revalde G. Mathematical modelling of the spectral line profiles in the high-frequency discharge. JQSRT 1999;61:717–27.
[14] Revalde G, Denisova N, Gavare Z, Skudra A. Diagnostics of capillary mercury–argon high-frequency electrodeless discharge using line shapes. JQSRT 2005;94:311–24.
[15] Tikhonov A, Goncharsky A, Stepanov V, Jagola A. Numerical solution's methods of the ill-posed problem. Moscow: Nauka; 1990.
[16] Tikhonov A, Arsenin V. The solution's methods of the ill-posed problem. Moscow: Nauka; 1979.
[17] Preobrazhenskii NG. Spectroscopy of optical thick plasma. Novosibirsk: Nauka; 1971. p. 177.
[18] Cowan RD, Dieke GH. Self-absorption of spectrum lines. Rev Mod Phys 1948;2:418.
[19] Bousquet C, Bras N. Broadening and shift of the absorption line Hg 1849 Å perturbed by noble gas. J Phys 1977;38:139.
[20] Leboucher E, Bousquet C, Bras N. The measure of the isotopic and hyperfine structure of the radiation Hg 1849 Å by means of the magnetic scanning method. Nouv Rev Optique 1974;5:121.

P2

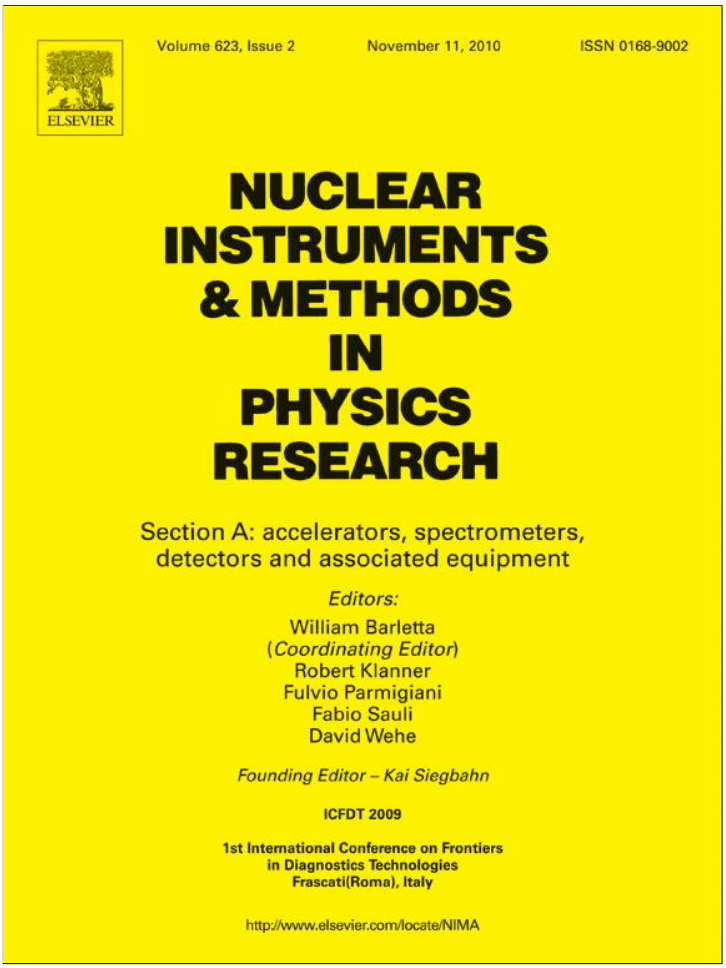

Nuclear Instruments and Methods in Physics Research A 623 (2010) 763–765

Contents lists available at ScienceDirect

Nuclear Instruments and Methods in Physics Research A

journal homepage: www.elsevier.com/locate/nima

Deconvolution of the spectral line profiles for the plasma temperature estimation

Natalja Zorina

Institute of Atomic Physics and Spectroscopy, University of Latvia, Skunu 4, LV-1050, Riga, Latvia

ARTICLE INFO

Available online 13 February 2010

Keywords:
Electrodeless discharge lamps
Temperature estimation
Instrumental function
Deconvolution
Tikhonov regularization

ABSTRACT

The Hg 253.7 nm spectral line profiles, emitted from the mercury–argon high-frequency electrodeless discharge lamps (HFEDL) have been measured by means of a high-resolution scanning Fabry–Perrot interferometer at the mercury cold spot temperature value at 20 °C, different discharge current and buffer gas values. The deconvolution procedure by means of the Tikhonov's regularization method was performed to obtain the real spectral line shape. The influence of the instrumental function and absorption, real width of the Hg 253.7 nm resonance line and temperature of the radiating atoms are obtained. The results were compared with the results of the nonlinear multiparameter mathematical modeling by means of a nonlinear multiparameter χ^2 fit.

1. Introduction

For plasma diagnostics it is important to know the real shape of the spectral line. The instrument function can destroy the real spectral line shape significantly, for example, it changes the width of the spectral line that leads to the uncertainties in the determination of such important plasma parameters as temperature. It can also cover detailed structure, like the self-reversal that is important to know different applications, for example atomic absorption analysis. Therefore the decomposition should always be performed while using the spectral line shapes for plasma diagnostic purposes.

2. Experiment

In this work are reported the studies of the line profiles of 253.7 nm Hg resonance line emitted from the spherical part of the bar-bell like high-frequency electrodeless discharge lamp (HFEDL), manufactured at the Institute of Atomic Physics and Spectroscopy. The lamp was filled with Hg of a high isotopic abundance (99.3% of 202 isotope) and Ar as a buffer gas.

Spectral line profiles were recorded by means of a high-resolution scanning Fabry–Perrot interferometer with two different Ar pressures of 2 and 10 Torr, in dependence on the discharge current (80–190 mA) at the Hg cold spot temperature value of 20 °C.

3. Theoretical approach

To obtain the real shape of a spectral line it is necessary to solve the Fredholm first kind integral equation:

$$\int_a^b A(v-v_0)y(v_0)dv_0 = f(v), \quad c \le v \le d. \tag{1}$$

Eq. (1) is a convolution of an unknown real profile y (v_0) with instrument function A (v, v_0), where a, b and c, d are the limits of the real and measured (experimental) profiles accordingly. In our case A is the instrumental function of Fabry–Perrot interferometer. It is described by the Airy function.

$$A(v) = A_{\max}\frac{1}{1+\frac{4R}{(1-R)^2}\sin^2\frac{\pi\Delta}{\lambda}}, \tag{2}$$

where Δ is the difference of the optical ways; R the effective refraction coefficient of mirrors.

Eq. (1) is an inverse ill-posed task. Therefore the solution is not possible directly [1–3]. In this work we performed our calculation using Tikhonov [1,3,4] regularization method. In detail the mathematical model for the case of spectral line real shapes obtained is described in Ref. [5]. By this algorithm an initial, ill-posed task (1) can be transformed to a solution of the following matrix Eq. [1]:

$$(\tilde{A}^*\tilde{A}+\alpha E)Y = \tilde{A}^*\tilde{f} \tag{3}$$

where α is the parameter of regularization, A_{ij} the elements of $N \times N$ size matrix A, which approximates kernel $K(x,x)$, f_i-vectors the column with initial dates, Y_i-vector the column of solution.

The motion of the atoms in accordance to the Maxwell low is isotropic in the space and thus the width at half of maximum

E-mail address: natalja.zorina@gmail.com

0168-9002/$ - see front matter © 2010 Elsevier B.V. All rights reserved.
doi:10.1016/j.nima.2010.02.085

(FWHM) corresponds to the Doppler effect. That is why the temperature of the radiating atoms can be obtained by the following expression [6,7]:

$$T = \frac{\mu}{(7.16 \times 10^{-7} \nu_0)^2} \Delta \nu_D^2 \quad (4)$$

where T is the absolute temperature of the emitting atoms, μ the atomic mass, ν_0 the position of the scale of the frequencies when the Gauss function reaches its maximum value and $\Delta\nu_D$ the FWHM of Gaussian function.

The self-absorption in the lamp was taken into account using the following expression [6]:

$$A_S = \frac{1}{2}\sqrt{\frac{\pi}{\ln 2}} \Delta\nu_D \kappa_0 l S(\kappa_0 l), \quad (5)$$

where $\kappa_0 l$ is the optical density, l the optical way, $S(\kappa_0 l)$ the Ladenburg–Levi function. All calculations were made for the Hg 253.7 nm line ($6^3P_1 - 6^1S_0$ transition).

4. Results and discussion

The measured profiles were processed in two stages, before temperature estimation. First of all, the deconvolution procedure or solving of this (Eq. (1)) ill-posed inverse problem by means of the Tikhonov's regularization method was performed to obtain the real spectral line shape. After that, the influence of the self-absorption was taken into account (Eq. (5)).

In Fig. 1 we can see the influence of the instrumental function and self-absorption to the FWHM of the measured spectral line profiles. In the case of the 253.7 nm line, emitted from the HFEDL with 10 Torr Ar, the FWHM of the measured (experimental) spectral lines were in the range of 0.15–0.20 cm^{-1}, but real FWHM were obtained to be in the range of 0.1–0.15 cm^{-1} after deconvolution and in the range of 0.048–0.066 cm^{-1} taking into account the absorption influence.

Examples of the experimental dependence of the FWHM from the generator current and the influence of the instrumental function and self-absorption to it in case of the 253.7 nm line emission from the HFEDL with 2 Torr Ar are shown in Fig. 2.

In case of Ar pressure of 2 Torr the FWHM of the experimental as well as the obtained real profiles are practically independent from the generator current. The estimated FWHM of the real profiles in average is broader by Ar pressure of 2 Torr in Hg HFEDL: about 0.14 cm^{-1} after deconvolution and about 0.07 cm^{-1} taking absorption into account.

Temperatures of the radiating atoms, estimated by Eq. (4) of the deconvoluted real spectral line profiles, taking into account the influence of the absorption are shown in Figs. 3 and 4. In Fig. 3 are shown the dependences of the temperatures from the discharge current for the case when Ar pressure was of 10 Torr. Clear maximum of dependence can be seen by 140–150 mA. The

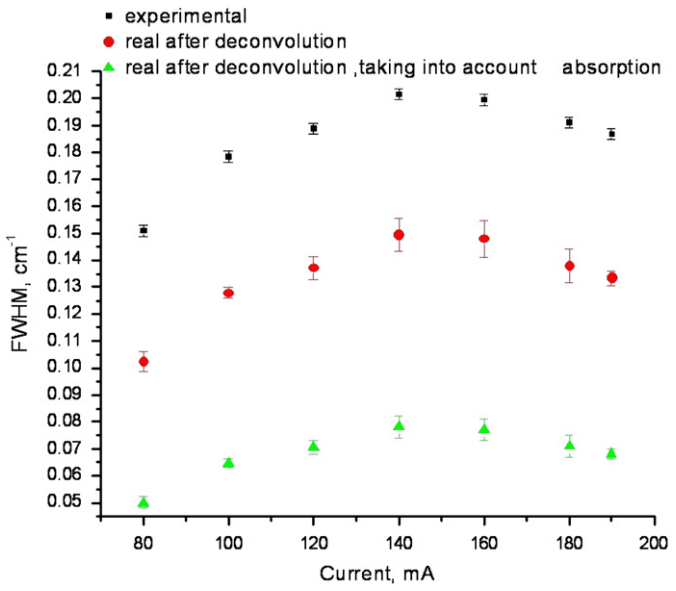

Fig. 1. The FWHM of the experimentally registered Hg 253.7 nm line profile (squares) and the FWHM of the results after deconvolution by means of the Tikhonov regularization method (circles) and after deconvolution taking absorption into account (triangles) in dependence on the generator current. The Ar pressure was 10 Torr.

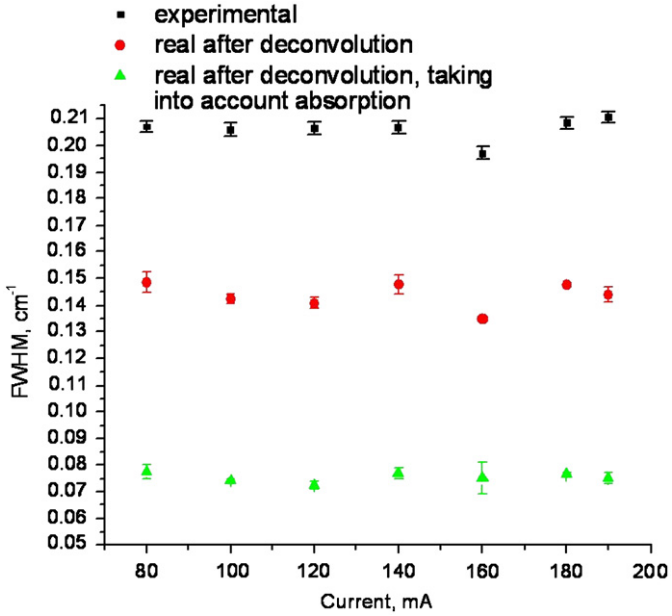

Fig. 2. The FWHM of the experimentally registered Hg 253.7 nm line profile (squares) and the FWHM of the results after deconvolution by means of the Tikhonov regularization method (circles) and after deconvolution taking absorption into account (triangles) in dependence on the generator current. The Ar pressure was 2 Torr.

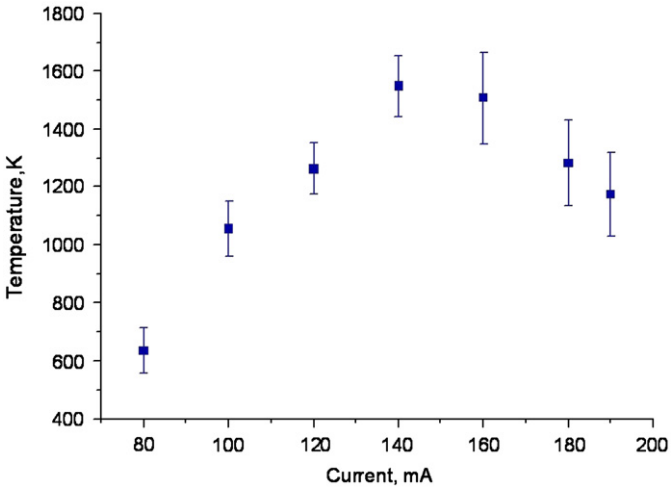

Fig. 3. The temperature of the radiating atoms dependence on the discharge current. Ar pressure was 10 Torr.

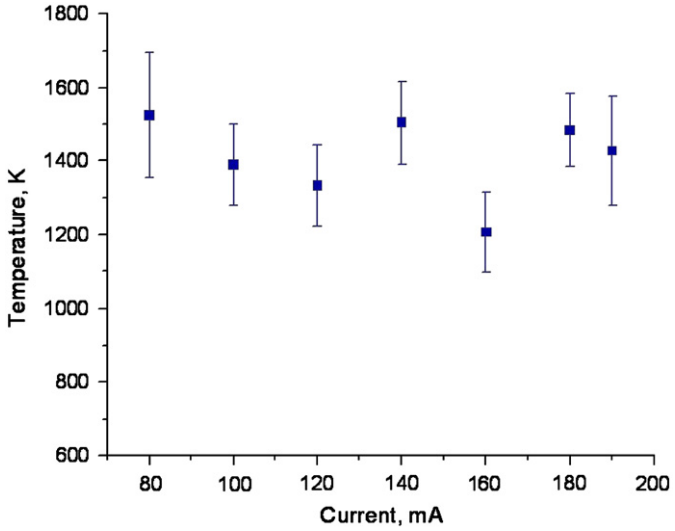

Fig. 4. The temperature of the radiating atoms dependence on the discharge current. Ar pressure was 2 Torr.

temperature varies from approximately 600–1700 K as a function of discharge generator current.

The results of the dependences of the temperatures as a function from the discharge current for the lamp with Ar pressure of 2 Torr are shown in Fig. 4. In this case the temperature of the radiating atoms is in the range of 1400–1500 K.

The tendencies of clear maximum appearance in the dependence FWHM from discharge current at the Ar pressure of 10 Torr and independence from discharge current at 2 Torr agree well with the previous results [8]. In that case the estimated FWHM of Hg 253.7 nm spectral line was obtained by another method, the mathematical modeling, described in Refs. [8,9]. This model is based on nonlinear multiparameter fitting procedure of the model profile to an experimental profile by varying the unknown parameters [8,9]. Model profile includes basic factors causing the spectral line broadening in a low-pressure discharge: Doppler, resonance, natural and collision broadening. Hyperfine splitting and shifts of the components due to the isotope effects are taken into account. The radiation trapping is accounted by means of the one ray approximation. The resulting profile is a convolution of the self-absorbed Voigt profile and the instrument function.

5. Conclusion

In this paper are presented the results of solution of the ill-posed inverse problem by means of the Tikhonov's regularization method in case of Hg 253.7 nm spectral line ($6^3\,P_1 - 6^1\,S_0$ transition) and discharge temperature estimation. In case of Ar pressure of 10 Torr, the real FWHM is obtained to be in the range of 0.1–0.15 cm^{-1} after deconvolution and in the range of 0.048–0.066 cm^{-1} taking into account the absorption influence. The temperature varies from approximately 600–1700 K as a function of discharge generator current. When Ar pressure was of 2 Torr, the estimated FWHM of the real profiles in average is 0.14 cm^{-1} and about 0.07 cm^{-1} taking absorption into account. The temperature of the radiating atoms is in the range of 1400–1500 K. The estimated results show a good agreement with previous calculations by means of a nonlinear multiparameter χ^2 fitting procedure.

Acknowledgments

The work was partly supported by the European Social Fund (ESF)-Projects: 2009/0138/1DP/1.1.2.1.2/09/IPIA/VIAA/004 and 2009/0210/1DP/1.1.1.2.0/09/APIA/VIAA/100.

Reference

[1] A. Verlan, V. Sizikov, The integral equations: the methods, algorithms, program, Kiev: Naukova dumka, (1986).
[2] G. Revalde, A. Skudra, N. Zorina, S. Sholupov, JQSRT 107 (2007) 164.
[3] A. Tikhonov, V. Arsenin, The solution's methods of the ill-posed problem, Nauka, Moscow, 1979.
[4] C.W. Groetsch, The theory of Tikhonov regularization for Fredholm equations of the first kind, Pitman, London, 1984.
[5] N. Zorina, G. Revalde, R. Disch, Proceedings of SPIE Sixth International Conference on Advanced Optical Materials and Devices (AOMD-6), 24–27 August (2008) Riga, Latvia, Vol. 7142 71420J-1.
[6] Frish E, Spectroscopy of the gas discharge plasma, Nauka, Leningrad, 25-26 (1970) p. 9.
[7] W. Demtroeder, Laser Spectroscopy, third ed, Springer, 2003, p. 70.
[8] G. Revalde, N. Denisova, Z. Gavare, A. Skudra, J.Q.S.R.T. 94 (2005) 311.
[9] G. Revalde, A. Skudra, 14th ICSLS 10 (1998) 179.

P3

Romanian Reports in Physics, Vol. 66, No. 4, P. 1099–1109, 2014

DECONVOLUTION OF THE LINE SPECTRA OF MICROSIZE LIGHT SOURCES IN MAGNETIC FIELD*

G. REVALDE[1,2], N. ZORINA[2], A. SKUDRA[2], Z. GAVARE[2]

[1] Riga Technical University, Institute of Technical Physics, Kalku str.1, LV 1050, Riga, Latvia, E-mail: Gita.Revalde@rtu.lv
[2] University of Latvia, Institute of Atomic Physics and Spectroscopy, Skunu 4, LV-1050,Riga, Latvia, E-mail: natalja.zorina@gmail.com; askudra@latnet.lv, Email: zanda.gavare@gmail.com

Received July 30, 2013

Abstract. We present our investigation of narrow spectral lines, emitted from microsize mercury/xenon electrodeless light source in magnetic field. The spectral line shapes were registered by the Fourier transform spectrometer and deconvoluted by means of a regularisation method. Two approaches were used to obtain the regularisation parameter. The plasma temperature and magnetic field intensity were obtained.

Key words: electrodeless light sources, microsize light sources, line shapes, Zeeman Effect, inverse problem, Tikhonov's regularisation method, calculated real line shape, low-pressure plasma temperature, regularisation parameter, instrumental function of the Fourier transform spectrometer.

1. INTRODUCTION

Our research is devoted to the preparation and optimisation of special type of electrodeless light sources for their use in different scientific devices [1]. Such light sources can be used in atomic absorption devices or as standards. Due to recent trends of miniaturisation, there is a need to find out right methods of diagnostics for small scale plasmas. In this paper we show our experience of diagnostics of micrometer size capillary lamps by means of spectral line shape measurements with Fourier transform spectrometer (FTS). Since the capillary sources emit very narrow lines, it is a challenge to get information about the form of spectral lines, though it is important for application of the lamps in high precision experiments.

In our previous research we did experiments of line shape investigation with such devices as Fabry Perrot spectrometer [2] and Zeeman scanning spectrometer [3, 4]. However, these methods have several restrictions and are not applicable for microsize light source diagnostics. FTS are becoming more and more widely used

* Paper presented at the 16th International Conference on Plasma Physics and Applications, June 20–25, 2013, Magurele, Bucharest, Romania.

in different experiments, where very high precision, especially in the IR spectral range, is needed. Though the light sources under investigation are used mainly in UV and visible spectral region, FTS can be used in this case too. The broadening of lines emitted from the capillary lamps is on the same order as the instrument function of FTS.

In this work we present investigation of the influence of FTS instrument function on spectral line shapes, used for diagnostics of capillary light sources. The method of diagnostics consists of obtaining the measurements of line shapes and following retrieval of the calculated real line shape from experimental shapes by means of the Tikhonov's regularisation method. In [5, 6] we reported the first results for capillary light source filled with mercury and buffer gases. Different emission properties were observed depending on the working position of capillary. In [7] the method of imaging and tomography was used to investigate this phenomenon. Detailed investigation of the influence of approximation of the instrument function of FTS was done in this work. In addition, two methods for finding the regularisation parameter were applied.

2. EXPERIMENTAL

The capillary lamps under investigation were manufactured at the Institute of Atomic Physics and Spectroscopy in Riga. The length of the capillary was of 2 cm and the discharge size was of 500 μm in radius (Fig. 1a). A Fourier transform spectrometer is basically a Michelson interferometer. Beam splitter is used in this type of interferometer to divide an incoming light beam in two parts. The first part is reflected on a fixed mirror, whereas the second part is reflected on a mobile mirror. The two beams are recombined at the beam splitter and shone on a detector. The principal scheme is shown below (Fig. 1b).

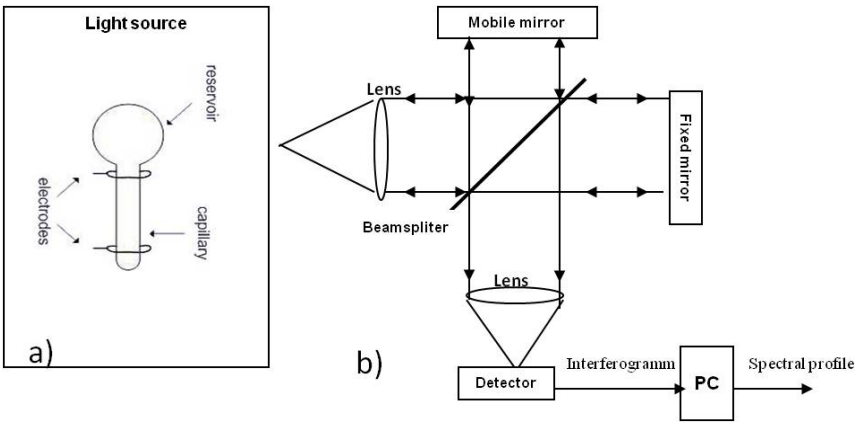

Fig. 1 – a) Design of the capillary electrodeless light source; b) Scheme of Fourier transform spectrometer as a Michelson interferometer.

At the end of capillary the lamp contains small reservoir for metal vapour. The discharge is ignited in the capillary part of lamp. In this case the lamp was filled with xenon of 2 Torr partial pressure and mercury isotope 198. The reservoir at the end of lamp is used as a cold spot to control the metal vapour pressure in lamp [8]. In this experiment the mercury isotope pressure was of 0.003 Torr [9].
The lamps were capacitatively excited using 100 MHz frequency applied to external electrodes. The lamps were operated in three different positions in accordance to the Earth plane, namely, horizontally, vertically with Hg reservoir up, and vertically with Hg reservoir down. The lamps were placed in magnetic field to observe Zeeman splitting, as necessary for their application in Zeeman Atomic Absorption Spectrometry (ZAAS). Magnetic field was perpendicular to the axis of capillary and the direction of observation was parallel to the magnetic field lines.

Spectral lines, emitted from Hg/Xe high frequency microsize capillary lamp, were measured using Fourier Transform spectrometer *Bruker IFS-125HR,* capable of registering lines in the wavelength region 330–2000 nm. We analyse the 404.7 nm Hg spectral line in this paper in detail. The examples of experimental measurements of the 404.7 nm line in three different working positions are shown in Fig. 2. As clearly can be seen in Fig. 2, the most intensive lines were obtained when the lamp was operated vertically, especially with the reservoir up. The smallest intensity was observed when the lamp was operated horizontally. This effect was observed in our previous research too, where we found that there is a difference between the distributions of atoms in different working positions [7].

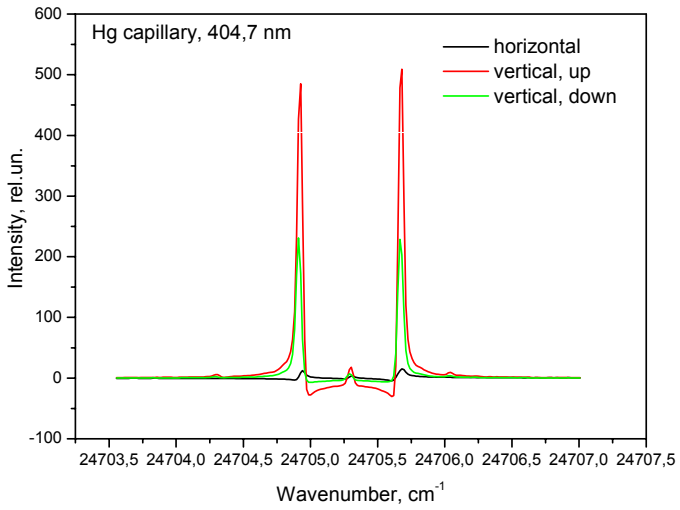

Fig. 2 – Example of experimentally measured Hg 404.7 nm line. The line was emitted from Hg/Xe capillary light source placed in three different working positions: horizontally (black line), vertically with Hg reservoir up (red line), and vertically with Hg reservoir down (green line).

3. THEORY

3.1. TIKHONOV'S REGULARISATION

For high precision spectroscopy it is necessary to retrieve the calculated real spectral line shape from the spectral line shape measured experimentally. The Fredholm first kind integral equation describes the convolution of real spectral line profile, measured (experimental) spectral line profile, and instrumental function:

$$\int_a^b A(x,s)y(s)\mathrm{d}s = f(x), \quad c \le x \le d, \tag{1}$$

where: *f(x)* – measured spectral line profile; *y(s)* – calculated real spectral line profile; *A(x,s)* – instrument function.

To retrieve the calculated real spectral line profile from experimental one without the instrumental function, it is necessary to solve the inverse ill-posed problem. Tikhonov's regularisation algorithm [10, 11] is one of the most useful tools for solving the task where small experimental uncertainties can cause large deviations in the solution.

Assuming, that the values on the right side and integral equation (1) kernel are known with accuracy:

$$\left.\begin{aligned} \left\| \tilde{f} - f \right\|_F &\le \delta; \\ \left\| \tilde{A} - A \right\| &\le \xi \end{aligned}\right\}, \tag{2}$$

where δ is the error of right part of (1) or the error of experimental $f(x)$ profile, ξ is the error of kernel of (1) or the error of instrument function $A(x,s)$, Tikhonov proved, that the initial, ill-posed task can be transformed into a task of searching for the minimum of smoothing functional:

$$M_\alpha\left[y, \tilde{f}\right] = \inf_{y \in Y} M_\alpha\left[y, \tilde{f}\right], \tag{3}$$

where: smoothing functional $M_\alpha\left[y, \tilde{f}\right]$, so called Tikhonov's functional, is given in the form:

$$M_\alpha\left[y, \tilde{f}\right] = \left\| \tilde{A}y - \tilde{f} \right\|_F^2 + \alpha\Omega[y], \tag{4}$$

stabilising functional Ω is described by the following expression:

$$\Omega[y] = \|y\|_Y^2, \tag{5}$$

where: $\alpha > 0$ – regularisation's parameter; number $\left\|\tilde{A}y - \tilde{f}\right\|_F^2$ discrepancy.

According to Tikhonov's method, instead of the initial ill posed problem, which is described by Fredholm integral equation of first kind, we get well posed task, which is described by Fredholm integral equation of second kind, which after changing the integrals to finite sums can be written as the system of linear equations:

$$\sum_{i=1}^{N} b_i \left(\sum_{m=1}^{N} b_m \tilde{A}_{mk} \tilde{A}_{mi} \right) y_i + \alpha y_k = \sum_{m=1}^{N} b_m \tilde{A}_{mk} \tilde{f}_m, \quad k = \overline{1, N} \tag{6}$$

or as matrix equation:

$$\left(\tilde{A}^* \tilde{A} + \alpha E\right) Y = \tilde{A}^* \tilde{f}, \tag{7}$$

where A_{ij} – elements of $N \times N$ size matrix A, which approximates kernel $K(x,x)$; f_i – vectors-column with initial dates; y_i – vector-column of solution; b_i – the coefficients of quadrature formula .

The mathematical model in detail is described in [4], in which Zeeman Scanning spectrometer was used for the registration of spectral lines.

3.2. REGULARISATION PARAMETER

It is well known, that the finding of regularisation parameter is crucial for application of Tikhonov's regularisation method. Two independent methods were used in this work to obtain the regularisation parameter α:

1) the minimisation of discrepancy [11]:

$$\left\|\tilde{A}y_\alpha - \tilde{f}\right\|_{L_2}^2 = \min_\alpha \left\|\tilde{A}y_\alpha - \tilde{f}\right\|_{L_2}^2; \tag{8}$$

2) the Kojdecki method [12]. According this method α is root of equation:

$$\alpha^{q+1} \left\| y_\alpha \right\| = \beta \, \| \tilde{A} \| \left(\delta + \xi \left\| y_\alpha \right\| \right). \tag{9}$$

In this work α was obtained from (9) in supposition that the error of kernel $\xi = 0$. The coefficients were chosen as $q = 0$ and $\beta = 1$. Variance of the errors of measured line is 0.017.

3.3. INSTRUMENT FUNCTION FOR FOURIER TRANSFORM SPECTROMETER

To obtain the calculated real profile from measured spectral profile by means of regularisation, it is necessary to know the instrument function very accurately.

First, we used an experimentally measured He spectral line of 632.8 nm wavelength emitted from the single mode He/Ne laser as a data array for instrument function matrix A in the formula (7) for deconvolution without any approximation, but it led to false maximums, especially in the far wings of the profile.

Second step was to test the instrument function given by the theory of Fourier transform spectrometry [13, 14], causing restrictions of the resolution of the device due to the limited optical path difference in the Michelson interferometer inside the Fourier transform spectrometer:

$$I(x) = 2L \bmod \left\{ \operatorname{sinc}\left[2\pi (x_0 - x) L \right] \right\} \tag{10}$$

where L – difference between lengths of two optical paths (optical path difference).

As we can see, usage of this function gives a lot of negative values and also false beats in the wings, where no real maxima can be present [14].

Afterwards we performed approximations of the instrument function trying to fit it with several known peak functions, for example, Voigt, Gauss and Lorentz functions.

The Voigt function was written in the form:

$$y = y_0 + A \frac{2\ln 2}{\pi^{3/2}} \frac{w_L}{w_G^2} \cdot \int_{-\infty}^{\infty} \frac{\mathrm{e}^{-t^2}}{\left(\sqrt{\ln 2}\, \dfrac{w_L}{w_G} \right)^2 + \left(\sqrt{4\ln 2}\, \dfrac{x - x_c}{w_G} - t \right)^2} \mathrm{d}t , \tag{11}$$

where w_L is full width at half of maximum (FWHM) of Lorentz function, w_G is FWHM of Gauss function, A – area, x_c – frequency at the line centre.

The Lorentz function was written in the form:

$$y = y_0 + 2Aw / \left(4\pi \left(x - x_c \right)^2 + w^2 \right), \tag{12}$$

where w – the FWHM of the line.

The Gauss function:

$$y = y_0 + \frac{A}{w\sqrt{\pi / 2}} \mathrm{e}^{-2\frac{(x - x_c)^2}{w^2}}, \tag{13}$$

where w – FWHM of the Gauss function.

Figure 3 shows the respective fitting results for the experimental instrument function (He laser line). We can see the experimental instrument function and its approximation with the Voigt function (fitting parameters are: the FWHM of Gaussian part ω_G is of 0.02926 (0.02012) cm^{-1}, the FWHM of the Lorentz part ω_L is of 0.02926 (0.01854) cm^{-1}); the fit to the Lorentz function (fitting parameters are: the FWHM ω_L is of 0.02862 (0.00341) cm^{-1}), and the fit to the Gauss function (fitting parameters are: the FWHM ω_G is of 0.03974 (0.00247) cm^{-1}).

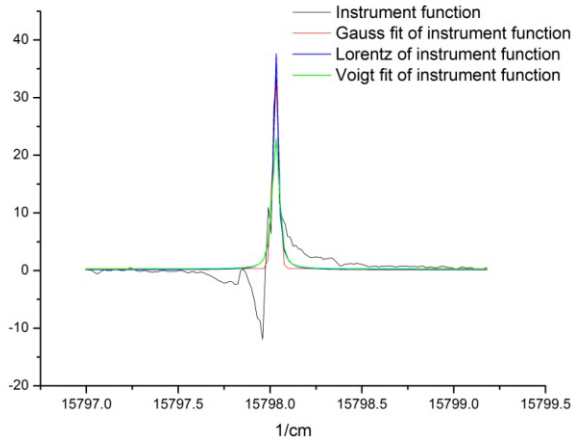

Fig. 3 – The experimentally measured instrument function (black line) of the Fourier transform spectrometer Bruker IFS-125HR and its approximation: the Voigt function (green line); the Lorentz function (blue line); the Gauss function (red line).

The best fitting results were obtained for the fitting with the Lorentz function (FWHM of 0.03 cm^{-1}), so we decided to use it for further tests.

In Fig. 4 the examples of deconvolution are shown when the instrument function was taken as a data array (blue line), Lorentz function (red line) and as a function described by Eq. 10 (green line). Figure 4 shows the deconvolution example for the measured 546 nm Hg line, emitted from Hg/Ar lamp without magnetic field. The example clearly demonstrates the case when the self-absorption dip in the centre of spectral line is covered by the instrument function.

The comparisons in figures below clearly demonstrate that the deconvolution procedure in cases, when instrument function was taken in a form of raw data, or as a theoretical instrument function described by equation (10), gave very noisy solutions on the wings of profiles. Also, this test illustrates that the best approximation of instrument function was its approximation with the Lorentz function.

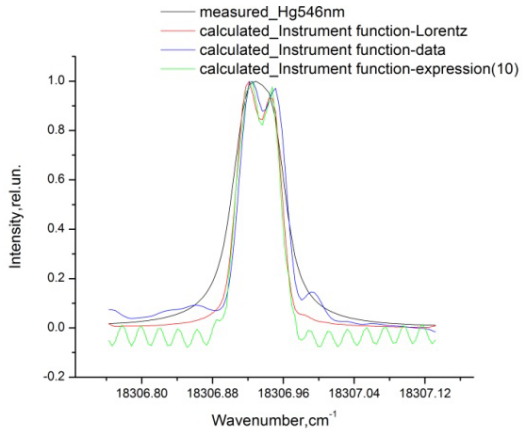

Fig. 4 – The example of the measured Hg 546 nm spectral line (black line) and calculated real lines in the case, when instrument function was taken as a data array (blue line), Lorentz function (red line) and as a function described by Eq.10 (green line). Line was emitted from Hg/Ar lamp without magnetic field.

4. RESULTS AND DISCUSSION

Figures 5a and 5b show the results for the vertical lamp operation, with Hg reservoir up and Hg reservoir down, respectively. All experimental lines were normalised for the line shape calculations and deconvolution. The line is split due to the Zeeman effect into one non-shifted π component and two σ components. The deconvolution was done using two independent methods Eq. (8) and Eq. (9) for finding the regularisation parameter.

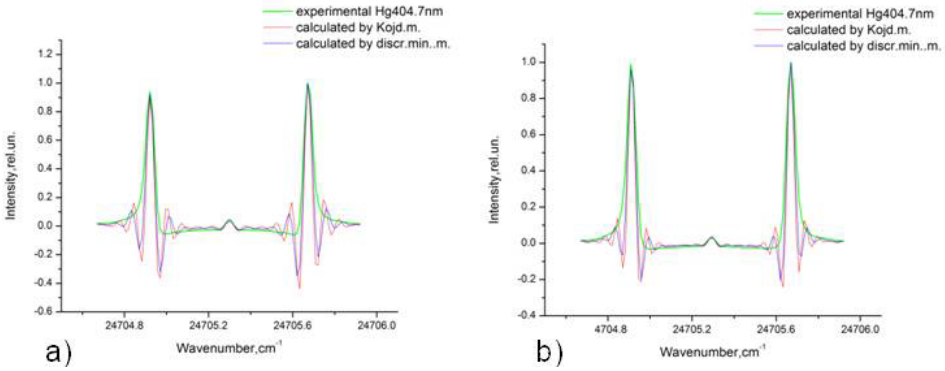

Fig. 5 – Measured and deconvoluted Hg 404.7 nm profiles: green line – experimental profile; blue and red lines – calculated real profiles, obtained using discrepancy minimization method for the getting of the regularisation parameter, and method when α is root of Eq. (9), respectively. a) Lamp was operated vertically with Hg reservoir up; b) lamp was operated vertically with Hg reservoir down**.**

After the deconvolution we performed Gauss fit to the calculated real lines, using expression (13).

In the Table 1 we can see the values of the full width at half of maximum (FWHM) of the Gauss profile. The values are shown for the Hg 404.7 nm emission line for vertical position of the lamp. The results of the solutions are shown for both methods of finding the regularisation parameter.

Table 1

The results of the deconvolution: the FWHM of the calculated real line shapes from the Gauss fit to the calculated real profiles for the Hg 404.7 nm emission line for both vertical positions of the lamp

FWHM(cm^{-1}) after Gauss fit	Peak 1	Peak 2	Peak 3	Lamp position
Experimental	0.05020	0.03148	0.04746	Vertically, with Hg reservoir up
Real calculated (discr.min.met.)	0.03541	0.03892	0.03437	
Real calculated (Kojdecki met.)	0.02893	0.02901	0.02826	
Experimental	0.05072	0.03176	0.05036	Vertically, with Hg reservoir down
Real calculated (discr.min.met.)	0.03518	0.02720	0.03539	
Real calculated (Kojdecki met.)	0.02873	0.02946	0.02903	

Both methods give credible results. However, we can observe that the Kojdecki method gives smaller values of the FWHM of the calculated real line shape than discrepancy method. It can be explained by the fact that the method proposed by Kojdecki strongly depends on errors of measurements and instrumental function. For application of the discrepancy minimization method it is necessary to know only the instrument function. We can also observe that the signal for the horizontal lamp position is very weak (see Fig. 2); therefore, the results of calculations for this working position were not taken into account for temperature estimation.

The motion of atoms in accordance to the Maxwell law is isotropic in the space, and therefore the width at half of maximum (FWHM) corresponds to the Doppler effect. Thus, the temperature of radiating atoms can be obtained by the following expression [15, 16]:

$$T = \frac{\mu}{\left(7.16 \times 10^{-7} x_0\right)^2} \Delta x_D^2 \,, \tag{14}$$

where T is the absolute temperature of emitting atoms, μ – the atomic mass, x_0 – the position of the scale of the frequencies, when the Gauss function reaches its maximum value, and Δx_D – the FWHM of Gaussian function. The average

calculated temperature value of radiating atoms is of 653.5 K, which is in good agreement with our initial calculations [5]. The relative error is 19%. No clear evidence of the temperature changes in different working positions was found. In addition, the magnetic field intensity was calculated from the Zeeman splitting of the spectral lines. The separation of the components Δx is dependent on the intensity of magnetic field $\boldsymbol{H}$:

$$\Delta x = \frac{1}{4\pi c}\frac{e}{m}\boldsymbol{H}. \tag{15}$$

Here e and m stands for charge and mass of electron, c – speed of light. Using this formula, we get the value of 4016 oersted ($3.1958 \cdot 10^5$ A/m) for the intensity of magnetic field. Further investigations are necessary to estimate the role of magnetic field inhomogeneity on the broadening of the line shapes.

5. CONCLUSION

In this paper we report the investigation of narrow multiple line shapes by means of the Fourier transform spectrometer. The lines were emitted from microsize capillary Hg/Xe discharge lamps, placed in magnetic field. Line shapes were deconvoluted from instrument function by means of the Tikhonov's regularisation method. Detailed analysis of the instrument function of the Fourier transform spectrometer was performed, leading to the conclusion that the best approximation for regularisation method was approximation with the Lorentz function. We proved the possibility to obtain the regularisation parameter by two different ways; however, more statistical data are necessary for the usage of Kojdecki method. The calculated temperature value of radiating atoms is of 655 K, which is in good agreement with our initial calculations [5]. Further research is necessary to understand the influence of operation position and magnetic field on the processes in the capillary discharge plasma.

Acknowledgments. G.Revalde acknowledges the support from the European Social Fund within the Project "Elaboration of Innovative Functional Materials and Nanomaterials for Application in Environment Control Technologies" 1DP/1.1.1.2.0/13/APIA/VIAA/30.

A.Skudra and Z.Gavare acknowledge the partial support from the ERDF project No.2010/0260/2DP/2.1.1.1.0/10/APIA/VIAA/166.

REFERENCES

1. A. Ganeev, Z. Gavare, V.I. Khutorshikov, S.V. Khutorshikov, G. Revalde, A. Skudra, G.M. Smirnova, N.R. Stankov, Spectrochimica Acta Part B, **58**, 879–889 (2003).
2. N. Zorina, Nuclear Instruments and Methods in Physics Research Section A, **623**, 763–765 (2010).
3. G. Revalde, A. Skudra, N. Zorina, S. Sholupov, J.Q.S.R.T., **107**,164–172 (2007).

4. N. Zorina, G. Revalde, R. Disch, in SPIE Sixth International Conference on Advanced Optical Materials and Devices, University of Latvia, Riga, **7142**, 71420J-1 (2008).
5. G. Revalde, N. Zorina, J.Skudra , A. Skudra, ICLS 2012, St. Petersburg, 2012.
6. G.Revalde, N.Zorina, A.Skudra, Imaging and Applied Optics: OSA Optics & Photonics Congress, 23–27 June 2013, VA, USA, JTu4A.12 (2013).
7. N. Denisova, G. Revalde, A. Skudra, and Ja. Skudra, Spatial Diagnostics of Hg/Ar and Hg/Xe Discharge Lamps by Means of Tomography, Jpn. J. Appl. Phys., **50**, 08JB03 (2011).
8. W. Bell, A.L. Bloom, Electrodeless discharge method and apparatus, US Patent 2975330, 1961.
9. *** Tables of physical quantities, Handbook, Moscow, Atomizdat, 199 (1976).
10. A. Tikhonov, V.Arsenin, *The solution's methods of the ill-posed problem*, Moscow, Nauka, 1979.
11. F. Verlan, V.S. Sizikov, *The integral equations: the methods, algorithms, program*, Kiev, Naukova Dumka, 1986.
12. M.A. Kojdecki, *New criterion of regularization parameter choice in Tikhonov's method*, Biuletyn WAT (Biul. Mil. Univ. Technol.), **49**, *1*, (569), 47–126 (2000).
13. V. Revalds, Spektrālie aparāti, University of Latvia, Part 3 (in Latvian), 1977, pp. 91–93.
14. P. Griffiths and J. de Haseth (Edit.), *Fourier transform infrared spectrometry*, Wiley & Sons, 1986.
15. E. Frish, Spectroscopy of the gas discharge plasma, Nauka, Leningrad, 25–26, 1970, p. 9.
16. W. Demtroeder, *Laser Spectroscopy*, third ed., Springer, 2003, p. 70.

Proceedings(Scopus)

Pr3

Deconvolution of the mercury 253.7 nm spectral line shape for the use in absorption spectroscopy

N.Zorina*[a], G.Revalde[a], R.Disch[b]
[a]Institute of Atomic Physics and Spectroscopy, University of Latvia, Skunu 4, Riga, LV-1050, Latvia
[b]Sieck Maihak GmbH, Nimburger Str.11, D-79276, Reute, Germany

ABSTRACT

In this work we present measurement and results of the deconvolution of the Hg 253.7 nm spectral line shapes, emitted from the mercury isotope high-frequency electrodeless discharge lamps, made at the Institute of Atomic Physics and Spectroscopy for the use in Zeeman Atomic Absorption Spectrometry. The emission line profiles of 254 nm Hg resonance line have been measured by means of a Zeeman scanning spectrometer at the mercury cold spot temperature value at 20 deg C. Then the deconvolution procedure or solving of this ill-posed inverse problem by means of the Tikhonov's regularization method [1] was performed to obtain the real spectral line shape.

Keywords: high-frequency electrodeless discharge lamps; Mercury 253.7 nm, absorption spectroscopy; deconvolution, Tikhonov regularization

1. INTRODUCTION

Light sources, based on high-frequency or radio-frequency electrodeless discharge are widely used for the atomic absorption analysis (AAA). Our research is connected with the preparation and diagnostics of new performance of high frequency electrodeless light sources (HF-EDLs), filled with different elements for their use in scientific devices [2]. Special attention is paid to the investigations of mercury and mercury isotope HF-EDLs, and their optimization for the use in atomic absorption analysis. Exploitation of Hg HF-EDLs in AAA demands specific conditions with taking into account lamp design, radiation, working time and other characteristics. In AAA high a quality emission line profile is needed. Therefore the high-resolution spectral line profile measurements and optimization of the lamp characteristics is necessary [3].

Zeeman Atomic Absorption Spectrometry (ZAAS) is a very sensitive method to determine mercury concentration in the environment. One of the core elements in the spectrometer is a mercury spectral lamp. To reach ambitious limits of the detection (for example, 1-2 ng/m3 for the mercury concentration in the air), the spectral lines used for the absorption has to be very narrow and without self-absorption.

Information about mercury 253.7 nm resonance line is important also in fluorescent lamp technology where mercury/argon discharge is used. Data about resonance lines structure in dependence on the cold spot temperature can be used not only for the lamp diagnostics but also for the validation of different type of calculations and models, considering radiation trapping [4].

In this work we have performed measurements of the 253.7 nm spectral line profile emitted from the natural Mercury and Mercury isotope high-frequency electrodeless discharge lamps by Zeeman spectrometry and recovering (doconvlution) of the real spectral line shape by means of Tikhonov's regularization method .

The measured line profile is distorted by the instrument function of the spectrometer. The instrument function can cover detailed structure of the spectral line, like the dip in the line centre caused by the self-absorption (self-reversal) and characterising the radiation trapping. To detect the quality of the spectral line shapes, emitted from the lamps, it is necessary to deconvolute the instrument function from the measured spectral line.

*zorina_n@pit.lv

Sixth International Conference on Advanced Optical Materials and Devices (AOMD-6), edited by
Janis Spigulis, Andris Krumins, Donats Millers, Andris Sternberg, Inta Muzikante, Andris Ozols, Maris Ozolinsh
Proc. of SPIE Vol. 7142, 71420J · © 2008 SPIE · CCC code: 0277-786X/08/$18 · doi: 10.1117/12.815460

To perform the restoring of the spectral line shape, preliminary information about instrument function of the spectrometer is necessary.

2. EXPERIMENTAL

In this work we have investigated HF electrodeless light sources of special type, manufactured at the Institute of Atomic Physics and Spectroscopy. The lamps are filled with mercury of natural abundance or with pure isotope Hg 198 and buffer gas argon of about 2 Torr pressure(Fig.1).

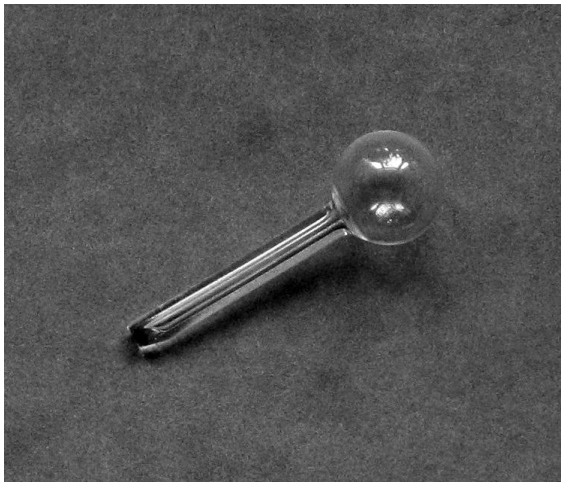

Fig.1. HF electrodeless discharge lamp.

The experimental set-up is shown in Fig. 2[5]. The working principles of spectrometer are following: radiation from the Hg light source (1) passes through a polarizer (2), where it has been separated into σ^+ and σ^- components. After that, in order to use the Zeeman scanning for the analysis of emission lines, one component has to traverse the same metal vapour cell(3). The mercury absorption line is separated due longitudinal Zeeman effect in the magnetic field of the electromagnet(4). The separation is proportional to intensity of magnetic field:

$$\Delta\nu = \frac{1}{4\pi c}\frac{e}{m}\vec{H}. \tag{1.4}$$

Or, in wavelength scale:

$$\Delta\lambda = \frac{1}{4\pi c^2}\left(\frac{e}{m}\right)\lambda^2\vec{H}. \tag{1.5}$$

By scanning of the magnetic field intensity using block (6), the distance between the separated lines is changing as shown in formula (1.5). When absorption line of Hg cell coincidences with the radiation line, emitted from the lamp, the level of lighting of photodetector (5) gets low. It allows registering the spectra of investigated lamp. The Holl detector(7) is applied for the scale obtaining.

The advantage of Zeeman spectrometer in comparison with commonly used Fabry-Perot interferometer [6] is quite narrow instrument function. The instrument function is given by the absorption spectral line profile, determined by the Doppler broadened profile for mercury vapour temperature in the absorption cell, in our case at the room temperature of 20 deg.C (0.046 cm^{-1}) .

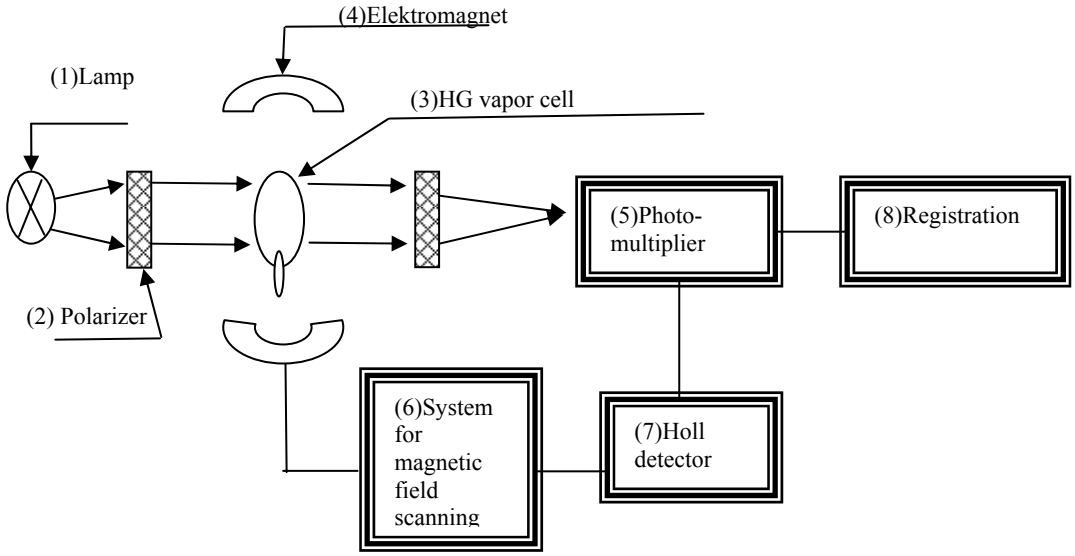

Fig.2. Experimental set-up of Zeeman spectrometer

3. THEORETICAL APPROACH

The measured (experimental) spectral line $f(x)$ is a convolution of the real line profile $y(x)$ of emitted spectral line and instrument function $A(x,s)$ It can be described by Fredholm first kind integral equation [1,7,8]:

$$\int_a^b A(x,s)y(s)ds = f(x), \quad c \le x \le d, \tag{1}$$

where: a, b and c, d the limits of the real and measured (experimental) profiles accordingly. Usually they are chosen such, that a=c and b=d.

To obtain the real spectral line shape it is necessary to solve an inverse ill-posed by Hadamard task (1) where small experimental uncertainties can cause large deviations in the solution. The solution of such problem is not possible directly [8]. For ill-posed problems in classical sense, the successful usage of the different methods of solution

are shown [9]. Some authors use Fourier transform and regularization method [10]. In this work we performed our calculation using Tikhonov regularization method. [1,8,11].

Tikhonov's regularization algorithm is one of the most useful tools for solving the task where small experimental uncertainties can cause large deviations in the solution [12,13].

He proved that an initial, ill-posed task can be transformed to a task of the minimum searching of the smoothing functional:

$$M_\alpha\left[y,\tilde{f}\right] = \inf_{y\in Y} M_\alpha\left[y,\tilde{f}\right], \tag{2}$$

Assuming, that values of the right side and integral equation (1) kernel are known with accuracy:

$$\left.\begin{aligned} \left\| \tilde{f} - f \right\|_F \le \delta; \\ \left\| \tilde{A} - A \right\| \le \xi \end{aligned}\right\} \tag{3}$$

where δ is error of right part of (1) or error of experimental $f(x)$ profile , ξ is error of kernel of (1) or error of instrument function $A(x,s)$.

Smoothing functional $M_\alpha\left[y,\tilde{f}\right]$ so called Tikhonov's functional, is given in form:

$$M_\alpha\left[y,\tilde{f}\right] = \left\| \tilde{A}y - \tilde{f} \right\|_F^2 + \alpha\Omega[y], \tag{4}$$

where $\alpha > 0$ -regularization's parameter; number-$\left\| \tilde{A}y - \tilde{f} \right\|_F^2$ - discrepancy.
Stabilizing functional Ω is described by following expression:

$$\Omega[y] = \|y\|_Y^2 \tag{5}$$

As the result of minimization (4) in case when $y \in W_2^1$ and $\tilde{f} \in L_2$ taking into account norm definitions in these spaces:

$$\left.\begin{aligned} \|y\|_{W_2^1} &= \sqrt{\int_a^b y^2(s)ds + \int_a^b \left(y'(s)\right)^2 ds} \\ \left\|\tilde{f}\right\|_{L_2} &= \sqrt{\int_c^d \tilde{f}^2(x)dx} \end{aligned}\right\} \tag{6}$$

instead of ill-posed first kind integral equation (1), we get the second kind integral equation:

$$\alpha\left(y_\alpha(t) - q y_\alpha''(t)\right) + \int_a^b k(t,s) y_\alpha(s)\,ds = F(t) \quad t \in [a,b], \tag{6}$$

where:

$$\begin{aligned} k(t,s) = k(s,t) &= \int_c^d \tilde{A}(x,t)\tilde{A}(x,s)\,dx; \\ F(t) &= \int_c^d \tilde{A}(x,t)\,\tilde{f}(x)dx. \end{aligned} \tag{7}$$

Changed integrals in (6) to finite sums we obtain the system of lineal equations:

$$\sum_{i=1}^N b_i \left(\sum_{m=1}^N b_m \tilde{A}_{mk} \tilde{A}_{mi} \right) y_i + \alpha y_k = \sum_{m=1}^N b_m \tilde{A}_{mk} \tilde{f}_m, \quad k = \overline{1,N} \tag{8}$$

or matrix equation

$$\left(\tilde{A}^* \tilde{A} + \alpha E\right) Y = \tilde{A}^* \tilde{f} \tag{9}$$

where, где A_{ij} – elements of N xN size matrix A, which approximates kernel $K(x,x)$; f_i – vectors– column with initial dates ; y_i –vector – column of solution, b_i.- the coefficients of quadrature formula .

In this work the solution was implemented in Math Cad (was used numerical algorithm of conjugate gradient) and Delphi (was used numerical algorithm of Brent) for case when $q = 0$ (zero order of regularization).

Regularization parameter α is determined using the minimization of discrepancy:

$$\left\| \tilde{A} y_\alpha - \tilde{f} \right\|_{L_2}^2 = \min_\alpha \left\| \tilde{A} y_\alpha - \tilde{f} \right\|_{L_2}^2 \tag{10}$$

and by Kojdecki method [14]. According this method α is root of equation:

$$\alpha^q \left\| \tilde{A}^* \tilde{A}\, y_\alpha - \tilde{A}^* \tilde{f} \right\| = \beta \,||\, \tilde{A} \,||\left(\delta + \eta \left\| y_\alpha \right\|\right) \tag{11}$$

or assumed (9):

$$\alpha^{q+1} \left\| y_\alpha \right\| = \beta \,||\, \tilde{A} \,||\left(\delta + \eta \left\| y_\alpha \right\|\right) \tag{12}$$

In this work α was obtained from (12) in supposition, that error of kernel η=0. The coefficients were chosen as q=0 and β=1. Variance of errors of measured line is 0.13.

4. RESULTS AND DISCUSSIONS

4.1. HF- ED lamp filled with natural Mercury mixture.

The natural mixture of Hg consists of seven isotopes, which gives the five resulting components in the spectra of the 253,7 nm line. In Fig.3 we can see measured 253,7 nm line profiles emitted from HF-EDL filled with natural mixture of Hg isotopes registered at the moment of switching the lamp (Fig.3a)and after 5 minutes of its operating (Fig.3b). Such investigation is necessary to obtain the lamp warming-up time. The lamp was operated with the HF electromagnetic field of about 100 MHz frequency and the discharge current was of 0.1 mA. In both figures, the deconvoluted real line profile, using Tichonov's regularisation method is shown as well.

As we can see, the total width of the 253,7 nm line profile, emitted from the natural Hg lamp, is quite broad- the total width of such line is about 0,8 cm^{-1}. Thus it can not be used for ZAAS, because this method needs very narrow spectral line to reach high sensitivity. Therefore we consider Mercury lamp filled with only one isotope.

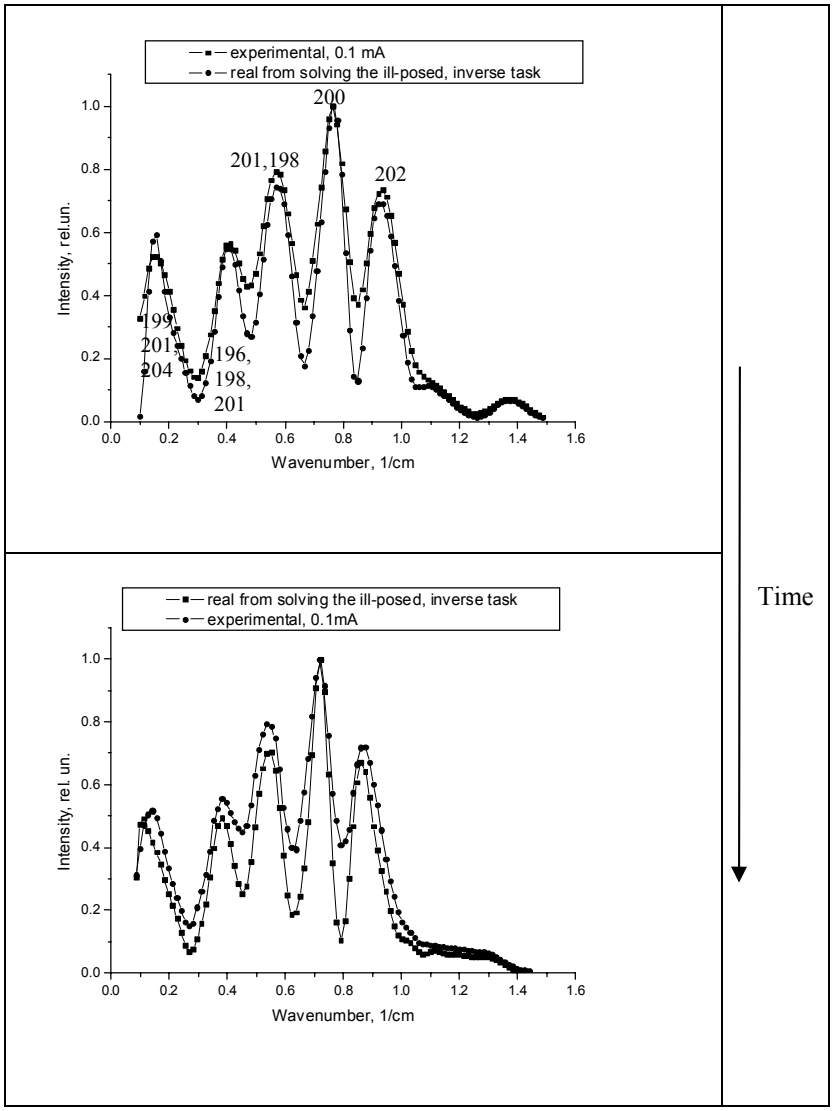

Fig. 3. The measured and deconvoluted line profiles emitted from HF-ED lamp filled with natural mixture of Hg (at time moment of ignition, (a) and after 5min of working (b))

4.2. HF- ED lamp filled with pure isotope Hg 198.

On the Fig.5. we can see measured line emitted from Hg HF-EDL filled with pure isotope Hg 198 (92.8%) and buffer gas argon of about 2 Torr pressure.

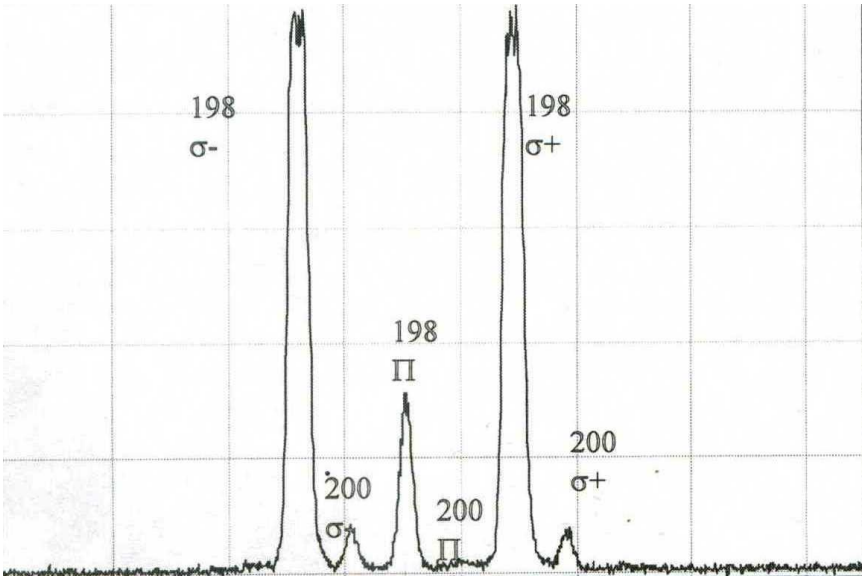

Fig. 4. The measured line profile emitted from HF-ED lamp filled with pure isotope Hg 198 (92.8%) and buffer gas argon of about 2 Torr pressure.

Results of the deconvolution of the right and left components are shown at Fig. 5a and Fig. 5b accordingly.

In this case parameter of regularization was determined by two ways. Using the minimization of discrepancy (10) and by Kojdecki (12).

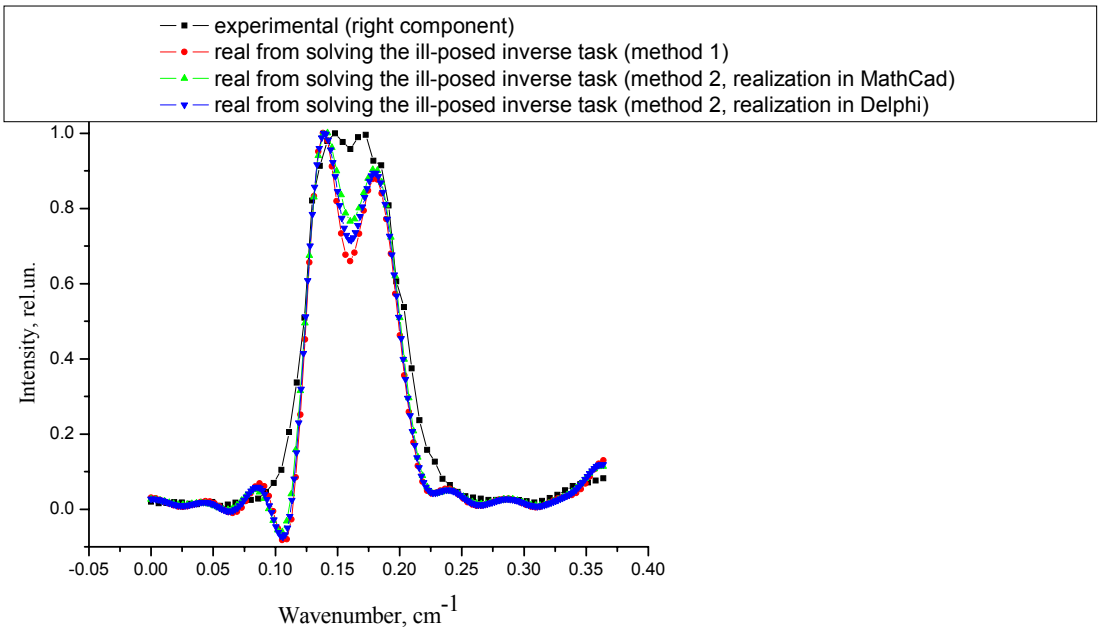

Fig.5(a). Measured and deconvoluted line profiles (right component) emitted from HF-ED lamp filled with pure isotope Hg 198 (92.8%) and buffer gas argon of about 2 Torr pressure. The solution by second method (formula(12)) was implemented in Delphi using algorithm of Brent (α=2.61318652730945E−5)and in Math Cad using algorithm of conjugate gradient (α=3.745E−5). The regularization parameter obtained in Mathcad from minimization of discrepancy is 1.664E-5. (Accuracy E-7).

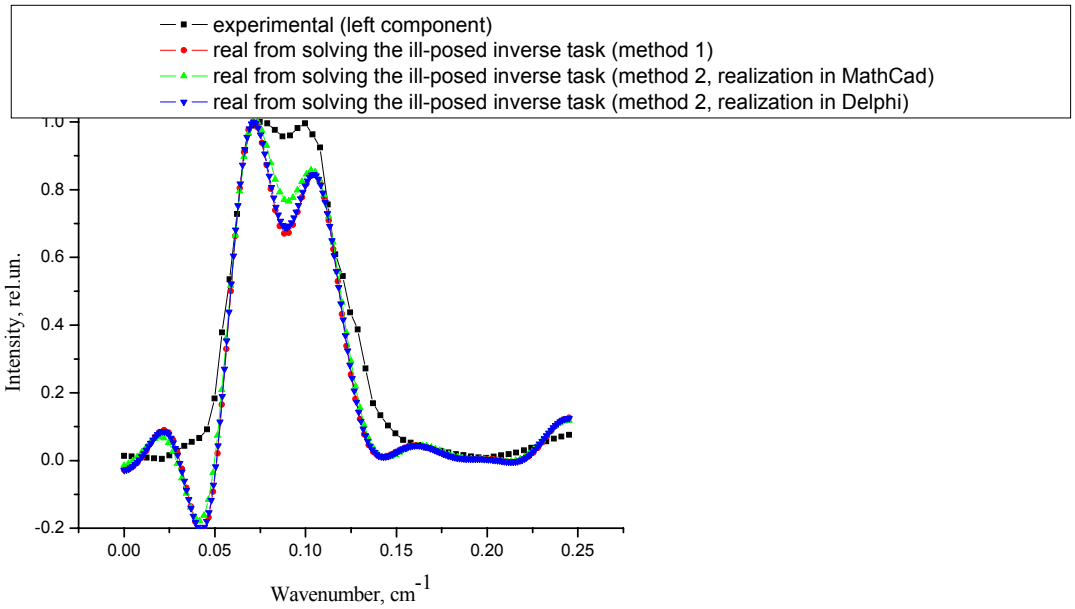

Fig.5(b). Measured and deconvoluted line profiles (left component) emitted from HF-ED lamp filled with pure isotope Hg 198 (92.8%) and buffer gas argon of about 2 Torr pressure. The solution by second method (formula(12)) was implemented in Delphi using algorithm of Brent (α=2.25700219881838E-5) and in Math Cad using algorithm of conjugate gradient (α=3.253E-5). The regularization parameter obtained in Mathcad from minimization of discrepancy is 2.068E-5. (Accuracy E-7)

The parameters of regularization determined for both components are shown in the table 1:

Table 1. The parameters of regularization determined for both components, using two different methods and two algorithms for numerical calculation

Method	Right component	Left component
Minimization of discrepancy	1.664E-5	2.068E-5
By Kojdecki(MathCad)	3.745E-5	3.253E-5
By Kojdecki(Delphi)	2.61318652730945E-5	2.25700219881838E-5

The waves observed in the left side wing of the obtained real spectral line profile in Fig.5 are due to the difficulty to stabilise the solution for the given level of errors of experimental data. The experimental profiles, shown in Fig.4, are very narrow, with very sharp increase and decrease of signal and this gives quite high level of uncertainty of numerical experimental. Nevertheless, from the obtained lines we can see that the doconvoluted profiles have larger dip in the line centre than the experimental ones. The centre of the spectral line profile is also the most interesting part for the deconvoluted spectral line for AAA, because the dip in the line centre shows that the self-absorption is present. In general good agreement can be observed between the deconvoluted real spectral line profiles using different methods of obtaining the regularisation parameter.

5. CONCLUSION

In this work we present measurement and results of the deconvolution of the Hg 253.7 nm spectral line shapes, emitted from the Mercury isotope high-frequency electrodeless discharge lamps, filled with the natural and pure isotope filling. The measurements was performed Zeeman atomic absorption spectrometry and the deconvolution from the instrument function was done by the Tikhonov regularization method. Good agreement of deconvoluted real spectral line profiles is reached using two different ways of obtaining the regularization parameter.

ACKNOWLEDGEMENTS

This work was partly supported by the European social fund and Latvian Council of Science grant Nr. 05.1866.

REFERENCES

[1] Tikhonov A., Goncharski A., Stepanov V., Jagola A., [Numerical solution's methods of the ill-posed problem], Nauka, Moscow, 5-231 (1990).
[2] Revalde G., Silinsh J., Spigulis J., Skudra A., "High-frequency electrodeless ligh sources for application", Proc.SPIE 4318, 78-83 (2000).
[3] Ganeev A., Gavare Z. et all, "High-frequency electrodeless discharge lamps for atomic absorption", Spectrochemica Acta, B 58, 879-889 (2003).
[4] Rajaraman K., Kushner M. J., "A Monte Carlo simulation of radiation trapping in electrodeless gas discharge lamps", J Phys D, 37,1780-1791 (2004).
[5] Vasiljev O., Kotkin A., Stoljarov D., Chopornjak D., Umorhodzhajev R., " High-frequency electrodeless light sources", Acta Universitatis Latviensis, 573, 105-110 (1992).
[6] Revalde G., Berzina D., Lhevkovski V., Luizova L., Putnina S., Reppo P., et al., " The automatic spectrometric complex for spectral line profile measurements", J Appl Spectrsc, 56, 681–686 (1992).
[7] Lebedeva V., [The technique of the optic spectroscopy], Moscow university, Moscow, 353-364 (1977).
[8] Tikhonov A., Arsenin V., [The solution's methods of the ill- posed problem], Nauka, Moscow, 9-285 (1979).
[9] Verlan F., Sizikov V., [The integral equations: the methods, algorithms, program], Naukova Dumka, Kiev, 223-321 (1986).
[10] Xiang-Tuan Xiong, Chu-Li Fu, Hong-Fang LiJ, "Fourier regularization method of a sideways heat equation for determining surface heat flux", Math Anal Appl, 317, 331–348 (2006).
[11] Groetsch C. W., [The theory of Tikhonov regularization for Fredholm equations of the first kind], Pitman, London, 3-100 (1984).
[12] Rajan M. P., "An efficient discretization scheme for solving ill-posed problems", J. Math. Anal. Appl., 313, 654–677 (2006).
[13] Revalde G., Skudra A., Zorina N., Sholupov S., "Investigation of Hg resonance 184.9nm line profile in a low-pressure mercury–argon discharge", JQSRT, 107, 164–172 (2007).
[14] Kojdecki M.A., "New criterion of regularization parameter choice in Tikhonov's method ", Biuletyn WAT (Biul. Mil. Univ. Technol.), 49(1), 47–126 (2000).

Pr5

Diagnostics of capillary light sources by means of line shape measurements and modeling

2012 J. Phys.: Conf. Ser. 397 012070

(http://iopscience.iop.org/1742-6596/397/1/012070)

Journal of Physics: Conference Series **397** (2012) 012070 doi:10.1088/1742-6596/397/1/012070

Diagnostics of capillary light sources by means of line shape measurements and modeling

G Revalde, N Zorina, J Skudra and A Skudra

Institute of Atomic Physics and Spectroscopy, University of Latvia, Šķunu str. 4, Riga, Latvia, LV 1050

E-mail: gitar@latnet.lv

Abstract. In this work the Hg visible triplet spectral lines were measured by means of Fourier Transform spectrometer and deconvoluted by Tikhonov's regularisation method and line shape modelling. The lines were collected from Hg/Ar and Hg/Xe high frequency capillary lamps. In our previous work, the spatial plasma homogeneity of isotope Hg/Xe and Hg/Ar capillary lamps was investigated by means of tomography. The lamps were operated in different working positions – horizontally and vertically. In this work the spectral diagnostics of capillary light sources by means of spectral line shape measurements and modelling is presented to obtain plasma temperature. The results are compared with the results for spectral line shapes emitted from the spherical light sources. The splitting of spectral lines in magnetic field due to Zeeman effect was observed.

1. Introduction

The capillary light sources are obtained an increasing attention due to the need in compact high-intensity light sources for different applications where narrow line sources are needed [1]. Spatial homogeneity of the plasma and emission profile is important for the use of such light sources in precision measurements. In addition, capillary light sources are difficult to investigate due to the small dimensions of the source, and spectral line shapes are one of the possibilities to get useful information about plasma properties, for example, plasma temperature.

The Hg/Ar, Hg/Xe, Hg/Kr high frequency (HF) capillary discharge lamps (figure 1) were manufactured in our laboratory. In our previous work, the spatial distribution of atoms in Hg/Xe, Hg/Ar, Hg/Kr spherical and capillary lamps was investigated by means of tomography [2-4]. In [3] the radial profiles of excited atoms showed differences in dependence of the horizontal or vertical operation position. To understand the mechanisms of this phenomenon, more information about processes in capillary lamps is necessary. In this work the results of spectral line shape diagnostics of capillary light sources are presented. The diagnostics include measurements of the spectral line shapes by high resolution Fourier spectrometer and later deconvolution to get the real spectral line shapes. The real lines shapes are modelled to estimate the plasma

Figure 1. Design of the capillary electrodeless light source - lamp together with HF generator.

temperature and homogeneity. The results are compared with the results for spherical discharge lamps.

2. Experimental

The capillary light sources were filled with mercury isotope of 0.003 Torr pressure and argon, xenon or krypton of 2 Torr pressure. The length of the capillary was of 2 cm. The discharge size was of 500 μm in radius. The lamp contains spherical mercury reservoir to control the vapour pressure inside the lamp, and it was kept at the room temperature. The lamps were operated by HF electromagnetic field of 100 MHz frequency, capacitive coupled from outer electrodes located at the ends of the capillary [1].

In this work the emission spectral line shapes from the Hg visible triplet 7^3S_1-$6^3P_{0,1,2}$ transitions (with the wave lengths Hg 404,7 nm, 435.8 nm, 546.1 nm respectively) were investigated for the Hg/Ar and Hg/Kr capillary lamps, operated in three different positions, horizontally, vertically with the Hg reservoir up and vertically Hg reservoir down. The spectral line profiles were registered also from spherical lamps of 1 cm diameter for comparison.

The spectral line shapes were registered by means of the Fourier Transform spectrometer *Bruker IFS-125HR*, allowing to register lines in the wavelength region 330-2000 nm. Examples of the registered spectral line shapes are shown in figure 2.

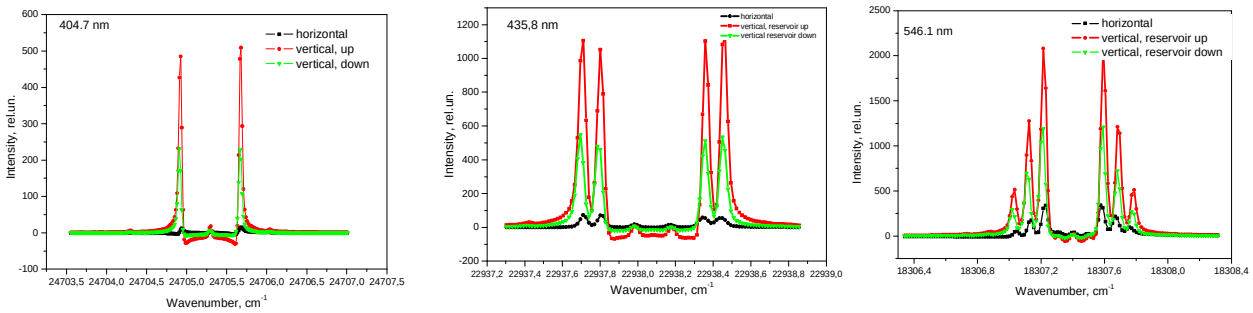

Figure 2. Experimental profiles of Hg visible triplet spectral lines 404.7 nm, 435.8 nm, 546.1 nm, emitted from the capillary light source. Light source was operated in three different operation positions: horizontally, vertically, Hg reservoir up, and vertically, Hg reservoir down. Line splitting is due to the magnetic field in the generator.

We can see that the FWHM of the experimental lines are about 0.06 cm^{-1}. In case of Fourier spectrometer the instrument broadening is on the same order as the width of real line shapes, emitted from low-pressure capillary discharge thus the deconvolution procedure has to be performed to get the real width without instrument distortion. The observed spectral lines are Zeeman split due to the magnetic field in the generator where the light sources are placed. The respective number of σ and π components can be observed. Clear difference of the intensities of the spectral lines in dependence of the operation position can be seen as already observed in our previous experiments [3].

3. Theoretical approach

3.1. Instrument function

The experimental instrument function of Fourier spectrometer is shown in figure 3. It was obtained registering 632.8 nm line from single mode He-Ne laser. For the detailed study of separate spectral line shapes, the influence of the approximation of instrument function of the Fourier spectrometer on the deconvolution results was estimated. The instrument function was approximated by Lorentz function, Gauss function, Voigt function and also the numerical data was taken for the calculations.

The best results were received for the approximation with the Lorentz function of 0.02 cm^{-1} FWHM which was used for the following calculations.

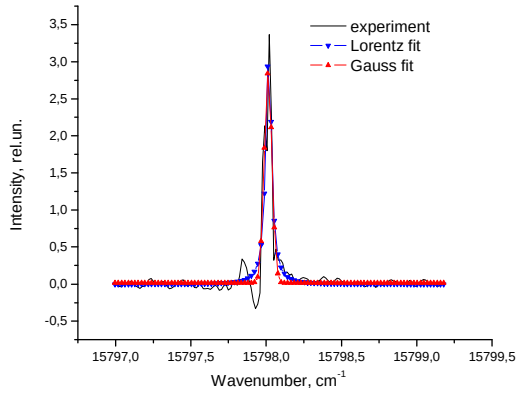

Figure 3. Instrument function of Fourier transform spectrometer and its approximation with Lorentz and Gauss functions.

3.2. Deconvolution method

Recovering the real spectral line profile from experimental line has always been an important problem in the high resolution spectroscopy. To study narrow emission lines like those emitted from capillary line sources, it is very important to deconvolute the instrument function to get the correct results for the plasma parameters. So-called problems of reduction to an ideal spectral device can be described by the first kind Fredholm integral equation:

$$\int_a^b A(\nu-\nu_0)y(\nu_0)d\nu_0 = f(\nu), \quad c \le \nu \le d, (1) \qquad (1)$$

Equation (1) is a convolution of an unknown real profile $y(\nu_0)$ with instrument function $A(\nu, \nu_0)$, where a, b and c, d are the limits of the real and measured (experimental) profiles accordingly. $A(\nu, \nu_0)$ is the instrument function of the Fourier spectrometer in our case. As well known, equation (1) is an inverse ill-posed task, where direct solution is not possible. To obtain the real spectral line shape we use two methods: solving the inverse non-linear problem by the Tickhonov's regularization method [5,6] and non-linear multi-parameter modeling, described in detail in [7]. Using Tikhonov's algorithm, the initial ill-posed task (1) can be transformed to solution of following matrix equation:

$$\left(\tilde{A}^*\tilde{A}+\alpha E\right)Y = \tilde{A}^*\tilde{f}\,, \qquad (2)$$

where, α – parameter of regularization; A_{ij} – elements of NxN size matrix A, which approximates kernel K(x,x); f_i –vectors– column with initial dates; Y_i –vector – column of solution. We use two different methods to determine the regularization parameter – method proposed by Kojdecki [6] and discrepancy method. After getting the real spectral line shape it was fitted to Gaussian profile. In the low-pressure discharge the main broadening mechanism is Doppler effect due to thermal motion of particles (the self-absorption is not present on the transitions under investigation). Thus the temperature of the radiating atoms was calculated from the FHWM of Gaussian profile [7].

4. Results and discussion

Figure 4 shows the example of the experimental and reconstructed line profiles using regularisation method. The wings of the real spectral line shape can be explained by the difficulties of the model to stabilise the solution by higher level of experimental uncertainties.

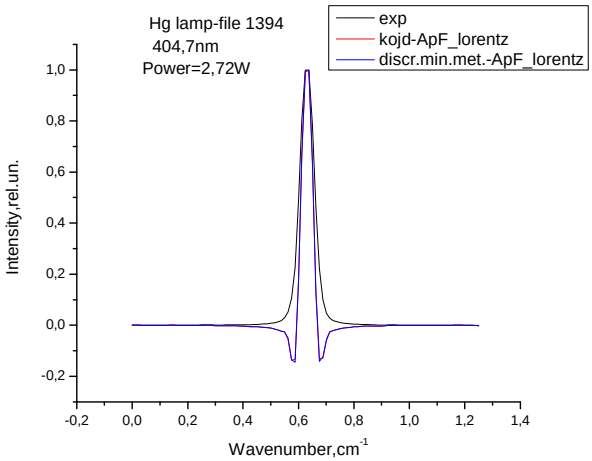

Figure 4. The experimental and reconstructed real Hg 404,7 nm spectral line profiles. Real line shape is reconstructed by two different methods for choosing the regularisation parameter – Kojdecki method and discrepancy method.

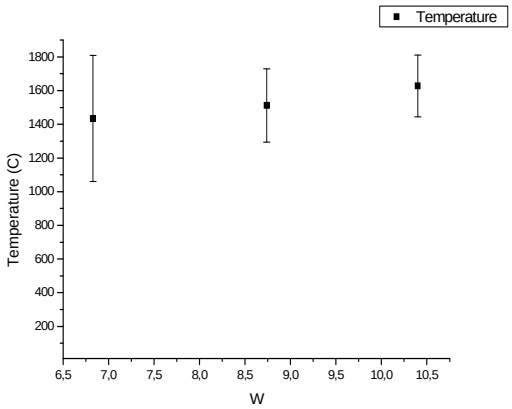

Figure 5. Calculated temperature of the emitting atoms in a spherical discharge in dependence of the discharge power.

For the capillary light sources, the temperature of emitting atoms was estimated to be about 600 K what is much lower than in spherical discharge lamps. The difference in line widths in dependence of observation positions could not be observed.

5. Conclusions

In this work we measured with Fourier spectrometer the profiles of Hg 404.7 nm, 435.8 nm, 546.1 nm lines, emitted from isotopic Hg/Ar and Hg/Xe capillary (500 μm diameter). The real spectral line shapes were obtained by means of the Tikhonov's regularisation method and mathematical modelling. The temperature of the emitting atoms was estimated. The calculations showed that the temperature of the atoms in the capillary light sources was about 600 K what is much lower than in a common spherical electrodeless discharge light source.

References

[1] Ganeev A et al 2003 *Spectrochem. Acta B* **58** 879
[2] Denisova N V 1998 *J.Phys.D: Appl.Phys* **31** 1888
[3] Denisova N, Revalde G, Skudra A and Skudra J 2011 *Jap. J. Appl. Phys.* **50** 08JB03
[4] Denisova N, Bogans E, Revalde G and Skudra J 2011 *Eur. Phys. J. Appl. Phys.* **56**, 24003
[5] Tikhonov A et al 1990 *Numerical solution's methods of the ill-posed problem* (Moscow: Nauka)
[6] Kojdecki M A 2000 New criterion of regularization parameter choice in Tikhonov's method, *Biuletyn WAT (Biul. Mil. Univ. Technol.),* V. 49. № 1 (569) 47–126
[7] Skudra A and Revalde G 1999 *J.Q.S.R.T.* **61** 717

Acknowledgments

The work was partially supported by ESF project "Spectrometric techniques for detection of heavy metal contaminants"(Nr.2009/0210/1DP/1.1.1.2.0/09/APIA/VIAA/100).

Pr6

Deconvolution of Multiple Spectral Lines Shapes by Means of Tikhonov's Regularization Method

G. Revalde[a], N. Zorina[b], A. Skudra[b]
[a]*Institute of Technical Physics, Riga Technical University, Kalku str.1, Riga, Latvia, LV 1050*
[b]*Institute of Atomic Physics and Spectroscopy, University of Latvia, Skunu 4, Riga, LV-1050, Latvia*
Gita.Revalde@rtu.lv; gitar@latnet.lv

Abstract: We present deconvolution of multiple narrow Zeeman split Hg lines, emitted from Hg/Xe micro-size capillary and measured by the Fourier Transform spectrometer. The ill-posed inverse problem was solved using the Tikhonov's regularization method.

1. Introduction

To determine the real spectral line shape from a noisy experimental profile it is necessary to solve an inverse ill-posed problem. In our previous works we used modeling of spectral line shapes taking into account all factors leading to spectral line shape creation [1]. Also Tikhonov's regularization method was applied to deconvolute an experimental spectral line shape for components σ^+ and σ^- separately [2] and for one component without magnetic field [3]. It was found that the method of the finding the regularization parameter is extremely important.

2. Experimental

In this work the emission spectral line shapes from the Hg visible triplet 7^3S_1-$6^3P_{0,1,2}$ transitions (with the Hg wave lengths of 404,7 nm, 435.8 nm, 546.1 nm respectively) were measured in magnetic field. Lines shapes were investigated for the Hg/Xe capillary lamp, manufactured at the Institute of Atomic Physics and Spectroscopy (University of Latvia) and operated by the electromagnetic field of 100 MHz frequency in three different positions, horizontally, vertically with the Hg reservoir up and vertically Hg reservoir down (Fig.1). The lamp was filled with mercury isotope of 0.003 Torr pressure and xenon of 2 Torr pressure. The length of the capillary was of 2 cm. The discharge size was of 500μm in radius.

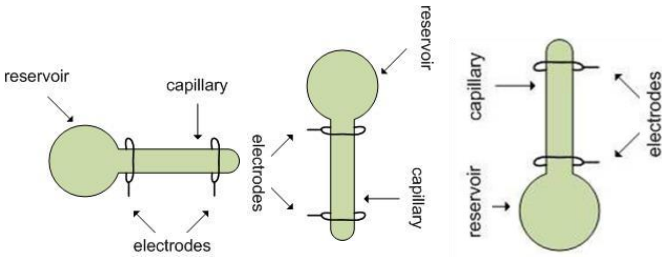

Fig. 1. Position of the Hg/Xe capillary lamp

Spectral lines were registered by means of the Fourier Transform spectrometer Bruker IFS-125HR, allowing to register lines in the wavelength region of 330-2000 nm.

Deconvolution to reach the real spectral line shape (without instrument function) was performed by means of Tikhonov's regularization method .

2. Theory

The measured (experimental) spectral line $f(x)$ is described by the Fredholm first kind integral equation [4]:

$$\int_a^b A(x,s)y(s)ds = f(x), \quad c \le x \le d, \qquad (1)$$

where : $y(x)$ - real line profile of emitted spectral line; $A(x,s)$ - instrument function; a, b and c, d - the limits of the real and measured (experimental) profiles accordingly.

Obtaining of the real spectral line shape is an inverse ill-posed problem where small experimental uncertainties can cause large deviations in the solution. The direct solution of such problem is not possible [4,5].

Tikhonov proposed the following smoothing functional:

$$M_\alpha\left[y,\tilde{f}\right]=\left\|\tilde{A}y-\tilde{f}\right\|_F^2+\alpha\Omega[y], \qquad (2)$$

where $\alpha>0$ -regularization's parameter; number-$\left\|\tilde{A}y-\tilde{f}\right\|_F^2$ - discrepancy; Ω- stabilizing functional is described by following expression:

$$\Omega[y]=\|y\|_Y^2 \qquad (3)$$

Tikhonov proved that the initial, ill-posed task can be transformed to a task of the minimum searching of the smoothing functional:

$$M_\alpha\left[y,\tilde{f}\right]=\inf_{y\in Y}M_\alpha\left[y,\tilde{f}\right], \qquad (4)$$

Assuming, that values of the right side and integral equation (1) kernel are known with accuracy:

$$\left.\begin{array}{l}\left\|\tilde{f}-f\right\|_F\le\delta;\\ \left\|\tilde{A}-A\right\|\le\xi\end{array}\right\}, \qquad (5)$$

where δ is error of right part of (1) or error of experimental $f(x)$ profile, ξ is error of kernel of (1) or error of instrument function $A(x,s)$, instead of the initial ill posed problem, which is described by Fredholm first kind integral equation, we have to solve the well posed Fredholm second kind integral equation. In matrix form it can be described by the following equation :

$$\left(\tilde{A}^*\tilde{A}+\alpha E\right)Y=\tilde{A}^*\tilde{f}\ , \qquad (6)$$

where: A_{ij} – elements of *NxN* size matrix *A*, which approximates kernel *K*(*x*,x); f_i – vectors– column with initial data; y_i –vector – column of solution, b_i.- the coefficients of quadrature formula. In detail it is described in [2].

The regularization parameter α is determined using the minimization of discrepancy:

$$\left\|\tilde{A}y_\alpha-\tilde{f}\right\|_{L_2}^2=\min_\alpha\left\|\tilde{A}y_\alpha-\tilde{f}\right\|_{L_2}^2 \qquad (7)$$

The solution was implemented in Math Cad for zero order of regularization. After deconvolution the real spectral line shapes were fitted to the Gaussian profiles and the temperature of the radiating atoms was calculated from the FHWM of Gaussian profile [1,3].

4. Results and discussion

On the Fig.2.-Fig.4 we can see the examples of the measured and deconvoluted Hg visible triplet spectral lines, emitted from Hg/Xe high frequency capillary lamp in case when it was operated vertically with the Hg reservoir up. For the deconvolution, the instrument function of the spectrometer was measured and approximated with the Lorentz profile with 0.03 cm^{-1} FWHM. Fig.2 presents our results for Hg 404.7nm line, Fig.3 and Fig.4 for the Hg lines of 435.8 nm, 546.1 nm wavelengths respectively. Due to the Zeeman effect, all lines are split.

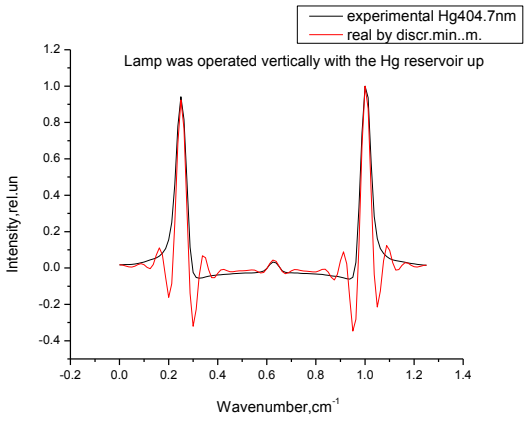

Fig. 2. Experimental and real line shapes of Hg 404.7nm line.

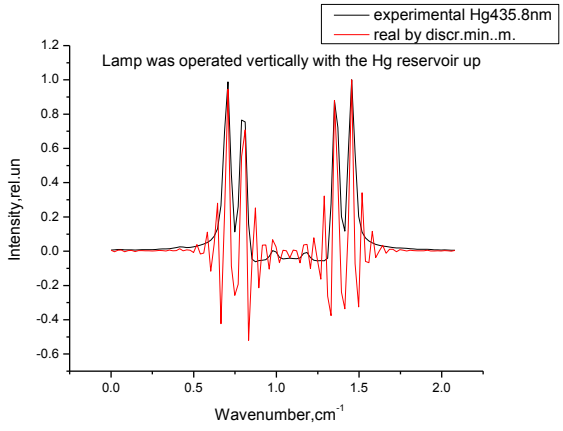

Fig. 3. Experimental and real line shapes of Hg 435.8 nm line.

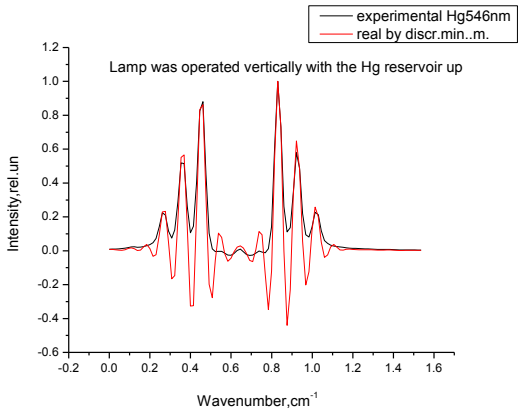

Fig. 4. Experimental and real line shapes, Hg 546.1nm line.

On the Table 1 the values of the full width at half of maximum (FWHM) of the Gauss profile are shown for the Hg 404.7nm emission line for all position of the lamp.

Table 1. The FWHM for Hg 404.7 nm

FWHM(cm^{-1})	Peak 1	Peak 2	Peak 3	Lamp position
Measured/Real	0.0485/0.0367	0.0471/0.0354	0.0718 /0.0586	Horizontally
Measured/Real	0.0502/0.0354	0.0515/0.0389	0.0475/0.0344	Vertically, with the Hg reservoir up
Measured/Real	0.0507/0.0352	0.0318/0.0272	0.0504/0.0354	Vertically with the Hg reservoir down

As can be seen on the figures and table, the deconvoluted profiles are significantly narrower than the measured ones. In low pressure plasma where the Doppler broadening is the dominant broadening effect, it is very important to take into account the instrument broadening and use the FWHM of the real line shapes for calculations. Since micro-size lamps are used for precision spectrometry, the deconvolution is necessary to detect the quality of the spectral line shapes.

5. Conclusions

In this work we show the possibility to implement Tikhonov's regularization method for deconvolution of real line shapes from the instrument function for multiple narrow Zeeman spectral line shapes, emitted from micro-size capillary light source. The FWHM of the real spectral line shapes was possible to obtain using zero order regularization and the minimum discrepancy method for estimation of regularization parameter, despite the fact that the stabilization of the solution in the wings of spectral line shapes was problematic especially in the case of many Zeeman components.

6. References

[1] Skudra A, Revalde G, "Mathematical modeling of the spectral line profiles in the high-frequency discharges" J.Q.S.R.T. **61** ,717-728 (1999).

[2] N. Zorina, G. Revalde, R. Disch, " Deconvolution of the mercury 253.7 nm spectral line shape for the use in absorption spectroscopy," in SPIE Sixth International Conference on Advanced Optical Materials and Devices, (University of Latvia, Riga, 2008), Vol. 7142, 71420J-1.

[3] N. Zorina, " Deconvolution of the spectral line profiles for the plasma temperature estimation," *Nuclear Instruments and Methods in Physics Research Section A*, **623**, 763-765(2010).

[4] A. Tikhonov, A. Goncharski, V. Stepanov, A. Jagola, "Numerical solution's methods of the ill-posed problem," Nauka**,** Moskow (1990).

[5] A. Tikhonov, V.Arsenin, "The solution's methods of the ill- posed problem)" Nauka**,** Moskow (1979).

Acknowledgement

Travel costs and participation fee for this conference are financially supported by ERDF project „ The development of international cooperation, projects and capacities in science and technology at Riga Technical University" Nr.2DP/2.1.1.2.0/10/APIA/VIAA/003.

Pr7

Validation of the solution method using Tikhonov regularization algorithm for spectral line diagnostics of microsize plasma

Natalia Zorina[a*], Gita Revalde[b,c], Atis Skudra[a]
[a]Institute of Atomic Physics and Spectroscopy, University of Latvia, Skunu str. 4, Riga, Latvia;
[b]Ventspils University College, Inzenieru str. 101, Ventspils, Latvia , [c]Institute of Technical Physics, Riga Technical University, Azenes str. 14/24,Riga,Latvia

ABSTRACT

This paper is devoted obtaining the threshold of the credibility of the solution by means of Tikhonov's regularization method in case of spectral lines, emitted from microsize plasma sources. The reliability of Tikhonov algorithm was verified by means of solving model tasks with different ratio between instrumental function and measured profile and, with different levels of noise.

Keywords: Tikhonov regularization, non-linear multi-parameter modeling, spectral line diagnostics, microsize plasma

1 INTRODUCTION

Since the capillary sources emit very narrow lines it is a challenge to get information about the form of the spectral lines what is important for application of the lamps in high precision experiments. The instrument function can destroy the real spectral line shape significantly, for example, it changes the width of the spectral line that leads to the uncertainties in the determination of such important plasma parameters as temperature [1],it can cover detailed structure of the spectral line, like the dip in the line centre caused by the self-absorption (self-reversal) and characterizing the radiation trapping. That is why to detect the quality of the spectral line shapes, emitted from the lamps, it is necessary to deconvolute the instrument function from the measured spectral lines.

.

1.1 Tikhonov algorithm

The properties of the well posed problems [2] are:
1. Existence of the solution.
2. Uniqueness of the solution.
3. Continuous dependence of the solution on the data.

The problem is ill posed, if, at least, one of properties is not satisfied. In case of inverse tasks the third condition is wrong: small experimental uncertainties can cause large deviations in the solution. The instrument function deconvolution from the measured spectral lines is an inverse ill-posed task.

The measured (experimental) spectral line f(ν) is a convolution of the real line profile y(ν') of the emitted spectral line and instrument function A(ν , ν'). It can be described by Fredholm first kind integral equation:

$$\int_a^b A(\nu,\nu')y(\nu')ds = f(\nu), \quad c \le \nu \le d, \tag{1}$$

where a, b and c, d the limits of the real and measured (experimental) profiles accordingly.

* natalja.zorina@gmail.com

Eighth International Conference on Advanced Optical Materials and Devices (AOMD-8), edited by Janis Spigulis,
Proc. of SPIE Vol. 9421, 94210H · © 2014 SPIE · CCC code: 0277-786X/14/$18 · doi: 10.1117/12.2083842

Tikhonov's regularization algorithm [3] is one of the most useful tools for solving the task where small experimental uncertainties can cause large deviations in the solution. Assuming, that values of the right side and integral equation (1) kernel are known with accuracy:

$$\left.\begin{aligned} \left\| \tilde{f} - f \right\|_F \le \delta; \\ \left\| \tilde{A} - A \right\| \le \xi \end{aligned}\right\} \tag{2}$$

where δ is error of right part of (1) or error of experimental f(*v*) profile ,ξ is error of kernel of (1) or error of instrument function A(*v*,*v*'). According Tikhonov regularization method by minimizing the following functional:

$$M_\alpha \left[y, \tilde{f} \right] = \inf_{y \in Y} M_\alpha \left[y, \tilde{f} \right], \tag{3}$$

we obtain Fredholm second kind integral equation:

$$\alpha \left(y_\alpha (t) - q y_\alpha'' (t) \right) + \int_a^b k(t,v') y_\alpha (v') dv' = F(t) \quad t \in [a,b], \tag{4}$$

where

$$k(t,v') = k(v',t) = \int_c^d \tilde{A}(v,t) \tilde{A}(v,v') dv;$$

$$F(t) = \int_c^d \tilde{A}(v,t)\, \tilde{f}(v) dv.$$

It is well posed task instead of first kind integral equation (1), and the further solution can be implemented by means of the classical methods. The mathematical model is described in the paper [4] in detail.

It is well known that the finding of regularization parameter is crucial for all regularization methods. The inaccurate determination of the regularization parameter leads to major errors in the solution. In this work we used two independent methods to obtain it. There is method of the discrepancy minimization [5]:

$$\left\| \tilde{A} y_\alpha - \tilde{f} \right\|_{L_2}^2 = \min_\alpha \left\| \tilde{A} y_\alpha - \tilde{f} \right\|_{L_2}^2 \tag{5}$$

and method proposed in work [6].According this method regularization parameter is root of equation:

$$\alpha^q \left\| \tilde{A}^* \tilde{A} y_\alpha - \tilde{A}^* \tilde{f} \right\| = \beta \left\| \tilde{A} \right\| \left(\xi + \eta \left\| y_\alpha \right\| \right) \tag{6}$$

All calculations in this work were performed for zero order of regularization (q=0) using programs written in MathCad13. Regularization parameter *a* was obtained in supposition, that error of kernel, in cases when instrumental function was given by formula, is equal of zero, (ξ=0).

1.2 Modeling of the spectral line profiles

The mathematical model is described in the paper [7] in detail. This model includes the basic factors causing the spectral line broadening in a low-pressure discharge: natural, Doppler, resonance and collisional. These effects are accounted by means of the Voigt profile which is a convolution of the Doppler and Lorentz profiles. Normally, the Doppler width (FWHM), $\delta\nu_D$, and Lorentz width, $\delta\nu_L$, are used as the parameters characterizing the Voigt profile.

For a quantitative description of self-absorption, the approximations of the radiation source are used: i) the approximation of a uniformly excited source; ii) source with spatially separated emitting and absorbing atoms; iii) model suggested by Cowan and Dieke [8,9]:

$$I(\nu-\nu_0) = I_0 P(\nu-\nu_0) e^{-\mu} \sum_{j=0}^{\infty} \frac{n!\mu^{2j}}{(2j+n)!} \tag{7}$$

where n is the integer characterizing the homogeneity of the radiation source and

$$\mu = \kappa_0 l \frac{P(\nu-\nu_0)}{P(0)} \tag{8}$$

where $P(\nu-\nu_0)$ is the line profile of radiation in a unity volume, $k_o l$ is the optical density at the centre of the line.

The resulting profile is a convolution of the self-absorbed Voigt profile and the instrument function.

The real spectral line profiles, estimated using described above method, were used for the comparison with the results obtained by means of Tikhonov regularization method. Below are mentioned some advantages and disadvantages of the both methods.

The disadvantage of the line profile modeling method is that the functions of the line profiles have to be known before and we can apply it manly for the symmetric lines. For the using the Tikhonov's regularization method, the only parameter what we have to know is the instrument function. The advantage of the modeling is that we can it apply also for the fit of the width of the instrument function if the type of the instrument function is known.

2 VALIDATION OF THE SOLUTION METHOD

2.1 Test

The reliability of the solution method using Tikhonov regularization algorithm was verified by means of solving model tasks. The test was performed in three stages. First of all several "real profiles" were generated using non-linear multi-parameter modeling with different values of the variable parameters: Doppler broadening, $\Delta\delta_D$, Lorentz broadening, $\Delta\delta_L$, optical density in the line centre, $k_o l$, homogeneity of the radiation source, n. Thus the "real profiles" – the self-absorbed Voigt profile and Voigt profile without self absorption are created. The values of the parameters were chosen so, that the 'experimental' model profiles were maximally close to real spectral profiles, emitted from microsizes light sources. The "experimental profiles" are generated performing a convolution of these "real profiles" with the instrument function (Gauss profile) with a given value of the full width at half of maximum- FWHM ($\Delta\delta_{Instr}$) . The influence of the different ratio of FWHM of 'instrumental function' and FWHM of 'experimental' model profile to result was observed. At the end the several sets of "experimental" errors with different variances were generated and overlapped. In the second stage, the real profiles deconvoluted from the instrumental function using the Tikhonov's regularization method, were obtained.

In the third stage, the deconvoluted real profiles were compared with the initial "experimental profiles". The dependence of these parameters from 1) width of instrument function, 2) values of the variance of the "experimental" errors 3) method of estimation of the regularization parameter were investigated.

Below we can see the examples of the our calculations. On the Fig.1.- Fig3. we can see comparisons between "modeled - real" profile and "calculated- real" profiles. "Modeled -real" profile was generated with following parameters: Doppler width (FWHM), $\delta\nu_D=0.03cm^{-1}$, and Lorentz width, $\delta\nu_L=0.01cm^{-1}$, instrumental function, Gauss profile, $\delta\nu_{Instr.}=0.06cm^{-1}$, optical density in the line centre, $k_o l=4$, homogeneity of the radiation source, n=13. The "experimental" errors were: variance1=0.01(Fig.1), variance2=0.02,(Fig2) variance3=0.05(Fig.3) accordingly .

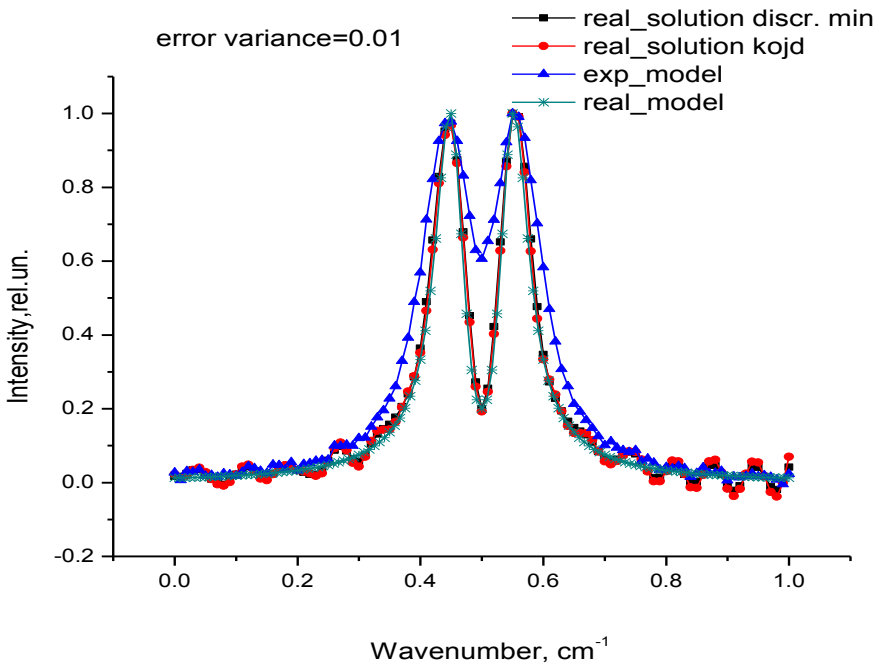

Figure 1. Comparison between "Real modeled" (modeled by means of non-linear multi-parameter modelling)profile and "Real solution" profile(obtained by means of Tikhonov regularization method). "Experimental" errors-variance 0.01.

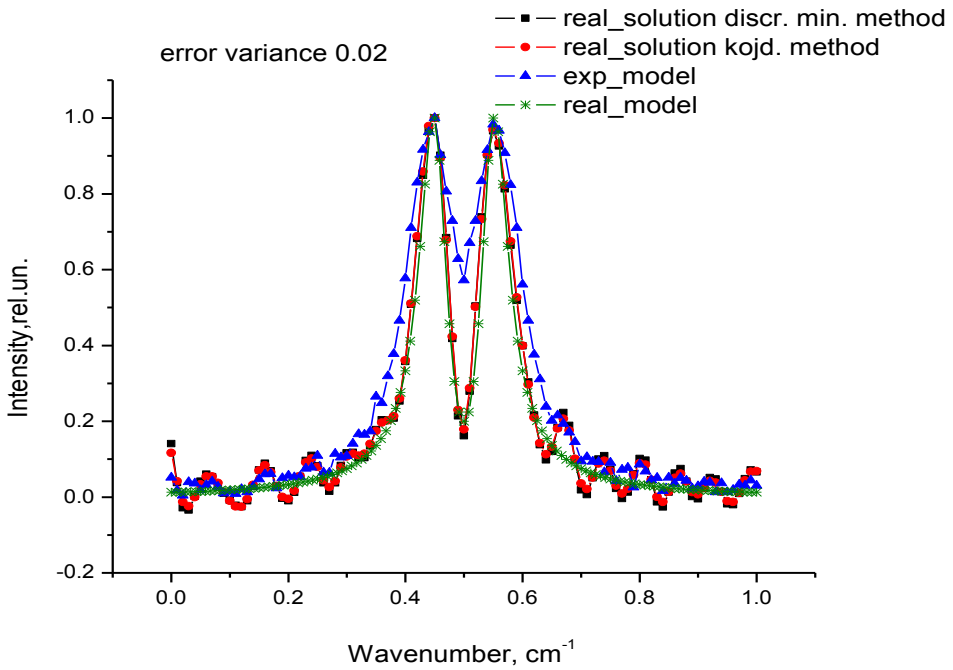

Figure 2. Comparison between "Real modeled" (modeled by means of non-linear multi-parameter modeling)profile and "Real solution" profile(obtained by means of Tikhonov regularization method). "Experimental" errors-variance 0.02.

Solution was implemented by means of Tikhonov regularization method, using two independent method to obtain regularization parameter: 1 method-discrepancy minimization method, 2 method- using equation (5) .

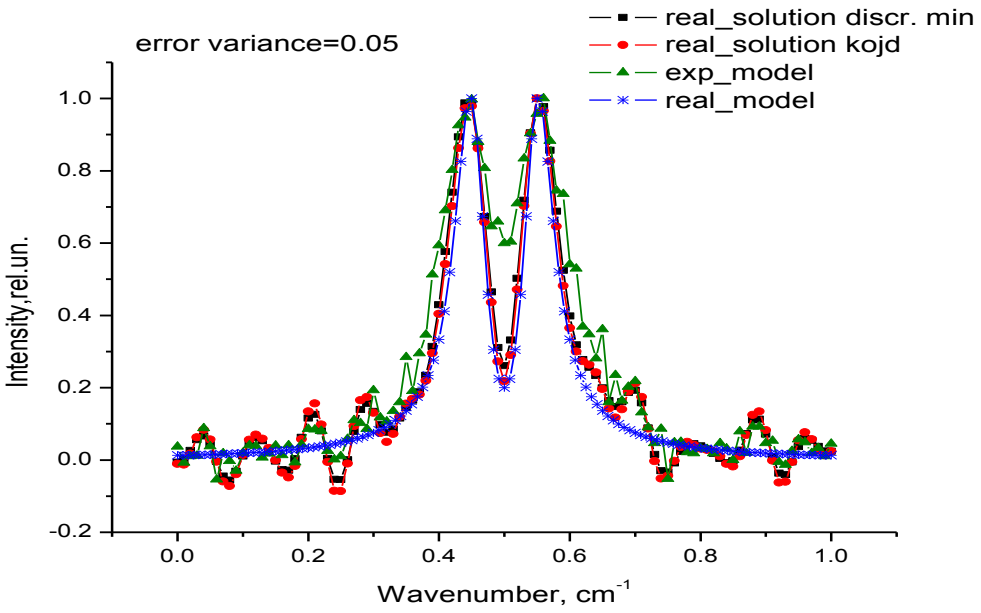

Figure 3. Comparison between "Real modeled" (modeled by means of non-linear multi-parameter modeling)profile and "Real solution" profile(obtained by means of Tikhonov regularization method). "Experimental" errors-variance 0.05.

On the Figs.4 - 7 we can see comparisons between "modeled -real" profile and "calculated- real" profiles.

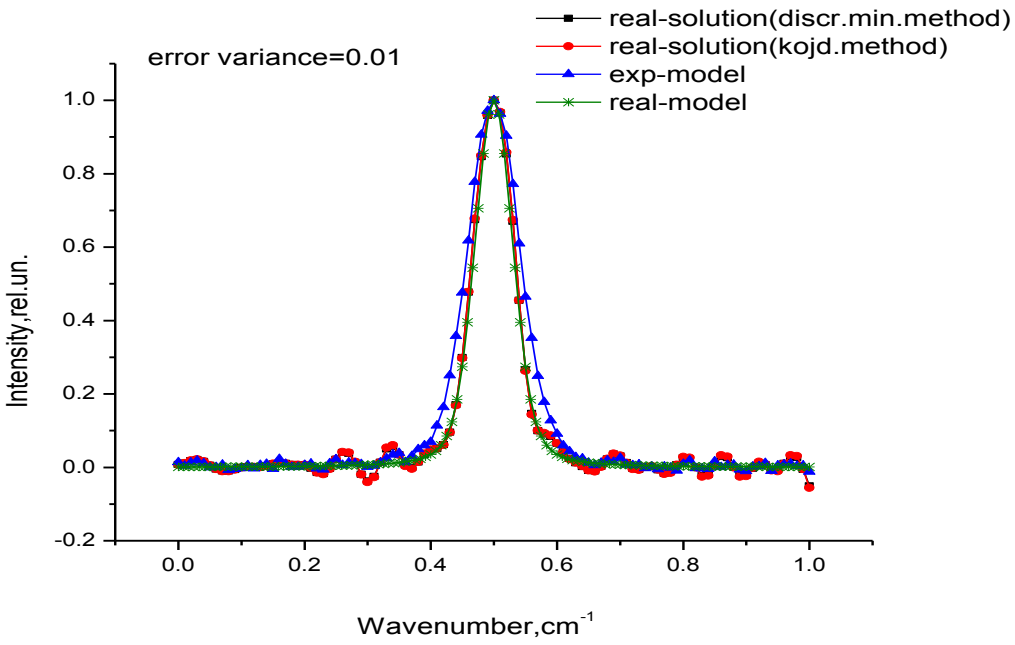

Figure 4. Comparison between "Real modeled" (modeled by means of non-linear multi-parameter modelling)profile and "Real solution" profile(obtained by means of Tikhonov regularization method). "Experimental" errors-variance 0.01.

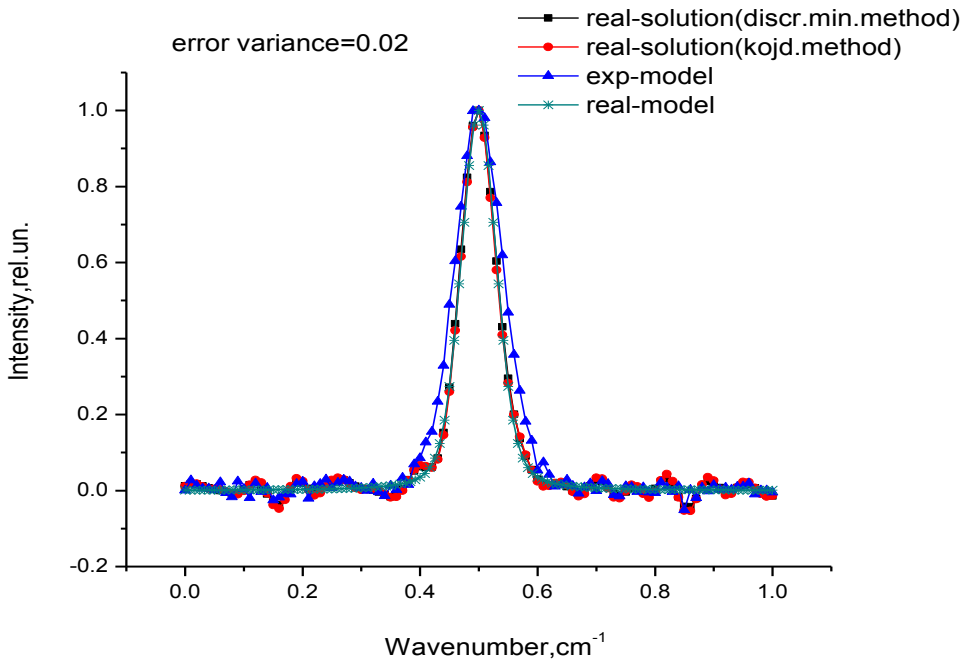

Figure 5. Comparison between "Real modeled" (modeled by means of non-linear multi-parameter modelling)profile and "Real solution" profile(obtained by means of Tikhonov regularization method). "Experimental" errors-variance 0.02.

"Modeled -real" profile was generated with following parameters: Doppler width (FWHM), $\delta\nu_D$=0.03cm^{-1}, and Lorentz width, $\delta\nu_L$=0.01cm^{-1}, instrumental function, Gauss profile, $\delta\nu_{Instr.}$=0.06cm^{-1}, without self absorption. The "experimental" errors were: variance1=0.01(Fig4), variance2=0.02(Fig5), variance3=0.05(Fig6), variance4=0.1 (Fig7).

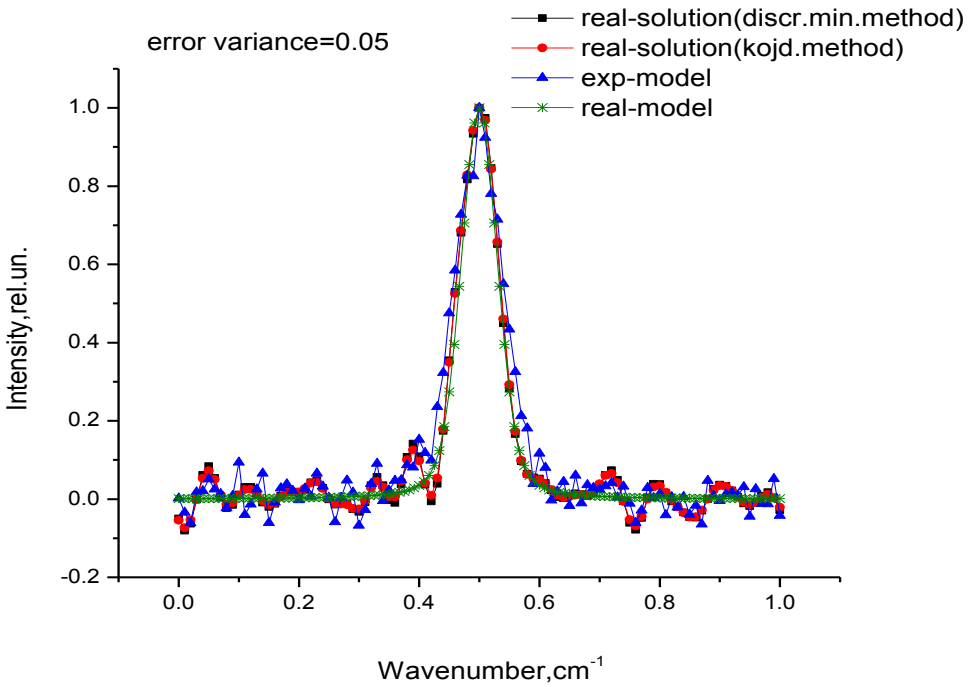

Figure 6. Comparison between "Real modeled" (modeled by means of non-linear multi-parameter modeling)profile and "Real solution" profile(obtained by means of Tikhonov regularization method). "Experimental" errors-variance 0.05.

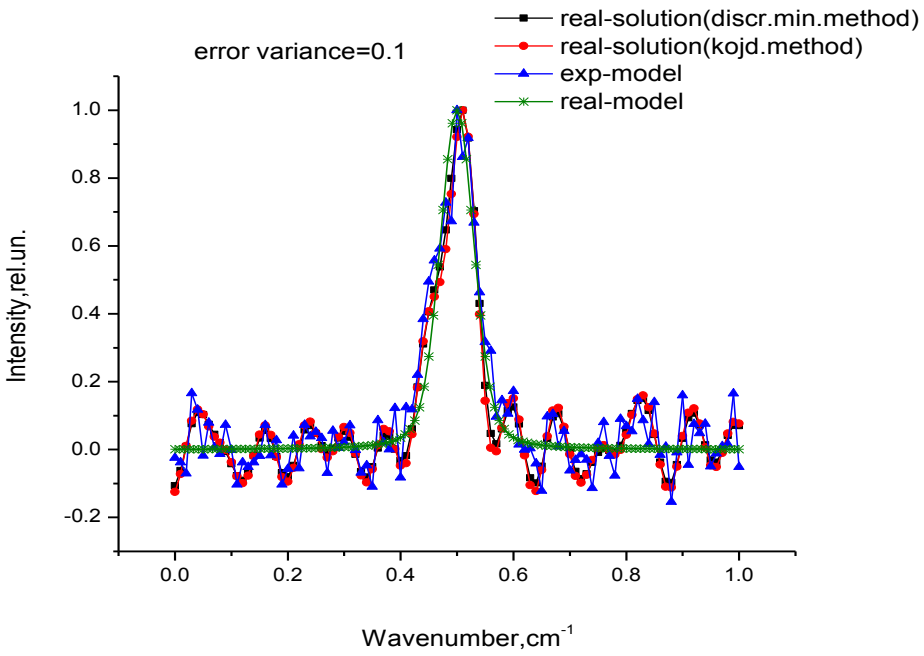

Figure 7. Comparison between "Real modeled" (modeled by means of non-linear multi-parameter modeling)profile and "Real solution" profile(obtained by means of Tikhonov regularization method). "Experimental" errors-variance 0.1.

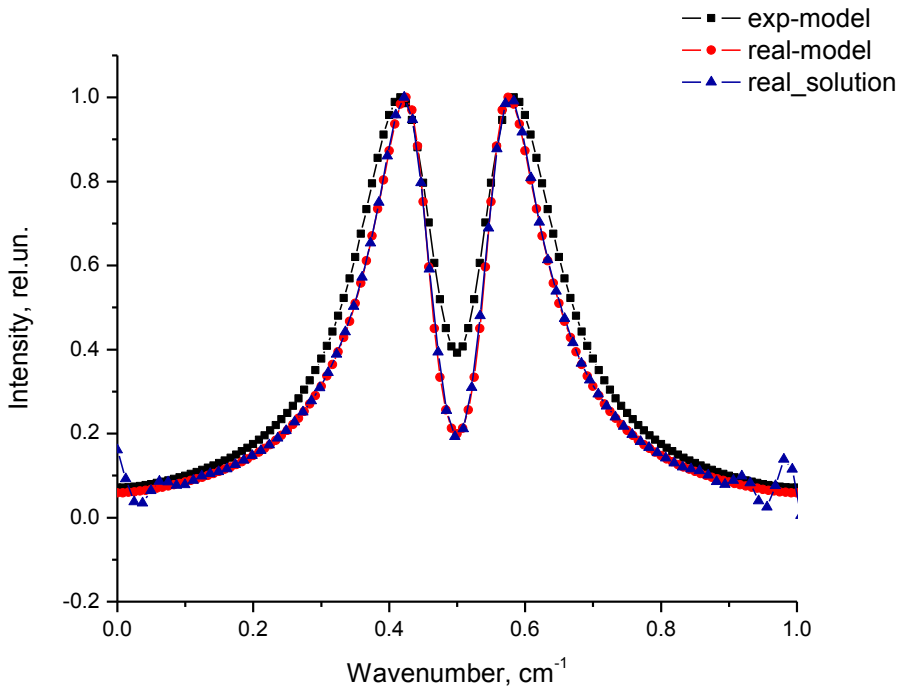

Figure 8. Comparison between "Real modeled" (modeled by means of non-linear multi-parameter modeling)profile and "Real solution" profile(obtained by means of Tikhonov regularization method).

As we can see on Figs.1- 7 the values of self absorption(Figs.1-3) and values of FWHM (Figs.4-7) of modeled "real" profile and of calculated "real" profile coincides quite well. But the greater values of variance lead to larger solution instabilities on the wings of profiles.

On the Fig.8 we can see comparison between comparisons between "modeled -real" profile and "calculated- real" profiles. In this case "modeled- real" profile was generated with equal values of Doppler width (FWHM) and Lorentz width $\delta\nu_D == \delta\nu_L = 0.03 cm^{-1}$ and without the "experimental errors" .The instrumental function, Gauss profile, $\delta\nu_{Instr.} = 0.06 cm^{-1}$. The density in the line centre, $k_o l = 4$, homogeneity of the radiation source, n=13. As we can see in case, when modeled profile was generated without "experimental" errors, modeled "real" profile and calculated "real" profile coincides perfectly.

On the Fig.9 we can see we can see comparison between comparisons between "modeled -real" profile and "calculated- real" profiles. In this case the instrumental function, Gauss profile, $\delta\nu_{Instr.} = 0.1 cm^{-1}$. which is significantly more than in previous cases. The "modeled- real" profile was generated with Doppler width (FWHM), $\delta\nu_D = 0.03 cm^{-1}$, and Lorentz width, $\delta\nu_L = 0.01 cm^{-1}$ and without the "experimental errors" .The density in the line centre, $k_o l = 4$, homogeneity of the radiation source, n=13.

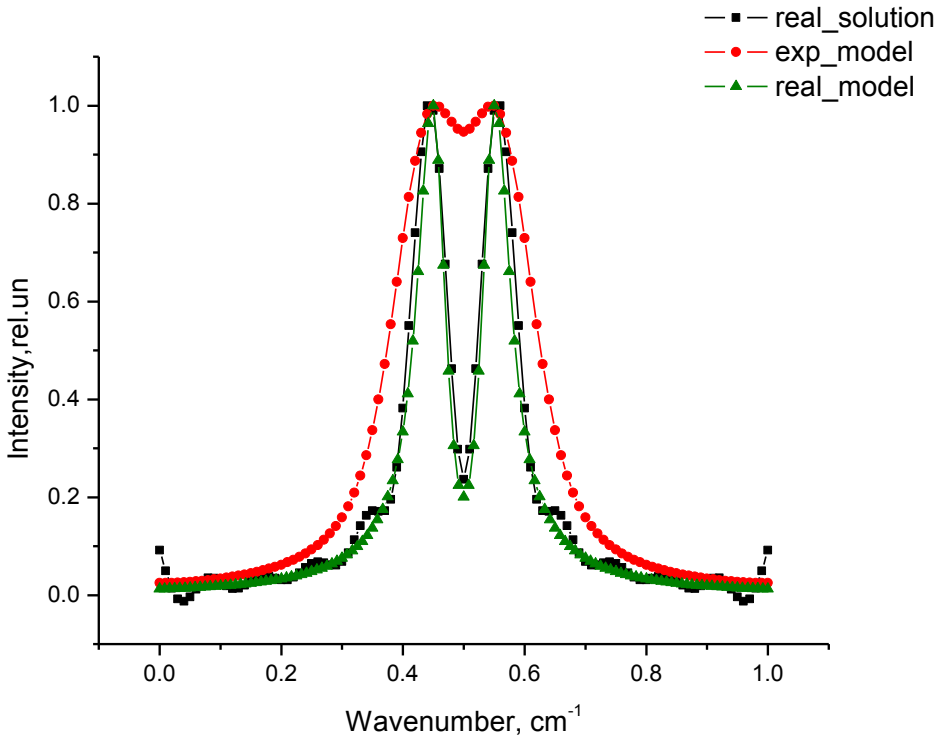

Figure 9. Comparison between "Real modeled" (modeled by means of non-linear multi-parameter modeling)profile and "Real solution" profile(obtained by means of Tikhonov regularization method).

As we can see on Fig.9., such wide instrumental function leads to unstable solution and to difference in values of self absorption in cases of modeled "real" profile and calculated "real" profile. And it leads to unstable solution.

"Real calculated" profiles on Figs.8-9 were obtained using discrepancy minimization method for regularization parameter determination.

2.2 Statistics

Below we can see correlation matrix (Spearman coefficient) [10], obtained in IBM SPSS Statistics 22 for case when "modeled -real" profile was generated with following parameters: Doppler width (FWHM), $\delta\nu_D = 0.03 cm^{-1}$, and Lorentz width, $\delta\nu_L = 0.01 cm^{-1}$, instrumental function, Gauss profile, $\delta\nu I_{nstr.} = 0.06 cm^{-1}$, optical density in the line centre, $k_o l = 4$, homogeneity of the radiation source, n=13. The "experimental" errors were: variance1=0.01, variance2=0.02, variance3=0.05. Solution was implemented by means of Tikhonov regularization method, using two independent method to obtain regularization parameter: 1 method-discrepancy minimization method, 2 method- using equation(6) .

As we can see was obtained significant correlations ($p<0.001$) between values, obtained by both method and between values of each of methods and values of "real-modeled" profile.

Table 1. Correlation matrix (Spearman's rho) -modeled profiles with self-absorption

Spearman's rho		variance0_01_2met.	variance0_02_2met.	variance0_05_2met.	real-modeled
variance0_01_1met.	Correlation Coefficient	,993**	,803**	,803**	,714**
	Sig. (2-tailed)	,000	,000	,000	,000
	N	101	101	101	101
variance0_02_1met.	Correlation Coefficient	,789**	,996**	,631**	,644**
	Sig. (2-tailed)	,000	,000	,000	,000
	N	101	101	101	101
variance0_05_1met.	Correlation Coefficient	,809**	,679**	,992**	,660**
	Sig. (2-tailed)	,000	,000	,000	,000
	N	101	101	101	101
real-modeled	Correlation Coefficient	,702**	,661**	,636**	1,000
	Sig. (2-tailed)	,000	,000	,000	.
	N	101	101	101	101

**. Correlation is significant at the 0.01 level (2-tailed).

In following case (Table 2) "modeled -real" profile was generated with following parameters: Doppler width (FWHM), $\delta\nu_D$=0.03cm^{-1}, and Lorentz width, $\delta\nu_L$=0.01cm^{-1}, instrumental function, Gauss profile, $\delta\nu_{Instr.}$=0.06cm^{-1}, without self absorption. The “experimental” errors were: variance1=0.01, variance2=0.02, variance3=0.05, variance4=0.1. Solution was implemented by means of Tikhonov regularization method, using two independent method to obtain regularization parameter: 1 method-discrepancy minimization method, 2 method- using equation(5) .

As we can see on Table2 was obtained significant correlations between values, obtained by both method ($p<0.001$) and between values of each of methods and values of "real-modeled" profile ($p<=0.01$).

Table 2. Correlation matrix (Spearman's rho)- modeled profiles without self-absorption

Spearman's rho		variance0_01_2met.	variance0_02_2met.	variance0_05_2met.	variance0_1_2met.	real-modeled
variance0_01_1met.	Correlation Coefficient	,999**	,544**	,551**	.297**	,435**
	Sig. (2-tailed)	,000	,000	,000	.003	,000
	N	101	101	101	101	101
variance0_02_1met.	Correlation Coefficient	,570**	,981**	,574**	.281**	,417**
	Sig. (2-tailed)	,000	,000	,000	.004	,000
	N	101	101	101	101	101
variance0_05_1met.	Correlation Coefficient	,533**	,520**	,992**	.356**	,437**
	Sig. (2-tailed)	,000	,000	,000	,000	,000
	N	101	101	101	101	101
variance0_1_1met.	Correlation Coefficient	,342**	,281**	,398**	.991**	,272**
	Sig. (2-tailed)	,000	,004	,000	.000	,006
	N	101	101	101	101	101
real-modeled	Correlation Coefficient	,427**	,393**	,447**	.254	1,000
	Sig. (2-tailed)	,000	,000	,000	.010	.
	N	101	101	101	101	101

**. Correlation is significant at the 0.01 level (2-tailed). *. Correlation is significant at the 0.05 level (2-tailed).

3 CONCLUSION

The solution of the model examples shows that this method can be used for real profile restoring for further diagnostic of the HFEDL if the following conditions can be performed is satisfied the following conditions:

- normal level of the noise. The variance of data must be less than 0.1;
- the ratio between instrumental function and measured profile can be less or equal of 2.

There are significant correlation between values , obtained by means of method1(discrepancy minimization method) and method 2 (Eq. 6). As we can see on Table 1(case with self- absorption), the correlation coefficients are: 0.993, 0.996, 0.992 in cases, when variances of modeled data are 0.01, 0.02, and 0.05 accordingly. We can see the significant correlation between values, obtained by two independent methods in case when modeled profile was without self-absorption too (Table 2). In this case the correlation coefficients are 0.999, 0.981, 0.992, 0.991 in cases, when variances of modeled data are 0.01, 0.02, 0.05, 0.1 accordingly.

As well significant correlation is observing between values of calculated "real" profiles and modeled "real" profiles. In case of modeled profile with self-absorption, the correlation coefficients are 0.714(method 1) and 0.702(method 2) for case when variance of modeled data is 0.01;, 0.644(method 1) and 0.661(method 2) in case when variance is 0.02; 0.660(method 1) and 0.636(method 2),variance of modeled data is 0.05. In case of modeled profile without self-absorption, the correlation coefficients are 0.435(method 1) and 0.427(method 2) for case when variance of modeled data is 0.01; 0.417(method 1) and 0.393(method 2) in case when variance is 0.02; 0.437(method 1) and 0.447(method 2),variance of modeled data is 0.05; 0.272(method 1) and 0.254(method 2), variance of modeled data is 0.1.

AKNOWLEDGEMENTS

This research has been partly supported by the European Social Fund within the project “Elaboration of Innovative Functional Materials and Nanomaterials for Application in Environment Control Technologies” 1DP/1.1.1.2.0/13/APIA/VIAA/30.

REFERENCES

[1] Zorina, N., “Deconvolution of the spectral line profiles for the plasma temperature estimation”, Nuclear Instruments and Methods in Physics Research Section A,623, 763-765,(2010).
[2] Tikhonov, A.N, Arsenin, V., [The solution’s methods of the ill- posed problem], Moscow, Nauka (1979)
[3] Revalde, G., Skudra, A., Zorina, N., Sholupov, S. ,“Investigation of Hg resonance 184.9nm line profile in a low-pressure mercury–argon discharge”, JQSRT 107, 164–172(2007)
[4] Zorina, N., Revalde, G., Disch, R., “Deconvolution of the mercury 253.7 nm spectral line shape for the use in absorption spectroscopy”, in SPIE Sixth International Conference on Advanced Optical Materials and Devices, (University of Latvia, Riga), Vol. 7142, 71420J-1(2008).
[5] Verlan, F, Sizikov, V. S , [The integral equations: the methods, algorithms, program] ,Kiev, Naukova Dumka), (1986)
[6] Kojdecki, M.A., “ New criterion of regularization parameter choice in Tikhonov's method”, Biuletyn WAT (Biul. Mil. Univ. Technol.), V. 49. № 1 (569),47–126, (2000)
[7] Skudra, A., Revalde, G., “Mathematical modeling of the spectral line profiles in the high-frequency discharge” , JQSRT 61, N6, pp 717-728, (1999)
[8] Preobrazhenskii, N.G., [Spectroscopy of Optical Thick Plasma], Novosibirsk, Nauka, , p. 177,(1971)
[9] Cowan R D, Dieke, G H., “ Self-Absorption of Spectrum Lines”, Rev. Mod. Phys2, 418,(1948)
[10] Buhl, A, Zofel P, SPSS., [Art of information processing], Moscow, St. Petersburg, Kiev, DiaSoft, (2005)

Pr8

Line Shape Measurement and Modelling for Plasma Diagnostics

2014 J. Phys.: Conf. Ser. 548 012034

(http://iopscience.iop.org/1742-6596/548/1/012034)

Journal of Physics: Conference Series **548** (2014) 012034 doi:10.1088/1742-6596/548/1/012034

Line Shape Measurement and Modelling for Plasma Diagnostics

G Revalde[1], N Zorina[2] and A Skudra[2]

[1]Institute of Technical Physics, Riga Technical University, Āzenes str. 14/24, Riga, Latvia

[1]Ventspils University College, Inženieru str.101, Ventspils, Latvia

[2]Institute of Atomic Physics and Spectroscopy, University of Latvia, Skunu str. 4, Rīga, Latvia, LV 1050

gitar@latnet.lv

Abstract. In this paper we discuss different methods of narrow spectral line shape measurements for a wide spectral range by means of high-resolution spectrometers such as the Fabry-Perot spectrometer, Zeeman spectrometer and Fourier transform spectrometer as well as a theoretical model for spectral line shape modelling and solving of the inverse task based on Tikhonov's regularization method. Special attention is devoted to the line shape measurements for the optically thin light sources filled with Hg, Ar, Xe, Kr for their use in high precision analysers for detection of heavy metals and benzene.

1. Introduction

Line shape diagnostics are essential when light sources with well-defined shapes of the emission lines are required. In this paper we present the spectral line shape measurement and calculation methods created for optimisation needs for special types of low pressure lamps for their application in atomic absorption spectrometers (AAS). Novel type AA analysers are developed for detection of heavy metals, benzene, toluene and other pollutants in air, water and food in real time [1].High selectivity and very low limits of detection depend on the quality of the spectral line shape.

Spectral line shapes are known as important tools for emission plasma diagnostics in different type of plasma since the form of the line is determined by all plasma processes. However many processes act at the same time, and it is not easy to resolve partial effects on the total line shape. In addition, the processes often correlate with each other. We have to take into account also the influence of spectral apparatus. Reconstructing the real line shape from the measured one is a so called inverse ill-posed task since small uncertainties in the measurement give large deviations in solution. Since it is a complex task, sometimes consideration of the instrument function is omitted. It can be done if the width of the instrument function is much smaller than the real spectral line shape which is true in general for high temperatures and dense plasmas. However in the case of low–pressure plasma the instrument function is on the same order as experimental profile and it has to be taken into account.

In this work we will focus on the deconvolution of narrow real spectral line shapes from experimental profiles registered by different spectrometers with high precision. The influence of the

instrument functions on Hg emission lines from low-temperature discharges will be discussed for Fabry-Perot, Zeeman and Fourier transform spectrometers. The influence of the instrument function on the FWHM of spectral line shapes and gas temperature estimation will be elaborated.

2. Experimental details

The developed light sources contain reservoir with working element, capillary and excitation electrodes located outside the capillary and exciting the discharge at 100 MHz frequency. The discharge can be excited also in the bulb of the lamp. Set-up of capillary light source is shown in Fig.1. In this work, experiments were conducted with mercury light sources with different buffer gases Ar, Kr and Xe. To avoid the splitting and consequently the broadening of the spectral line, the isotopes of the metal are used as filling elements.

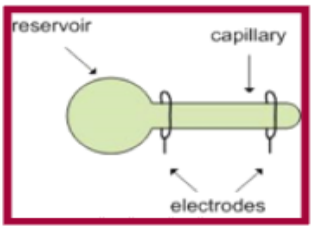

Figure 1. Set-up of a capillary light source

2.1. Fabry-Perot Interferometer

Since the working lines, selected for the needs of AAS, are narrow and often in the UV, the registration instrument should have high sensitivity in broad spectral region. Direct spectral line shape's measurements were done by three different methods in this work. In Fig. 2, the experimental arrangement of a high resolution scanning Fabry-Perot spectrometer is illustrated. The heart of this experimental arrangement is the Fabry-Perot interferometer, consisting of two parallel mirrors, placed into a vacuum chamber which is connected with the pumping system and evacuated. When the air is gradually let to refill the vacuum chamber the refraction index of the mirrors is changing and the spectrum lines are registered by a PMT. The instrument function of the Fabry-Perot interferometer is so called Airy function which can be approximated also by Voigt profile [2].

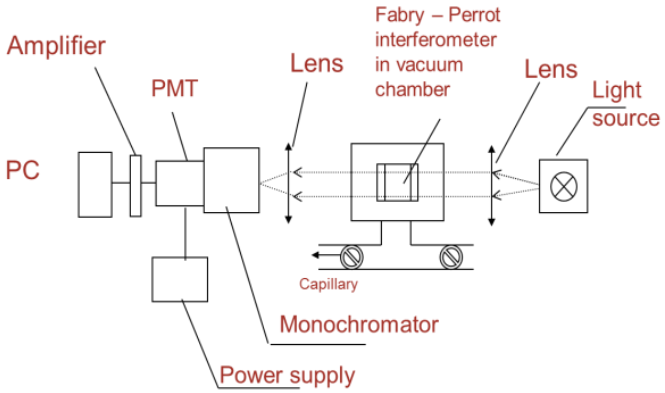

Figure 2. Set-up of a Fabry Perot high resolution spectrometer.

The finesse of the interferometer is restricted by the effective refraction coefficient of the mirrors which includes both, the refraction coefficient and inaccuracy of the adjustment. For example at the effective refraction coefficient R = 80%, the full width at half of maximum (FWHM) of the instrument function $\Delta\nu_{instr}$ amounts to 0.071 cm^{-1}.

2.2. Zeeman Spectrometer

Since The principle set-up of the scanning Zeeman spectrometer is shown in Fig. 3(a). This type of spectrometer is very useful to measure the resonance line shapes in UV region [3, 4]. Examples of the measured Hg VUV resonance line of 185 nm wavelength are shown in Fig.3 (b). By our knowledge this is the only available spectrometer which makes possible direct registration of the Hg 185 nm spectral line shape. The light from the plasma source traverses the same metal vapour cell. The frequency scanning is ensured by changing the magnetic field strength in the absorption cell. The signal is registered by the PMT.

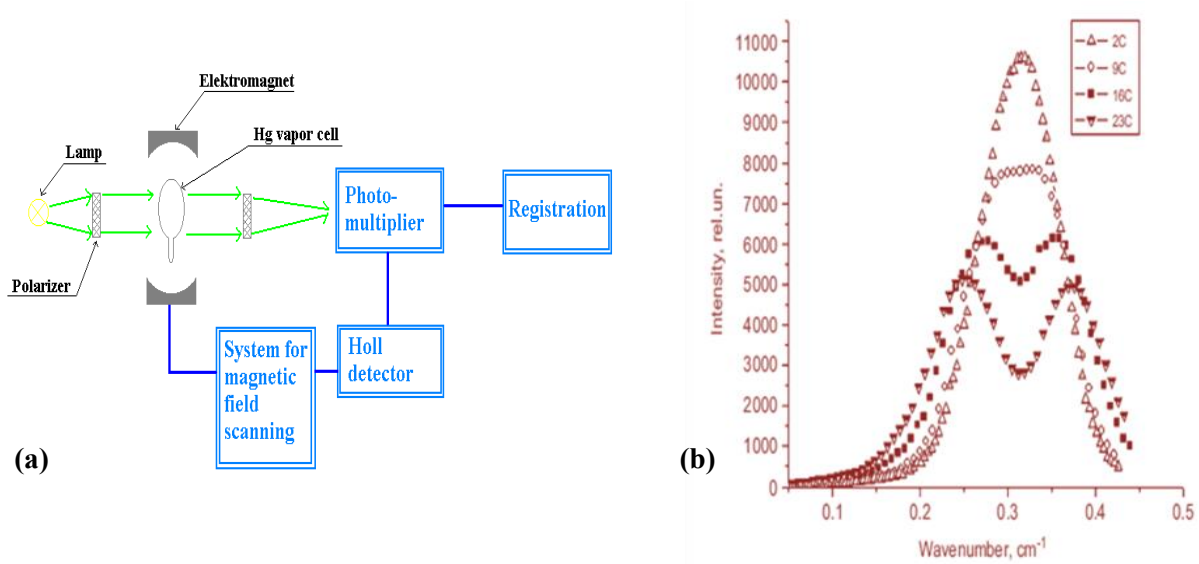

Figure 3. (a) Set-up of Zeeman high resolution spectrometer for the line shape measurements based on absorption of light in the cell placed in magnetic field; **(b)** experimentally measured Hg resonance line shape of 185 nm emitted from the Hg isotope 198 lamp in dependence of the Hg cold spot temperature (metal vapour pressure) [4].

For the Zeeman spectrometer, the instrument function is absorption profile of the metal vapor in the absorption cell. If the cell is hold at the room temperature of 20^{o} C, the Doppler broadened absorption profile has FWHM of 0.036 cm^{-1} which gives better resolution than for the Fabry-Perot interferometer.

2.3. Fourier Transform Spectrometer

The Fourier Transform Spectrometer model Bruker IFS 125 HR can be used to measure spectral line shapes in wide spectral range from 320 - 910 nm, about 2000 pixels/nm. The theoretical instrument function of the Fourier spectrometer is function sinc(x) = sin(x)/x shown in Fig.4. However the measured function using the He laser line of wavelength 632.8 nm, shown in Fig.5 looks differently.

Since the reconstruction takes into account the theoretical or measured prompt function and since we encountered issues with finding stable solutions, we first applied a fitting procedure. Subsequently, we found that the best approximation of the instrument function is a Lorentz profile with FWHM of 0.02 cm^{-1} [5]. Thus all further calculations were performed with this function. Experimentally measured spectral line shapes of 435.8 nm for two Hg isotope lamps, 202 and 198 isotopes, respectively, depend on the discharge power. Fig. 6 displays these results.

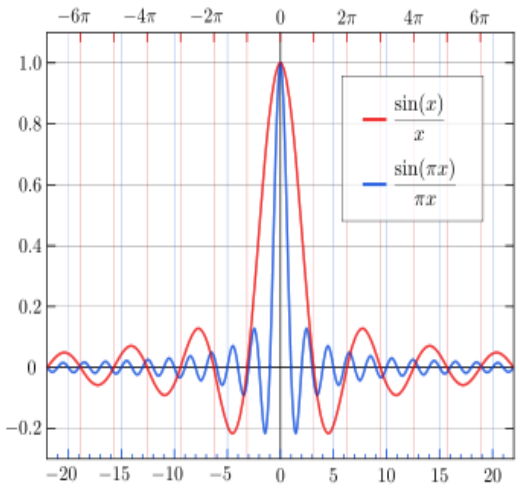

Figure 4. Theoretical instrument function of Fourier transforms spectrometer.

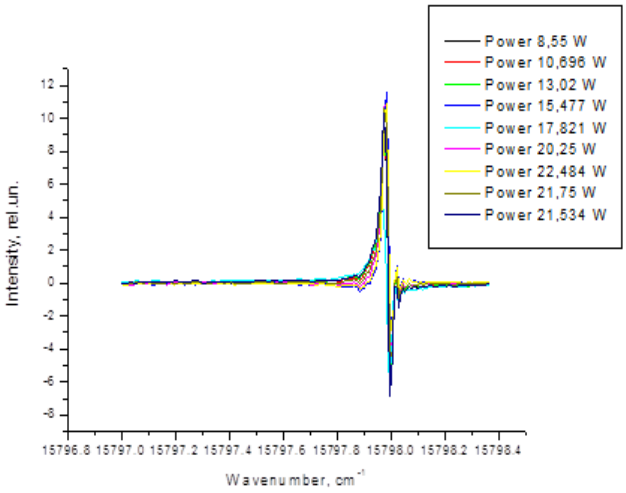

Figure 5. Experimentally measured Fourier transform spectrometer instrument function.

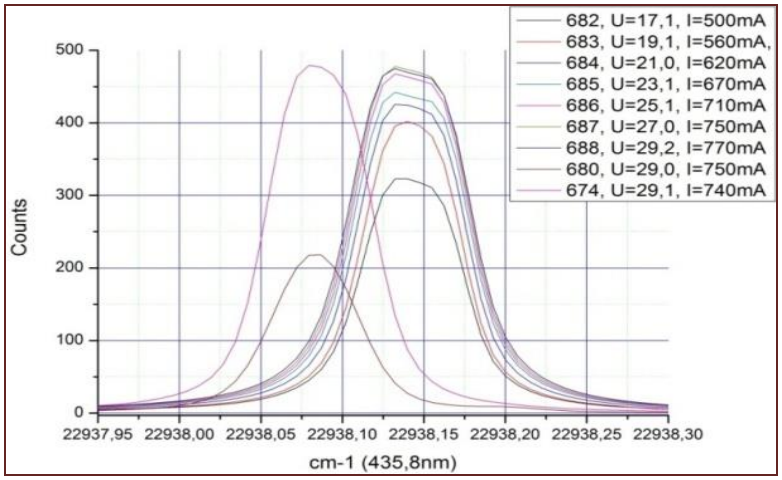

Figure 6. Experimentally measured Fourier spectra of the Hg 435.8 nm line shapes for the two Hg isotopes 198 and 202.

3. Theoretical Approach

As is well known, the experimentally registered spectral line shape, influenced by the instrument function, can be expressed in form of a Fredholm integral equation of first kind:

$$\int_a^b A(x,s)y(s)ds = f(x), \quad c \le x \le d, \quad (1)$$

where *f(x)*- measured spectral line profile; *y(s)*- real spectral line profile; *A(x,s)*-instrument function and a, b and c, d -the limits of the real and experimental profiles, accordingly.

To calculate the real spectral line profile from experimental line, it is necessary to solve this inverse ill-posed task where small experimental uncertainties can cause large deviations in the solution. Our experience showed that the Tikhonov's regularisation algorithm [6] is one of the most useful tools for solving the task.

Assuming, that the values on the right side and integral equation (1) kernel are known with accuracy:

$$\left.\begin{aligned} \left\| \tilde{f} - f \right\|_F \le \delta; \\ \left\| \tilde{A} - A \right\| \le \xi \end{aligned}\right\} \qquad (2)$$

where δ is the error of right part of (1) or the error of experimental $f(x)$ profile, ξ is the error of kernel of (1) or the error of instrument function $A(x,s)$, Tikhonov proved, that the initial, ill-posed task can be transformed into a task of searching for the minimum of a smoothing functional:

$$M_\alpha\left[y, \tilde{f}\right] = \inf_{y \in Y} M_\alpha\left[y, \tilde{f}\right], \qquad (3)$$

where the smoothing functional $M_\alpha\left[y, \tilde{f}\right]$, so called Tikhonov's functional, is given in the form:

$$M_\alpha\left[y, \tilde{f}\right] = \left\| \tilde{A}y - \tilde{f} \right\|_F^2 + \alpha\Omega[y]. \qquad (4)$$

The stabilising functional Ω is described by the following expression:

$$\Omega[y] = \|y\|_Y^2 \qquad (5)$$

$\alpha > 0$ is the regularisation's parameter; the number discrepancy is denoted by $\left\| \tilde{A}y - \tilde{f} \right\|_F^2$.

According to Tikhonov's method, instead of the initial ill posed problem (1) we get well posed task, which is described by the Fredholm integral equation of second kind. After changing the integrals to finite sums, one can write the system of linear equations are

$$\sum_{i=1}^{N} b_i \left(\sum_{m=1}^{N} b_m \tilde{A}_{mk} \tilde{A}_{mi} \right) y_i + \alpha y_k = \sum_{m=1}^{N} b_m \tilde{A}_{mk} \tilde{f}_m, \quad k = \overline{1, N} \qquad (6)$$

where A_{ij} – elements of *N xN* size matrix *A,* which approximates kernel; f_i – vectors-column with initial dates; y_i – vector-column of solution; b_i – the coefficients.

The system of Equations (6) can be solved with classical methods. All calculations in this work were done for zero order of regularization (q=0) using programs written in MathCad. Regularisation parameter α was obtained in supposition, that the error of kernel is equal to zero (ξ=0) in cases when the instrumental function is known analytically. Typically we use two independent methods to obtain the regularisation parameter α [7,8].

However the deconvoluted real spectral line shape still needs to be modelled because we want to obtain plasma parameters. In the low temperature plasma the real spectral line shape can be approximated Voigt profile which is a convolution of the Doppler and Lorentz profiles. Normally, the Doppler width (FWHM), $\delta\nu_D$, and Lorentz width, $\delta\nu_L$, are used as the parameters characterizing the Voigt profile. Voigt profile includes the basic factors causing the spectral line broadening in a low-pressure discharge: natural, temperature, collisional. The main problem is to take into account the self-absorption. Spectral line modelling is further described in [2-4]. Along the line of sight the intensity distribution in the line shape *I(ν)* can be written as:

$$I(\nu) = I_0 \int_{-\infty}^{+\infty} \bar{n}_e(r) P_e(\nu, r) \exp\left[-s \int_r^{\infty} P_a(\nu, x) \bar{n}_a(x) dx \right] dr \qquad (7),$$
$$\bar{n}_a(r) = \frac{n_a(r)}{N_a}; \quad \bar{n}_e = \frac{n_e(r)}{N_e}$$

where

$$N_a = \frac{1}{2} \int_{-\infty}^{+\infty} n_a(r) dr; \qquad N_e = \int_{-\infty}^{+\infty} n_e(r) dr \,.$$

It is important to know the distributions of the absorbing and emitting particles $n_a(r)$ and $n_e(r)$. For our calculations we use several approximations: uniform distribution of emitting and absorbing particles (homogenous light source), light source with spatially resolved emitting and absorbing particles (inhomogeneous light source), experimentally determined distributions as well as model supposed by Cowan and Dicke which gives some kind of intermediate distributions of the excitation function of the light source [9].

4. Results and discussion

Mercury 202 isotope 253.7 nm line shapes, recorded with a Zeeman spectrometer and the Fabry-Perot spectrometer are shown in Fig. 7.

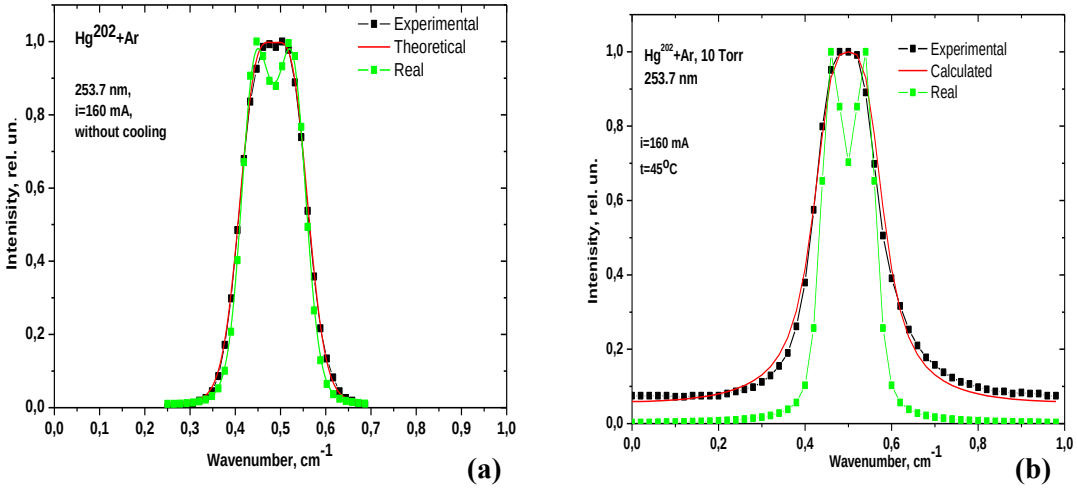

Figure 7. Comparison of mercury 202 isotope 253,7 nm line shapes, registered with Zeeman **(a)** and Fabry-Perot spectrometers **(b)** and the calculated real spectral line (green squares).

As we can observe, in both cases the dip due to the self-absorption is covered by the instrument functions of the spectrometers despite the fact that the instrument functions in both cases are narrow (the broadening is on the same order as the line shape itself). The Fabry-Perot spectrometer gives more influence on the wings of the shape. For the calculation of the real profile, the model of the inhomogeneous light source excitation function was applied. In Fig. 8, the results of deconvolution procedure are shown for Hg 546.1 nm visible triplet line.

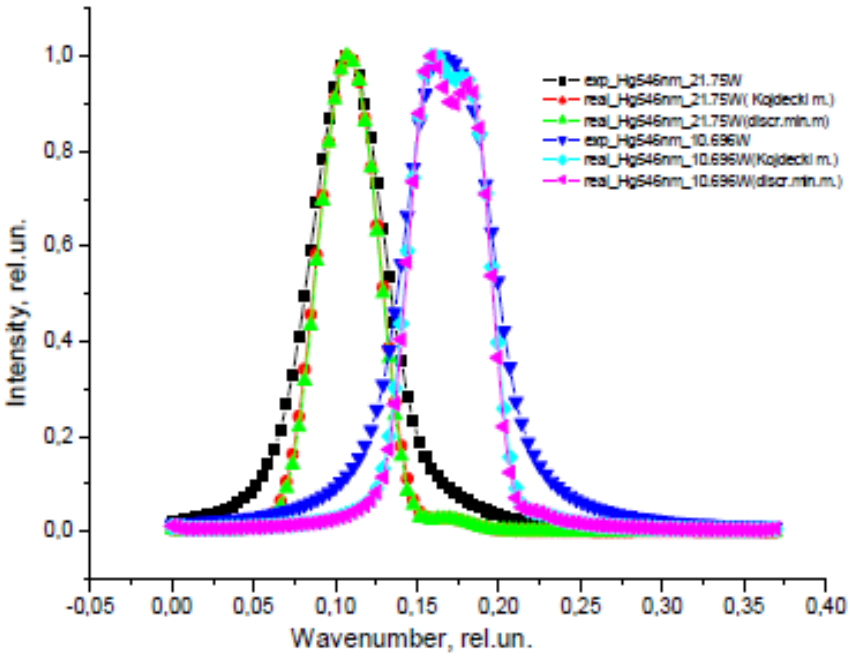

Figure 8. Experimental Fourier spectra of the Hg 546.1 nm line and deconvoluted shapes for the two Hg isotope lamps, 202 and 198.

The results are given for two methods of finding the regularization parameter α, the Kojdecki method [7] and minimum of discrepancy method [8]. Both methods give similar results. It is interesting to observe that the line, emitted from the 198 isotope lamp, is self-absorbed because the lamp contains higher concentration of mercury.

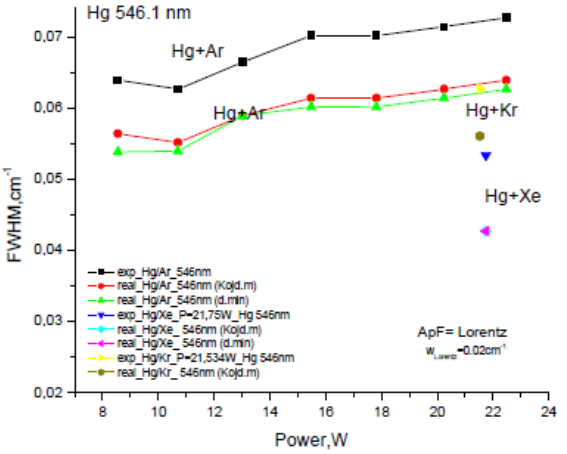

Figure 9. FWHM in dependence from the discharge power, calculated from the deconvoluted line shapes of Hg line 546.1 nm emitted from the Hg/Ar, Hg/Kr, Hg/Xe discharge plasmas.

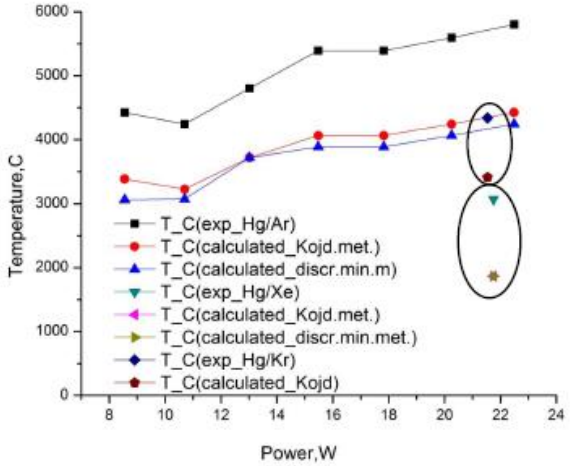

Figure 10. FWHM in dependence from the discharge power, calculated from the deconvoluted line shapes of 435.8 nm Hg line emitted from the Hg/Ar, Hg/Kr, Hg/Xe discharge plasmas.

We can obtain the real FWHM for all the registered lines that allows us to determine temperature of the emitting particles. Examples of the results of the calculated FWHM of the 546.1 nm line and temperatures (T) are shown in the Figs. 9 and 9. It is clearly demonstrated that the neglecting instrument function can lead to large error of about 1500° C in the temperature calculations. Clear

dependence of the temperature of the type of buffer gas can be observed – the heavier the buffer gas, the colder the plasma. Adding Kr instead of Ar decreases temperature of about 900^{o} C, adding Xe instead of Ar decreases temperature about 2000^{o} C.

5. Conclusion

Narrow spectral line shapes, emitted from the light sources, developed for the atomic absorption spectrometry for detection of heavy metals and benzene, are analysed by three different measurement methods in UV and visible spectral regions. The regularisation method and mathematical modelling is used to extract the real spectral line shape. Neglecting the instruments function gives an error of about 1500^{o} C for the discharge temperature. Clear influence of buffer gas type was found on the mercury discharge temperature.

Acknowledgement

This research has been partly supported by the European Social Fund within the project "Elaboration of Innovative Functional Materials and Nanomaterials for Application in Environment Control Technologies" 1DP/1.1.1.2.0/13/APIA/VIAA/30.

References

[1] Ganeev A, Gavare Z, Khutorshikov V I, Khutorchikov S V,Revalde G, Skudra A, Smirnova GM, Stankov N R 2003 *Spectrochim. Acta Part B* **58** 879
[2] Skudra A, Revalde G 1999 *J. Quant. Spectrosc. Rad. Transfer* **61** 717
[3] Revalde G, Denisova N, Gavare Z, Skudra A 2005 *J. Quant. Spectrosc. Rad. Transfer* **94** 311
[4] Revalde G, Skudra A, Zorina N, Sholupov S 2007 *J. Quant. Spectrosc. Rad. Transfer* **107** 164
[5] Revalde G, Zorina N, Skudra A, Gavare Z 2014 *Romanian Reports in Physics* **66** (in press: *N4*)
[6] Tikhonov A, Arsenin V 1979 *The solution's methods of the ill-posed problem* (Moscow: Nauka)
[7] Verlan F, Sizikov V S 1986 The integral equations: the methods, algorithms, program (Kiev: Naukova Dumka)
[8] Kojdecki M F 2000 New criterion of regularization parameter choice in Tikhonov's method *Biuletyn WAT* (Biul. Mil. Univ. Technol.) **49** № 1 (569) 47
[9] Cowan R D, Dieke G H 1948 *Rev. Mod. Phys*. **2** 418